
A PHYSICAL MODEL AND A MONTE CARLO ESTIMATE FOR THE SPECIFIC INTENSITY SPATIAL DERIVATIVE, ANGULAR DERIVATIVE AND GEOMETRIC SENSITIVITY.

A PREPRINT

Paule Lapeyre^{1*}, Zili He², Stéphane Blanco³, Cyril Caliot⁴, Christophe Coustet⁵, Jérémi Dauchet⁶, Mouna El Hafi², Simon Eibner², Eugene d'Eon⁷, Olivier Farges⁸, Richard Fournier³, Jacques Gautrais⁹, Nada Chems Mourtaday³, and Maxime Roger¹⁰

¹*Department of Mechanical and Mechatronics Engineering, University of Waterloo, 200 Ave. W. Waterloo ON, Canada, N2L 3G1*

²*Université de Toulouse, IMT Mines Albi, UMR 5302 - Centre RAPSODEE, Campus Jarlard, F-81013, Albi CT Cedex 09, France*

³*LAPLACE, UMR 5213 - Université Paul Sabatier, 118, Route de Narbonne - 31062 Toulouse Cedex, France*

⁴*LMAP, UMR 5142, E2S UPPA, Université de Pau et des Pays de l'Adour, 1 allée du Parc Montaury, 64600 Anglet, France*

⁵*Méso-star, 8 rue des pechers, 31410 Longages, France*

⁶*Université Clermont Auvergne, Clermont Auvergne INP, CNRS, Institut Pascal, F-63000 Clermont-Ferrand, France*

⁷*NVIDIA, Wellington, New Zealand*

⁸*Université de Lorraine, UMR 7563 CNRS, LEMTA, F-54000 Nancy, France*

⁹*Centre de Recherches sur la Cognition Animale (CRCA), Centre de Biologie Intégrative (CBI), Université de Toulouse; CNRS, UPS, France*

¹⁰*Univ. Lyon, CNRS, INSA-Lyon, Université Claude Bernard Lyon 1, CETHIL UMR5008, F-69621, Villeurbanne, France*

July 28, 2022

Abstract

Starting from the radiative transfer equation and its usual boundary conditions, the objective of this work is to design Monte Carlo algorithms estimating the specific intensity spatial and angular derivatives as well as its geometric sensitivity. The present document is structured in three parts, each of them dedicated to a specific derivative of the intensity. Although they are all assembled here in one document each derivative is of interest independently whether it be for radiative transfers analysis or engineering conception. Therefore, they are thought to be written as three different papers and are presented here as such. Estimating derivatives of the specific intensity when solving radiative transfers using a Monte-Carlo algorithm is challenging. Finite differences are often not sufficiently accurate and directly estimating the derivative from a specific Monte-Carlo algorithm can lead to arduous formal or numerical developments. The proposition here is to work from the radiative transfer equation and its boundary conditions to design a physical model for each derivatives. Only then Monte-Carlo algorithms are built from the derivatives differential equations using the usual equivalent path integral. Since the same methodology is applied to the specific intensity spatial derivative, angular derivative and geometric sensitivity we chose to keep the same writing structure for all three parts so that all common ideas and developments appears exactly the same. We believe this choice to be coherent to facilitate the reader's understanding. Finally, these are preliminary versions of the final papers: for each parts the theory is fully described, but,

* plapeyre@uwaterloo.ca

although they have been implemented, the examples and algorithms sections are not always complete. This will be mentioned in the introductions of the concerned sections.

PART 1: A physical model and a Monte Carlo estimate for the spatial derivative of the specific intensity

Abstract

Starting from the radiative transfer equation and its usual boundary conditions, the objective of the present article is to design a Monte Carlo algorithm estimating the spatial derivative of the specific intensity. There are two common ways to address this question. The first consists in using two independent Monte Carlo estimates for the specific intensity at two locations and using a finite difference to approximate the spatial derivative; the associated uncertainties are difficult to handle. The second consists in considering any Monte Carlo algorithm for the specific intensity, writing down its associated integral formulation, spatially differentiating this integral, and reformulating it so that it defines a new Monte Carlo algorithm directly estimating the spatial derivative of the specific intensity; the corresponding formal developments are very demanding [1]. We here explore an alternative approach in which we differentiate both the radiative transfer equation and its boundary conditions to set up a physical model for the spatial derivative of the specific intensity. Then a standard path integral translation is made to design a Monte Carlo algorithm solving this model. The only subtlety at this stage is that the model for the spatial derivative is coupled to the model for the specific intensity itself. The paths associated to the spatial derivative of the specific intensity give birth to paths associated to specific intensity (standard radiative transfer paths). When designing a Monte Carlo algorithm for the coupled problem a double randomization approach is therefore required.

1 Introduction

We address the question of modeling and numerically simulating the spatial derivative $\partial_{1,\vec{\gamma}}I \equiv \partial_{1,\vec{\gamma}}I(\vec{x},\vec{\omega})$ of the specific intensity $I \equiv I(\vec{x},\vec{\omega})$ at location \vec{x} in the transport direction $\vec{\omega}$. This spatial derivative is made along a given direction, namely along a unit vector $\vec{\gamma}$, which means that

$$\partial_{1,\vec{\gamma}}I = \vec{\gamma} \cdot \vec{\nabla}I \quad (1)$$

Intensity I has two independent variables $(\vec{x},\vec{\omega})$; the spatial derivative $\partial_{1,\vec{\gamma}}I$ has three independent variables $(\vec{x},\vec{\omega},\vec{\gamma})$. As two of these variables are directions (vectors in the unit sphere), they will be distinguished by specifying the transport direction for $\vec{\omega}$ and the differentiation direction for $\vec{\gamma}$ (see Figure 1).

The reason why we address $\partial_{1,\vec{\gamma}}I$, a scalar quantity, instead of the vector $\vec{\nabla}I$ as a whole, is the attempt to make explicit connections between the modeling of spatial derivatives and standard radiative transfer modeling. Starting from the available transport physics for I , our main objective is to introduce a new, very similar transport physics for $\partial_{1,\vec{\gamma}}I$. Then all the standard practice of analysing and numerically simulating I can be directly translated into new tools for analysing and numerically simulating spatial derivatives.

Standard radiative transfer physics can be gathered into two equations: the partial differential equation governing I at any location inside the field G (the radiative transfer equation) and an integral constraint at the boundary ∂G (the incoming radiation equation), relating I in any direction toward the field to I in all the directions exiting the field. Recognizing, in the writing of these equations, the processes of volume emission/absorption/scattering and surface emission/absorption/reflection, translating them into path statistics, is quite straightforward. We will do the same with $\partial_{1,\vec{\gamma}}I$:

* plapeyre@uwaterloo.ca

We make the very same choice in PART 2 as far as angular derivatives are concerned (considering only one rotation around a given axis).

- Two equations will be constructed for $\partial_{1,\vec{\gamma}}I$ by differentiating the radiative transfer equation and the incoming radiation equation (differentiating the equations of the I model).
- The resulting equations will be physically interpreted using transport physics processes, defining volume emission/absorption/scattering and surface emission/absorption/reflection processes for the spatial derivative. A particular attention will be devoted to the identifications of the sources of the spatial derivative.
- Statistical paths will then be defined for $\partial_{1,\vec{\gamma}}I$, from the sources to the location and direction of observation.

Numerically estimating $\partial_{1,\vec{\gamma}}I$ will then be simply achieved using a Monte Carlo approach, i.e. sampling large numbers of paths. We will display the observed variance of the resulting Monte Carlo estimate but no attempt will be made to optimize convergence in the frame of the present article. Configurations for which $\partial_{1,\vec{\gamma}}I$ is known analytically will be used both to validate the formal developments and to illustrate the physical meaning of each of the identified processes of emission, absorption, scattering and reflection as far as spatial derivatives are concerned.

Even if the presentation of the mathematical developments remains strictly formal, we will try to stick to the spirit of radiative transfer: trying to write down the physics of spatial derivatives by maintaining a parallel, as strict as possible, with the physics of photon transport. This parallel will not be complete. Beer-Lambert and phase functions will be entirely recovered, BRDFs also but with a significant new feature: reflection changes the differentiation direction (note that a far parallel can be made with surface reflection modifying the polarization state).

The text is essentially a short note with three sections:

- Section 2 provides the model in its differential form for boundary surfaces without any discontinuities.
- Section 3 deals with the specific case of discontinuities at the junction between two plane surfaces.
- Section 4 provides the associated statistical paths and illustrates how a standard Monte Carlo approach can be used to estimate $\partial_{1,\vec{\gamma}}I$ (or any radiative transfer observable defined as an integral of $\partial_{1,\vec{\gamma}}I$).

2 Convex domain with differentiable boundaries

Noting \mathcal{C} the collision operator, the stationary monochromatic radiative transfer equation is

$$\vec{\nabla}I \cdot \vec{\omega} = \mathcal{C}[I] + S \quad \vec{x} \in G \quad (2)$$

with

$$\mathcal{C}[I(\vec{x}, \vec{\omega})] = -k_a(\vec{x})I(\vec{x}, \vec{\omega}) - k_s(\vec{x})I(\vec{x}, \vec{\omega}) + k_s(\vec{x}) \int_{4\pi} p_{\Omega'}(-\vec{\omega}'|\vec{x}, -\vec{\omega})d\vec{\omega}' I(\vec{x}, \vec{\omega}') \quad (3)$$

where k_a is the absorption coefficient, k_s the scattering coefficient and $p_{\Omega'}(-\vec{\omega}'|\vec{x}, \vec{\omega})$ is the probability density that the scattering direction is $-\vec{\omega}'$ for a photon scattered at \vec{x} coming from direction $-\vec{\omega}$ (the single scattering phase function, see Figure 2 for a single collision and Figure 3 for a multiple-scattering photon trajectory). $S \equiv S(\vec{x}, \vec{\omega})$ is the volumic source. When this source is due to thermal emission, under the assumption that the matter is in a state of local thermal equilibrium, then it is isotropic and $S = k_a I^{eq}(T)$ where T is the local temperature and I^{eq} is the specific intensity at equilibrium (following Planck function).

At the boundary, noting \mathcal{C}_b the reflection operator, the incoming radiation equation is

$$I = \mathcal{C}_b[I] + S_b \quad \vec{x} \in \partial G ; \vec{\omega} \cdot \vec{n} > 0 \quad (4)$$

with

$$\mathcal{C}_b[I] = \rho(\vec{x}, -\vec{\omega}) \int_{\mathcal{H}'} p_{\Omega',b}(-\vec{\omega}'|\vec{x}, -\vec{\omega})d\vec{\omega}' I(\vec{x}, \vec{\omega}') \quad (5)$$

where \vec{n} is the normal to the boundary at \vec{x} , oriented toward the inside, $\vec{\omega}$ is a direction within the inside hemisphere \mathcal{H} , $\vec{\omega}'$ is any direction within the outside hemisphere \mathcal{H}' , $\rho(\vec{x}, -\vec{\omega})$ is the surface reflectivity for a photon impacting the boundary in direction $-\vec{\omega}$, and $p_{\Omega',b}(-\vec{\omega}'|\vec{x}, -\vec{\omega})$ is the probability density that the refaction direction is $-\vec{\omega}'$ for a photon reflected at \vec{x} coming from direction $-\vec{\omega}$ (the product $\rho p_{\Omega',b}$ is the bidirectional reflectivity density function, see Figure 4 collision at the boundary and Figure 5 for a multiple-reflection photon trajectory). When the surfacic source $S_b \equiv S_b(\vec{x}, \vec{\omega})$ is due to the thermal emission

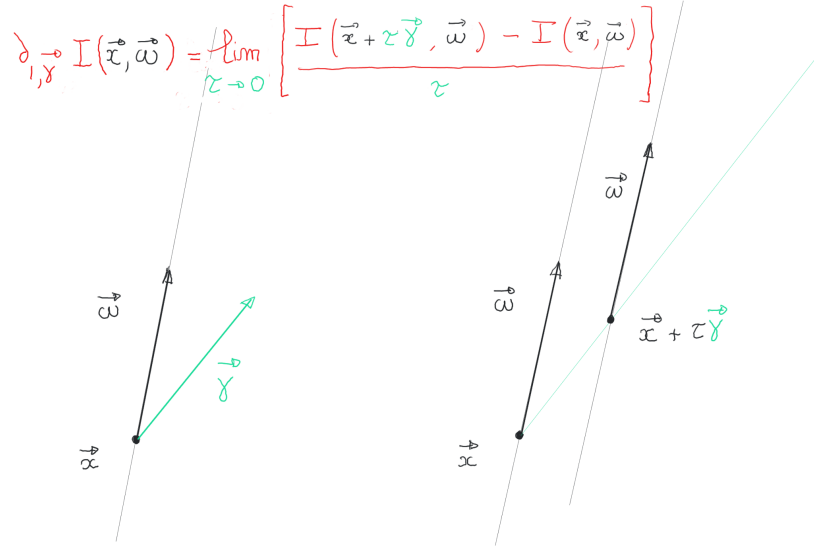


Figure 1: The spatial derivative $\partial_{1, \vec{\gamma}} I$ pictured as an elementary displacement in the differentiation direction $\vec{\gamma}$ according to $\partial_{1, \vec{\gamma}} I(\vec{x}, \vec{\omega}) = \vec{\gamma} \cdot \vec{\nabla} I = \lim_{\tau \rightarrow 0} \frac{I(\vec{x} + \tau \vec{\gamma}, \vec{\omega}) - I(\vec{x}, \vec{\omega})}{\tau}$. When picturing photon transport, we need to draw the location \vec{x} and the line of sight, i.e. the transport direction $\vec{\omega}$. When picturing the physics of spatial derivatives, we will need to draw the location \vec{x} and two vectors: $\vec{\omega}$ for the transport direction and $\vec{\gamma}$ for the differentiation direction.

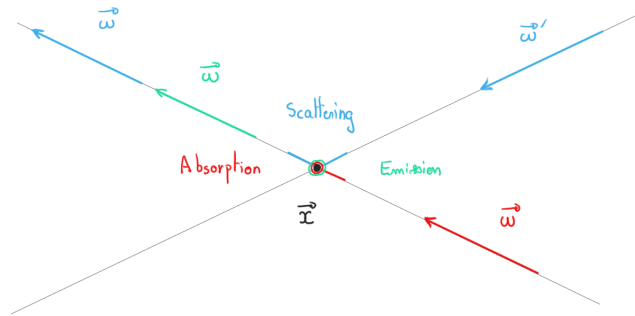


Figure 2: Sources (emission) and collisions (absorption and scattering) within the volume. The formulation of Eq. 3 favors a reciprocal/adjoint interpretation thanks to the micro-reversibility relation $p_{\Omega'}(-\vec{\omega}' | \vec{x}, -\vec{\omega}) = p_{\Omega}(\vec{\omega} | \vec{x}, \vec{\omega}')$. The physical picture then becomes that of a photon initially in direction $-\vec{\omega}$ scattered in direction $-\vec{\omega}'$.

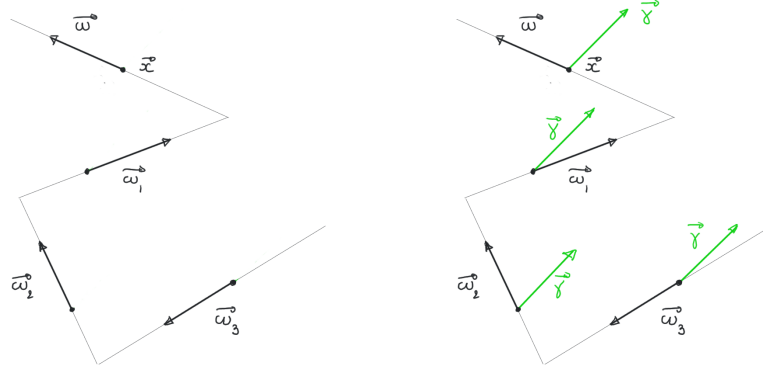


Figure 3: Left: a multiple-scattering photon trajectory leading to location \vec{x} and transport direction $\vec{\omega}$. Right: its correspondence for spatial derivatives (differentiation direction $\vec{\gamma}$). Nothing changes. The differentiation direction is preserved at each scattering event.

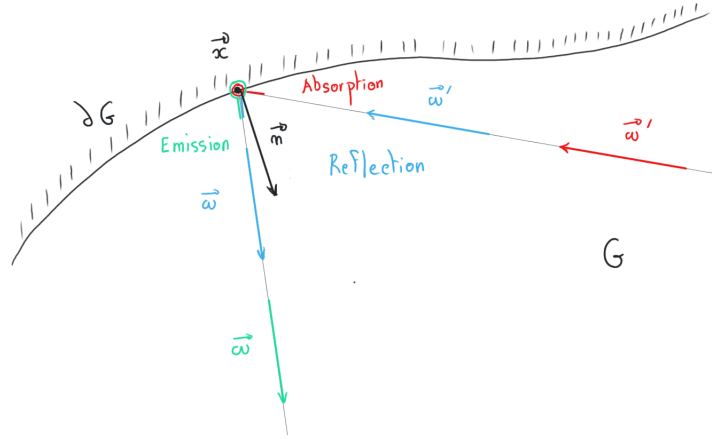


Figure 4: Sources (emission) and collisions (absorption and reflection) at the boundary. The formulation of Eq. 4 favors a reciprocal/adjoint interpretation thanks to the micro-reversibility relation $(\vec{\omega} \cdot \vec{n})\rho(\vec{x}, -\vec{\omega})p_{\Omega',b}(-\vec{\omega}'|\vec{x}, -\vec{\omega}) = -(\vec{\omega}' \cdot \vec{n})\rho(\vec{x}, \vec{\omega}')p_{\Omega,b}(\vec{\omega}|\vec{x}, \vec{\omega}')$. The physical picture then becomes that of a photon initially in direction $-\vec{\omega}$ reflected in direction $-\vec{\omega}'$.

of an opaque surface, under the assumption that the matter at this surface is in a state of local thermal equilibrium, then $S_b = (1 - \rho(\vec{x}, -\vec{\omega})) I^{eq}(T_b)$ where T_b is the local surface temperature.

Using the linearity of the collision operator, spatially differentiating equations 2 provides a transport model for $\partial_{1,\vec{\gamma}}I$:

$$\vec{\nabla}(\partial_{1,\vec{\gamma}}I) \cdot \vec{\omega} = \mathcal{C}[\partial_{1,\vec{\gamma}}I] + S_{\vec{\gamma}}[I] \quad \vec{x} \in G \quad (6)$$

with $S_{\vec{\gamma}}[I] = \partial_{1,\vec{\gamma}}\mathcal{C}[I] + \partial_{1,\vec{\gamma}}S$, leading to

$$\begin{aligned} S_{\vec{\gamma}}[I] &= -\partial_{1,\vec{\gamma}} k_a I - \partial_{1,\vec{\gamma}} k_s I \\ &+ \partial_{1,\vec{\gamma}} k_s \int_{4\pi} p_{\Omega'}(-\vec{\omega}'|\vec{x}, -\vec{\omega}) d\vec{\omega}' I(\vec{x}, \vec{\omega}') \\ &+ k_s \int_{4\pi} \partial_{1,\vec{\gamma}} p_{\Omega'}(-\vec{\omega}'|\vec{x}, -\vec{\omega}) d\vec{\omega}' I(\vec{x}, \vec{\omega}') \\ &+ \partial_{1,\vec{\gamma}}S \end{aligned} \quad (7)$$

Establishing the boundary condition for equation 6 is less straightforward because the boundary properties are attached to the boundary and spatially differentiating I in any direction α implies a differential step that is not parallel to the boundary. We retained the following approach that we believe is an essential argument when attempting to read the physics of $\partial_{1,\vec{\gamma}}I$ in pure transport terms:

- $\vec{\gamma}$ is decomposed as the sum of two vectors, one parallel to the direction of sight $\vec{\omega}$, the other parallel to a direction \vec{u} parallel to the boundary (see figure 6 and Appendix A), i.e.

$$\vec{\gamma} = \alpha\vec{\omega} + \beta\vec{u} \quad (8)$$

with

$$\alpha = \frac{\vec{\gamma} \cdot \vec{n}}{\vec{\omega} \cdot \vec{n}}; \quad \beta = \|\vec{\gamma} - \alpha\vec{\omega}\|; \quad \vec{u} = \frac{\vec{\gamma} - \alpha\vec{\omega}}{\beta} \quad \text{or} \quad \beta\vec{u} = \frac{(\vec{\omega} \wedge \vec{\gamma}) \wedge \vec{n}}{\vec{\omega} \cdot \vec{n}} \quad (9)$$

The spatial derivative in direction $\vec{\gamma}$ can then be addressed by successively considering the spatial derivative in direction $\vec{\omega}$ and the spatial derivative in direction \vec{u} :

$$\partial_{1,\vec{\gamma}}I = \alpha\partial_{1,\vec{\omega}}I + \beta\partial_{1,\vec{u}}I \quad (10)$$

- The spatial derivative in the direction of the line of sight is simply the transport term of the radiative transfer equation 2. It can therefore be replaced by field collisions and sources:

$$\partial_{1,\vec{\omega}}I = \mathcal{C}[I] + S \quad (11)$$

- The spatial derivative in a direction tangent to the boundary can finally be obtained by a straightforward differentiation of the incoming radiation equation 4:

$$\partial_{1,\vec{u}}I = \mathcal{C}_b[\partial_{1,\vec{u}}I] + \partial_{1,\vec{u}}\mathcal{C}_b[I] + \partial_{1,\vec{u}}S_b \quad (12)$$

Altogether, the boundary condition of the transport model for $\partial_{1,\vec{\gamma}}I$ is

$$\partial_{1,\vec{\gamma}}I = \beta\mathcal{C}_b[\partial_{1,\vec{u}}I] + S_b[\vec{\gamma}][I] \quad \vec{x} \in \partial G; \quad \vec{\omega} \cdot \vec{n} > 0 \quad (13)$$

with $S_b[\vec{\gamma}][I] = \alpha(\mathcal{C}[I] + S) + \beta(\partial_{1,\vec{u}}\mathcal{C}_b[I] + \partial_{1,\vec{u}}S_b)$, leading to

$$\begin{aligned} S_b[\vec{\gamma}][I] &= -\alpha k_a I - \alpha k_s I \\ &+ \alpha k_s \int_{4\pi} p_{\Omega'}(-\vec{\omega}'|\vec{x}, -\vec{\omega}) d\vec{\omega}' I(\vec{x}, \vec{\omega}') \\ &+ \alpha S \\ &+ \beta\partial_{1,\vec{u}}\rho(\vec{x}, -\vec{\omega}) \int_{\mathcal{H}'} p_{\Omega',b}(-\vec{\omega}'|\vec{x}, -\vec{\omega}) d\vec{\omega}' I(\vec{x}, \vec{\omega}') \\ &+ \beta\rho(\vec{x}, -\vec{\omega}) \int_{\mathcal{H}'} \partial_{1,\vec{u}}p_{\Omega',b}(-\vec{\omega}'|\vec{x}, -\vec{\omega}) d\vec{\omega}' I(\vec{x}, \vec{\omega}') \\ &+ \beta\partial_{1,\vec{u}}S_b \end{aligned} \quad (14)$$

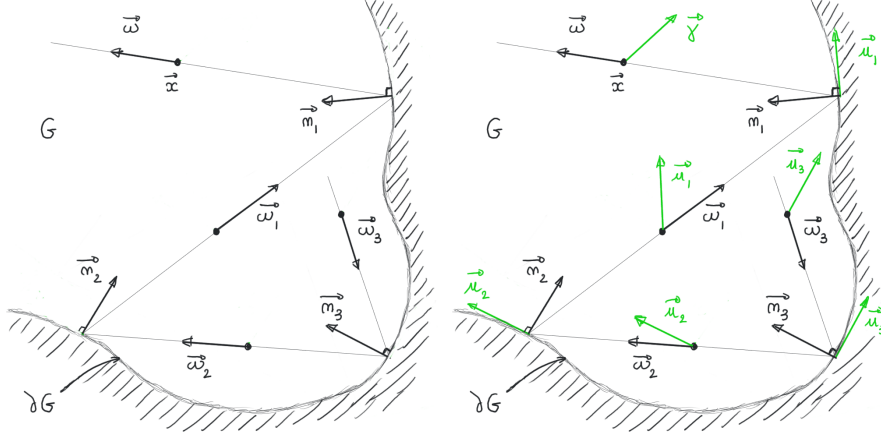


Figure 5: Left: a multiple-reflection photon trajectory leading to location \vec{x} and transport direction $\vec{\omega}$. Right: its correspondence for spatial derivatives (differentiation direction $\vec{\gamma}$). The characteristics of surface reflection are unchanged, but the differentiation direction is modified at each reflection event. Note that once again we favor a reciprocal reading of this transport physics: $\vec{\gamma}$ is transformed into \vec{u}_1 at the first reflection backward along the line of sight, then \vec{u}_1 is transformed into \vec{u}_2 at the second reflection, etc.

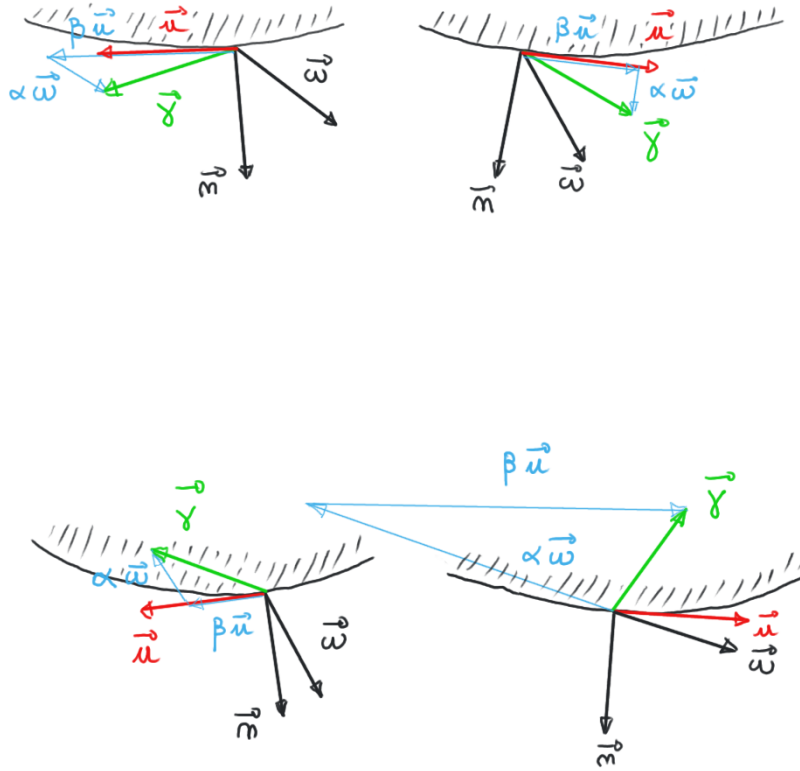


Figure 6: At the boundary, the differentiation direction $\vec{\gamma}$ is decomposed by projection along the transport direction $\vec{\omega}$ and along a unit vector \vec{u} tangent to the boundary: $\vec{\gamma} = \alpha\vec{\omega} + \beta\vec{u}$ with α that can be positive or negative and β always positive. Four configurations are illustrated. The bottom right configuration illustrates that when the transport direction is nearly tangent to the surface, then the coefficient β can take very large values. This will be an important point when discussing convergence issues for Monte Carlo simulations. β appears indeed as a factor in front of the collision operator, which is translated by the Monte Carlo weight being multiplied by β at each reflection, possibly leading to very large weight values.

The model for I was (see Eq. 2 and Eq. 4)

$$\begin{cases} \vec{\nabla} I \cdot \vec{\omega} = \mathcal{C}[I] + S & \vec{x} \in G \\ I = \mathcal{C}_b[I] + S_b & \vec{x} \in \partial G ; \vec{\omega} \cdot \vec{n} > 0 \end{cases} \quad (15)$$

The model for $\partial_{1,\vec{\gamma}} I$ is (see Eq. 6 and Eq. 13)

$$\begin{cases} \vec{\nabla} (\partial_{1,\vec{\gamma}} I) \cdot \vec{\omega} = \mathcal{C}[\partial_{1,\vec{\gamma}} I] + S_{\vec{\gamma}}[I] & \vec{x} \in G \\ \partial_{1,\vec{\gamma}} I = \beta \mathcal{C}_b[\partial_{1,\vec{u}} I] + S_{b,\vec{\gamma}}[I] & \vec{x} \in \partial G ; \vec{\omega} \cdot \vec{n} > 0 \end{cases} \quad (16)$$

The main differences are the following:

- At the boundary, the collision operator is multiplied by β , a pure geometrical quantity, function of $\vec{\omega}$, $\vec{\gamma}$ and \vec{n} , that is always positive but is not framed inside the unit interval. It can take large values when the transport direction is close to surface tangent (see Figure 6). At least this β factor cannot be interpreted as a simple modification of the surface reflectivity: at each reflection we will have to account for this multiplication factor as a additional amplification or attenuation mechanism.
- Again at the boundary, the collision operator is applied to another spatial derivative, $\partial_{1,\vec{u}} I$ instead of $\partial_{1,\vec{\gamma}} I$, i.e. a spatial derivative along a direction tangent to the boundary. In physical terms, there is still a surface reflection mechanism, with the same reflection properties, but the direction of the spatial derivative changes at each reflection (see Figure 5).
- In the standard radiative transfer model, the sources S and S_b are given quantities (functions of the volume and surface properties), but in the model for $\partial_{1,\vec{\gamma}} I$, the sources $S_{\vec{\gamma}}[I]$ and $S_{b,\vec{\gamma}}[I]$ depend on I . In pure mathematical terms, they are sources in the model for $\partial_{1,\vec{\gamma}} I$ only if this model is decoupled from the radiative transfer model. But the complete physics implies that the models are coupled: $S_{\vec{\gamma}}[I]$ and $S_{b,\vec{\gamma}}[I]$ express this coupling.

The sources $S_{\vec{\gamma}}[I]$ and $S_{b,\vec{\gamma}}[I]$ can be reformulated, depending on the configuration and the addressed question, in order to highlight a chosen set of features of spatial derivatives. Hereafter, as an example, we put forward the fact that when reaching a state of radiative equilibrium, intensity is uniform and therefore $\partial_{1,\vec{\gamma}} I$ is null whatever the derivation direction $\vec{\gamma}$: there must be no sources for $\partial_{1,\vec{\gamma}} I$. Equations 7 and 14 can be transformed the following way to help picturing this equilibrium limit:

$$\begin{aligned} S_{\vec{\gamma}}[I] &= \partial_{1,\vec{\gamma}} S - \partial_{1,\vec{\gamma}} k_a I \\ &+ \partial_{1,\vec{\gamma}} k_s \int_{4\pi} p_{\Omega'}(-\vec{\omega}'|\vec{x}, -\vec{\omega}) d\vec{\omega}' (I(\vec{x}, \vec{\omega}') - I) \\ &+ k_s \int_{4\pi} \partial_{1,\vec{\gamma}} p_{\Omega'}(-\vec{\omega}'|\vec{x}, -\vec{\omega}) d\vec{\omega}' (I(\vec{x}, \vec{\omega}') - I) \end{aligned} \quad (17)$$

and

$$\begin{aligned} S_{b,\vec{\gamma}}[I] &= \alpha (S - k_a I) \\ &+ \alpha k_s \int_{4\pi} p_{\Omega'}(-\vec{\omega}'|\vec{x}, -\vec{\omega}) d\vec{\omega}' (I(\vec{x}, \vec{\omega}') - I) \\ &+ \beta \int_{\mathcal{H}'} p_{\Omega',b}(-\vec{\omega}'|\vec{x}, -\vec{\omega}) d\vec{\omega}' (\partial_{1,\vec{u}} \rho(\vec{x}, -\vec{\omega}) I(\vec{x}, \vec{\omega}') + \partial_{1,\vec{u}} S_b) \\ &+ \beta \rho(\vec{x}, -\vec{\omega}) \int_{\mathcal{H}'} \partial_{1,\vec{u}} p_{\Omega',b}(-\vec{\omega}'|\vec{x}, -\vec{\omega}) d\vec{\omega}' (I(\vec{x}, \vec{\omega}') - I) \end{aligned} \quad (18)$$

This leaves us with three terms for $S_{\vec{\gamma}}[I]$ and four terms for $S_{b,\vec{\gamma}}[I]$:

- The first term of $S_{\vec{\gamma}}[I]$ expresses the fact that when moving along the differentiation direction $\vec{\gamma}$, if the absorption coefficient changes (k_a non-uniform) then extinction by volume absorption changes, and also if the source changes (S non-uniform) then amplification by volume sources changes. When the physical problem is compatible with equilibrium, then $S = k_a I^{eq}(T)$ and this first term of $S_{\vec{\gamma}}[I]$ becomes

$$k_a \partial_{1,\vec{\gamma}} I^{eq}(T) + \partial_{1,\vec{\gamma}} k_a (I^{eq}(T) - I) \quad (19)$$

Its physical meaning is the following: i) $k_a \partial_{1,\vec{\gamma}} I^{eq}(T)$ means that even for k_a uniform, the source may change spatially if the volume is non-isothermal; ii) as k_a is in factor of both extinction by

absorption and amplification by emission, the source associated to a non-uniform absorption coefficient is proportional to the difference $I^{eq}(T) - I$. Obviously both mechanisms vanish at equilibrium: $\partial_{1,\vec{\gamma}} I^{eq}(T) = 0$ because T is uniform and $I^{eq}(T) - I = 0$ because $I = I^{eq}(T)$. As expected, this first term (competition of volume emission and volume absorption) is null at equilibrium.

- The second term expresses the volume source associated to the competition between extinction by outgoing scattering and amplification by incoming scattering in the case of a non-uniform scattering coefficient. This expression is obtained by noting that

$$\int_{4\pi} p_{\Omega'}(-\vec{\omega}'|\vec{x}, -\vec{\omega})d\vec{\omega}' I = I \int_{4\pi} p_{\Omega'}(-\vec{\omega}'|\vec{x}, -\vec{\omega})d\vec{\omega}' = I \quad (20)$$

Again, this second term is null at equilibrium because intensity is isotropic and $I(\vec{x}, \vec{\omega}') = I$ for all $\vec{\omega}'$.

- The third term is strictly similar for non-uniform phase functions. It is obtained by observing that $\int_{4\pi} p_{\Omega'}(-\vec{\omega}'|\vec{x}, -\vec{\omega})d\vec{\omega}' = 1$ at all locations, therefore $\partial_{1,\vec{\gamma}} \int_{4\pi} p_{\Omega'}(-\vec{\omega}'|\vec{x}, -\vec{\omega})d\vec{\omega}' = 0$, or $\int_{4\pi} \partial_{1,\vec{\gamma}} p_{\Omega'}(-\vec{\omega}'|\vec{x}, -\vec{\omega})d\vec{\omega}' = 0$, leading to

$$\int_{4\pi} \partial_{1,\vec{\gamma}} p_{\Omega'}(-\vec{\omega}'|\vec{x}, -\vec{\omega})d\vec{\omega}' I = I \int_{4\pi} \partial_{1,\vec{\gamma}} p_{\Omega'}(-\vec{\omega}'|\vec{x}, -\vec{\omega})d\vec{\omega}' = 0 \quad (21)$$

- The first term of $S_{b,\vec{\gamma}}[I]$ expresses the fact that except when $\vec{\gamma}$ is strictly parallel to the surface, when moving along the differentiation direction $\vec{\gamma}$ the distance to the surface increases (if $\vec{\gamma} \cdot \vec{n} > 0$, i.e. $\alpha > 0$), which creates a new volume of emitting and absorbing medium between the current location and the surface, or the distance to the surface decreases (if $\vec{\gamma} \cdot \vec{n} < 0$, i.e. $\alpha < 0$), which suppresses some amount of emitting and absorbing medium. When the addressed radiative transfer problem is compatible with equilibrium, $S = k_a I^{eq}(T)$ and this first term of $S_{b,\vec{\gamma}}[I]$ becomes

$$\alpha k_a (I^{eq}(T) - I) \quad (22)$$

which is obviously null at the equilibrium state.

- The second term of $S_{b,\vec{\gamma}}[I]$ expresses the very same phenomenon, but as far as scattering is concerned: increase or decrease of the amount of participating medium between the current location and the surface when moving along the differentiation direction, therefore increasing or reducing the extinction by outgoing scattering as well as the amplification by incoming scattering. This second term is obtained by noting that

$$\int_{4\pi} p_{\Omega'}(-\vec{\omega}'|\vec{x}, -\vec{\omega})d\vec{\omega}' I = I \int_{4\pi} p_{\Omega'}(-\vec{\omega}'|\vec{x}, -\vec{\omega})d\vec{\omega}' = I \quad (23)$$

- The third term accounts for surfaces with a non-homogeneous reflectivity and/or a non-homogeneous surface emission. A displacement along the differentiation direction $\vec{\gamma}$ is associated to a displacement along the projected direction \vec{u} of the location where the line of sight intersects the surface. ρ and S_b are therefore spatially differentiated along \vec{u} . When the addressed radiative transfer problem is compatible with equilibrium, $S_b = (1 - \rho(\vec{x}, -\vec{\omega})) I^{eq}(T_b)$ and this third term of $S_{b,\vec{\gamma}}[I]$ becomes

$$\beta \rho(\vec{x}, -\vec{\omega}) \partial_{1,\vec{u}} I^{eq}(T_b) + \beta \partial_{1,\vec{u}} \rho(\vec{x}, -\vec{\omega}) \int_{\mathcal{H}'} p_{\Omega',b}(-\vec{\omega}'|\vec{x}, -\vec{\omega})d\vec{\omega}' (I(\vec{x}, \vec{\omega}') - I) \quad (24)$$

Its first part accounts for non-isothermal surfaces, even for uniform reflectivities. The second deals with ρ being non-uniform. At equilibrium both parts are null: T_b is uniform along the surface and intensity is isotropic ($I(\vec{x}, \vec{\omega}') = I$ for all $\vec{\omega}'$).

- The last term of $S_{b,\vec{\gamma}}[I]$ deals similarly with $p_{\Omega',b}$ non-uniform. Its expression is obtained by observing that $\int_{\mathcal{H}'} p_{\Omega',b}(-\vec{\omega}'|\vec{x}, -\vec{\omega})d\vec{\omega}' = 1$ at all locations along the surface, therefore $\partial_{1,\vec{u}} \int_{\mathcal{H}'} p_{\Omega',b}(-\vec{\omega}'|\vec{x}, -\vec{\omega})d\vec{\omega}' = 0$, or $\int_{\mathcal{H}'} \partial_{1,\vec{u}} p_{\Omega',b}(-\vec{\omega}'|\vec{x}, -\vec{\omega})d\vec{\omega}' = 0$, leading to

$$\int_{\mathcal{H}'} \partial_{1,\vec{u}} p_{\Omega',b}(-\vec{\omega}'|\vec{x}, -\vec{\omega})d\vec{\omega}' I = I \int_{\mathcal{H}'} \partial_{1,\vec{u}} p_{\Omega',b}(-\vec{\omega}'|\vec{x}, -\vec{\omega})d\vec{\omega}' = 0 \quad (25)$$

3 Boundary discontinuities at the junction of two plane surfaces

We have set up a transport model for $\partial_{1,\vec{\gamma}} I$. The corresponding source terms define the emission, in the elementary solid angle $d\vec{\omega}$ around $\vec{\omega}$ (see Figure 7),

- of any elementary volume $dv \equiv d\vec{x}$ around $\vec{x} \in G$:

$$\text{Volume emission: } S_{\vec{\gamma}}[I] dv d\vec{\omega} \quad (26)$$

- of any elementary surface $d\sigma \equiv d\vec{x}$, of normal \vec{n} , around $\vec{x} \in \partial G$

$$\text{Surface emission: } S_{b,\vec{\gamma}}[I](\vec{\omega} \cdot \vec{n}) d\sigma d\vec{\omega} \quad (27)$$

When the boundary is discrete as an ensemble of plane surfaces, typically an ensemble of triangles, then new linear emissions appear along the edge \mathcal{L}_{12} between adjacent plane surfaces ($\mathcal{S}_1, \mathcal{S}_2$). These emissions are nothing more than the extension of our previous developments to discontinuous intensities fields. The intensity in a given direction becomes discontinuous at the edge, either because the intensity sources are different on the two plane surfaces (discontinuous surface temperatures for thermal emission), or because reflection properties are different, or simply with the same reflection properties because the normals are different. In all such cases, the outgoing intensity is discontinuous when crossing the edge and this creates localised sources that require a Dirac formulation. When these Dirac sources are integrated over the surface, only the integral over the edge remains and an emission is associated to each elementary length $d\ell \equiv d\vec{x}$ around $\vec{x} \in \mathcal{L}_{12}$ (see Appendix B and Figure 7):

$$\text{Linear emission: } (\vec{\omega} \wedge \vec{\gamma}) \cdot \vec{t} (I_1 - I_2) d\ell d\vec{\omega} \quad (28)$$

where I_1 and I_2 are the two intensity values at the discontinuity and \vec{t} is a unit tangent to the edge. In this expression, the indexes 1 and 2 for the two adjacent surfaces \mathcal{S}_1 and \mathcal{S}_2 , of unit normals \vec{n}_1 and \vec{n}_2 , are chosen so that $\vec{m}_1 = \vec{t} \wedge \vec{n}_1$ is oriented toward the inside of \mathcal{S}_1 , and $\vec{m}_2 = -\vec{t} \wedge \vec{n}_2$ is oriented toward the inside of \mathcal{S}_2 (see Figure 8). As for the volume and surface sources of the preceding section, this linear source of spatial derivative is a function of intensity via its dependence on I_1 and I_2 : via its sources, the transport physics of the spatial derivative of intensity is coupled to the physics of intensity itself. Evaluating I_1 (or I_2) rises different questions depending on the sign of $\vec{\omega} \cdot \vec{n}_1$ (or $\vec{\omega} \cdot \vec{n}_2$). If $\vec{\omega} \cdot \vec{n}_1 > 0$, then I_1 is the sum of surface emission S_b and surface reflection $\mathcal{C}_b[I] = \rho(\vec{x}, -\vec{\omega}) \int_{\mathcal{S}'} p_{\Omega',b}(-\vec{\omega}'|\vec{x}, -\vec{\omega}) d\vec{\omega}' I(\vec{x}, \vec{\omega}')$, using the physical properties of \mathcal{S}_1 :

$$\begin{aligned} I_1 &= \lim_{\epsilon \rightarrow 0} I(\vec{x} + \epsilon \vec{m}_1, \vec{\omega}) \quad \text{for } \vec{\omega} \cdot \vec{n}_1 > 0 \\ &= \lim_{\epsilon \rightarrow 0} S_b(\vec{x} + \epsilon \vec{m}_1, \vec{\omega}) + \rho(\vec{x} + \epsilon \vec{m}_1, -\vec{\omega}) \int_{\mathcal{S}'} p_{\Omega',b}(-\vec{\omega}'|\vec{x} + \epsilon \vec{m}_1, -\vec{\omega}) d\vec{\omega}' I(\vec{x} + \epsilon \vec{m}_1, \vec{\omega}') \end{aligned} \quad (29)$$

If $\vec{\omega} \cdot \vec{n}_1 < 0$, then I_1 is not exiting \mathcal{S}_1 and cannot be expressed using surface emission and surface reflection: it corresponds to radiation tangential the edge, coming from the part of the system facing \mathcal{S}_1 (see Figure 9):

$$I_1 = \lim_{\epsilon \rightarrow 0} I(\vec{x} - \epsilon \vec{m}_1, \vec{\omega}) \quad \text{for } \vec{\omega} \cdot \vec{n}_1 < 0 \quad (30)$$

Anticipating Monte Carlo discussions, we need to emphasize that these linear emissions are the result of surface integrations over the boundary of a Dirac sources. This implies that when a Dirac source at \vec{x} is viewed from a point \vec{x}_{obs} at distance r , i.e. $\vec{x}_{obs} = \vec{x} + r\vec{\omega}$, the surface integration comes from the angular integration (see Figure 10). A typical formulation is therefore the following. At \vec{x}_{obs} , let us consider a solid angle Ω under which a subpart of the boundary ∂G is viewed, noted ∂G^Ω , including a subpart of the edge \mathcal{L}_{12} , noted \mathcal{L}_{12}^Ω . If we address the integration over Ω of the surface sources as they are viewed from \vec{x}_{obs} (temporarily ignoring extinction by absorption and scattering), each elementary solid angle $d\omega$ defines an elementary surface $d\sigma$ at the boundary according to $d\omega = \frac{(\vec{\omega} \cdot \vec{n}) d\sigma}{r^2}$ and the angular integration becomes

$$\int_{\Omega} \partial_{1,\vec{\gamma}} I(\vec{x}_{obs}, \vec{\omega}) d\omega = \int_{\partial G^\Omega} \frac{(\vec{\omega} \cdot \vec{n})}{r^2} (\beta \mathcal{C}_b[\partial_{1,\vec{u}} I] + S_{b,\vec{\gamma}}[I]) d\sigma + \int_{\mathcal{L}_{12}^\Omega} \frac{(\vec{\omega} \wedge \vec{\gamma}) \cdot \vec{t}}{r^2} (I_1 - I_2) d\ell \quad (31)$$

4 Path statistics and Monte Carlo

Notice: This is a preliminary version of the final paper, consequently the reader might find some missing parts, especially in the results section where some of the pseudo-algorithms and results tables are not included in this current version.

Our main point in this text is that the model of the spatial derivative of intensity resemble so much the model of intensity (the radiative transfer model) that the whole radiative transfer literature about path statistics

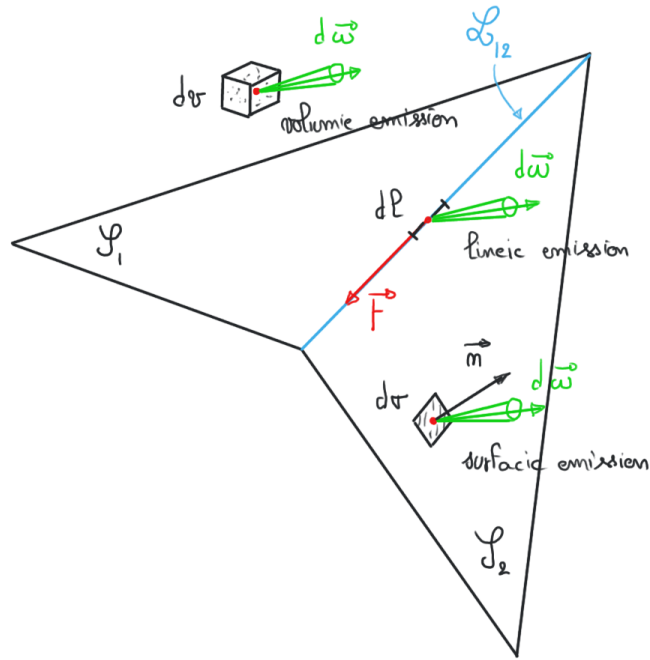


Figure 7: Volume, surface and linear emissions of spatial derivatives.

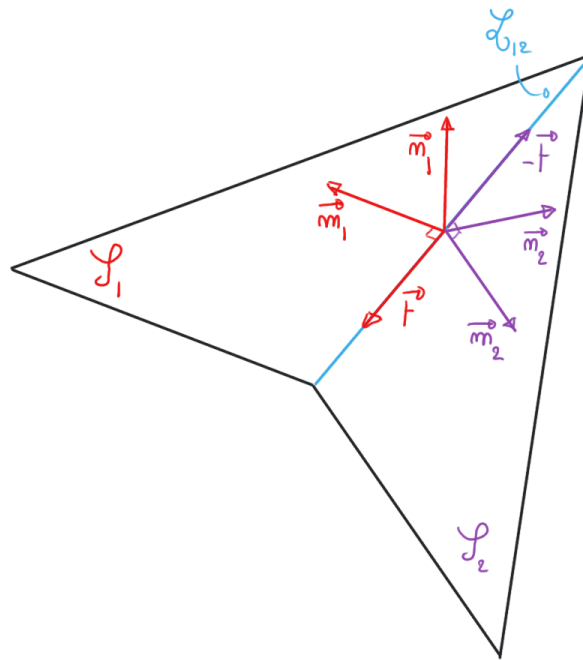


Figure 8: The unit vectors attached to \mathcal{S}_1 and \mathcal{S}_2 at the edge \mathcal{L}_{12} . They form two direct orthonormal basis: $(\vec{m}_1, \vec{t}, \vec{n}_1)$ and $(\vec{m}_2, -\vec{t}, \vec{n}_2)$.

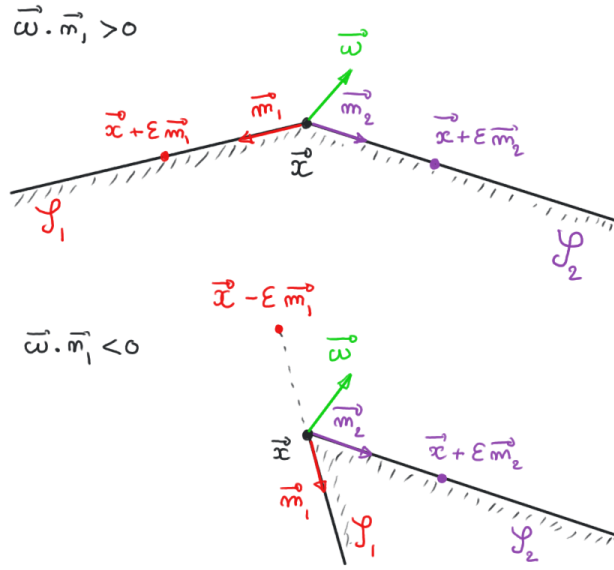


Figure 9: The two limit values of intensity, I_1 and I_2 , at the edge \mathcal{L}_{12} between \mathcal{S}_1 and \mathcal{S}_2 . Top: $\vec{\omega} \cdot \vec{n}_1 > 0$ and $\vec{\omega} \cdot \vec{n}_2 > 0$; both I_1 and I_2 are the limits of the intensity exiting the corresponding surface when reaching the edge: $I_1 = \lim_{\epsilon \rightarrow 0} I(\vec{x} + \epsilon \vec{m}_1, \vec{\omega})$ and $I_2 = \lim_{\epsilon \rightarrow 0} I(\vec{x} + \epsilon \vec{m}_2, \vec{\omega})$. Bottom: $\vec{\omega} \cdot \vec{n}_1 < 0$ and $\vec{\omega} \cdot \vec{n}_2 > 0$; I_2 is the limits of the intensity exiting \mathcal{S}_2 when reaching the edge, but I_1 corresponds to the intensity within the volume, tangencing the edge: $I_1 = \lim_{\epsilon \rightarrow 0} I(\vec{x} - \epsilon \vec{m}_1, \vec{\omega})$ and $I_2 = \lim_{\epsilon \rightarrow 0} I(\vec{x} + \epsilon \vec{m}_2, \vec{\omega})$

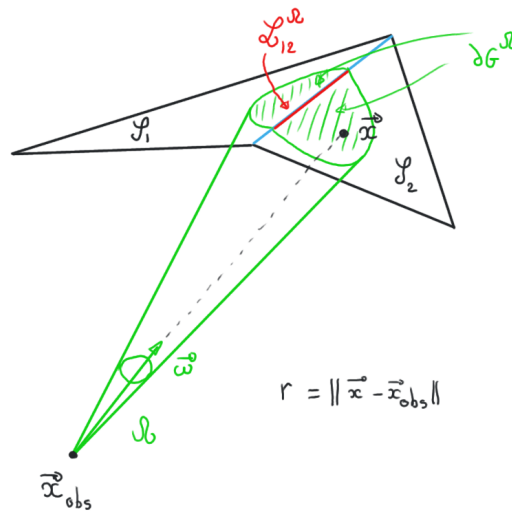


Figure 10: Surface and linear sources viewed from a distant point \vec{x}_{obs} within a solid angle Ω .

and Monte Carlo simulation can be reinvested in a straightforward manner to numerical estimate spatial derivatives. In this last section, we illustrate the practical meaning of this statement. The technical steps that we will highlight with some specificity are the following:

- As already mentioned, at each reflection event the projection factor β needs to be stored and the differentiation direction is changed (see Figure 5). Such a state change at reflection events leads to algorithmic steps that are very similar to those of the Monte Carlo algorithms designed for polarized radiation (note that here nothing similar occurs at scattering events).
- Via the volume, surface and linear sources of spatial derivatives, that depend on intensity, the model of spatial derivatives is coupled to the radiative transfer model. This coupling can be handled using the very same Monte Carlo techniques as those recently developed for the coupling of radiative transfer with other heat-transfer modes[2, 3, 4, 5], or the coupling of radiative transfer with electromagnetism and photosynthesis[6, 7, 8, 9]. In both cases, the main idea is double randomisation: in standard Monte Carlo algorithms for pure radiative transfer, when a volume source or a surface source is required it is known (typically the temperature is known for infrared radiative transfer); if it is not known but a Monte Carlo algorithm is available to numerically estimate the source as an average of a large number of sampled Monte Carlo weights, then in the coupled problem the source can be replaced by only one sample. The resulting coupled algorithm is rigorously unbiased thanks to the law of expectation (“the expectation of an expectation is an expectation”). In practice, this means that the Monte Carlo algorithms estimating spatial derivatives can be designed as if the sources were known, and when a source is required that depends on $I(\vec{x}', \vec{\omega}')$ then one single radiative path is sampled as if estimating the intensity $I(\vec{x}', \vec{\omega}')$ with any available Monte Carlo algorithm.
- The linear sources need a specific treatment otherwise they would be missed by the standard algorithms integrating over surfaces or solid angles. This can be achieved using the techniques developed to handle collimated Dirac sources for solar/laser applications[10, 11, 12, 13, 14] or satellite observation: at each reflection or scattering event, the directions of the Dirac sources are first sampled, specifically, before continuing the path in another sampled reflected or scattered direction.

We provide hereafter some examples of algorithms that illustrate these three points. They estimate either $\partial_{1,\vec{\gamma}}I$ at a location \vec{x} in a direction $\vec{\omega}$, or the spatial derivative of the incident flux density φ at a location \vec{x} on a surface of unit normal \vec{n} , i.e. $\partial_{\vec{\gamma}}\varphi = \int_{2\pi}(\vec{\omega} \cdot \vec{n}) \partial_{1,\vec{\gamma}}I(\vec{x}, -\vec{\omega}) d\vec{\omega}$. Each example is implemented and tested against exact solutions (see Fig. 11):

- Solution 1: the solution provided by Chandrasekhar for a uniform flux in a stratified heterogeneous scattering atmosphere[15] (see Appendix C). This one-dimension solution is cut by a three-dimension closed boundary (a sphere or a cube) and the boundary conditions are adjusted to insure that Chandrasekhar’s solution is still satisfied. In Chandrasekhar’s solution, there is no volume absorption; when we need to add volume absorption, we compensate it by introducing an adjusted volume emission insuring that Chandrasekhar’s solution is again still satisfied.
- Solution 2: a transparent slab between a black isothermal surface at T_{hot} and an emitting/reflecting diffuse surface of temperature T_{cold} everywhere except for a square subsurface where the temperature is T_{hot} ;

These algorithms sample Monte Carlo weights noted w_Z for each quantity Z , meaning that N samples $w_{Z,1}, w_{Z,2} \dots w_{Z,N}$ are required to estimate Z as $\tilde{Z} = \frac{1}{N} \sum_{i=1}^N w_{Z,i}$,

- w_I for the intensity I when referring to a standard Monte Carlo algorithm estimating the solution of the radiative transfer equation;
- $w_{\partial_{1,\vec{\gamma}}I}$ for the spatial derivative of intensity;
- $w_{\partial_{\vec{\gamma}}\varphi}$ for the spatial derivative of the incident flux density.

4.1 Emissive surfaces, no reflection, uniform scattering, no volume absorption, no volume emission

Convex domain with differentiable boundaries The intensity I and its spatial derivative $\partial_{1,\vec{\gamma}}I$ are estimated at location \vec{x}_{obs} and direction $\vec{\omega}_{obs}$ as described in Fig. 11. The geometrical configuration is a sphere, which center is located at $\vec{x} \cdot \vec{e}_3 = 0$, inserted into an infinite scattering medium. The scattering coefficient k_s lead to the optical thickness $\tau = k_s \vec{x} \cdot \vec{e}_1$. In this example there is no volume absorption ($k_a = 0$)

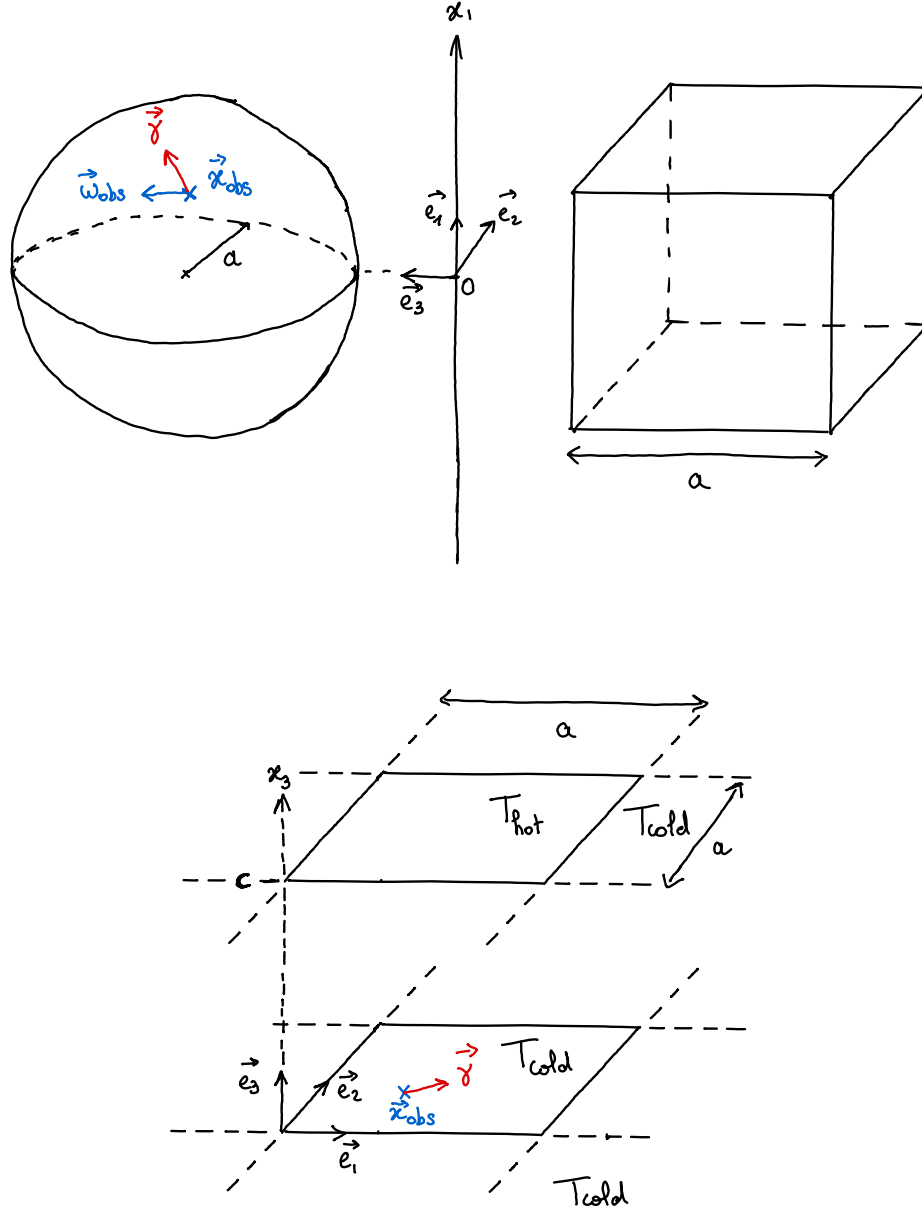


Figure 11: The two configurations used for illustration. Top: the solution provided by Chandrasekhar for a uniform flux in a stratified heterogeneous scattering atmosphere cut by a three-dimension closed boundary (a sphere of radius a or a cube of side a). Bottom: a transparent slab of thickness c between a black isothermal surface at T_{hot} and an emitting/reflecting diffuse surface of temperature T_{cold} everywhere except for a square subsurface of side a where the temperature is T_{hot} . The emissivity ϵ of the emitting/reflecting diffuse surface is uniform.

and no volume emission. The radiative configuration is built so that Chandrasekhar's analytical solution \mathcal{L} (Appendix. C) apply at any $(\vec{x}, \vec{\omega})$. Therefore, the sphere volume has the same properties than the rest of the infinite medium and the sphere surface is considered as a black body with boundary conditions set in Eq. 32 as Chandrasekhar's solution \mathcal{L} for each position on the sphere boundary $\vec{x} \in \partial G$ and each $\vec{\omega} \cdot \vec{n} > 0$.

$$I = S_b = \mathcal{L}(\vec{x}, \vec{\omega}) \quad \vec{x} \in \partial G; \vec{\omega} \cdot \vec{n} > 0 \quad (32)$$

The intensity Monte-Carlo weight w_I sampling is detailed in Algorithm 16 and the resulting intensity estimated by Monte-Carlo at $(\vec{x}_{obs}, \vec{\omega}_{obs})$ is compared to the analytical solution $\mathcal{L}(\vec{x}_{obs}, \vec{\omega}_{obs})$ in Fig. 12 and table (the table is not included in the current state of the paper). The spatial derivative $w_{\partial_{1,\vec{\gamma}}I}$ weight sampling is detailed in Algorithm 23 and the resulting spatial derivative estimated by Monte-Carlo at $(\vec{x}_{obs}, \vec{\omega}_{obs})$ is compared to the analytical solution $\partial_{1,\vec{\gamma}}\mathcal{L}(\vec{x}_{obs}, \vec{\omega}_{obs})$ in Fig. 12 and table (the table is not included in the current state of the paper).

Supplementary informations on the algorithms and the spatial derivative boundary conditions will be found in Appendix. E.1.

Boundary discontinuities The density flux φ and its spatial derivative $\partial_{1,\vec{\gamma}}\varphi$ are estimated at location \vec{x}_{obs} as described in Fig. 11. The geometric configuration is composed by two parallel planes, the lower plane (∂G_{bottom}) is modelled as a black body at temperature T_{cold} and the upper plane ∂G_{top} as a black body at temperature T_{hot} in a square surface \mathcal{S}_{hot} and T_{cold} outside the square surface. The observation position is located on the lower plane so that we aim to estimate the flux density outgoing the lower plane. The analytical solution of the flux density in this configuration is stated in Appendix. D and will be compared with the Monte-Carlo estimations of the flux density and its spatial gradient.

The flux density is solved by sampling w_φ (see Algorithm 4) and results are compared to analytical solution in Fig. 13 and table (the table is not included in the current state of the paper). The spatial derivative of the flux density is solved by sampling $w_{\partial_{1,\vec{\gamma}}\varphi}$ (see Algorithm 15) and results are presented in Fig. 13 and compared with the analytical solution.

Supplementary informations on the algorithms and the spatial derivative boundary conditions will be found in Appendix. E.1.

4.2 Emissive and reflective surfaces, uniform scattering, no volume absorption, no volume emission

Convex domain with differentiable boundaries The intensity I and its spatial derivative $\partial_{1,\vec{\gamma}}I$ are estimated at location \vec{x}_{obs} and direction $\vec{\omega}_{obs}$ as described in Fig. 11. The geometrical configuration is the same as in Sec. 4.1: a sphere, which center is located at $\vec{x} \cdot \vec{e}_3 = 0$, inserted into an infinite scattering medium. Again the radiative configuration is built so that Chandrasekhar's analytical solution \mathcal{L} apply at any $(\vec{x}, \vec{\omega})$. The only difference with Sec. 4.1 is that this time the sphere boundaries are looked at as emissive and reflective (diffuse) surfaces with reflection coefficient $\rho = 0.6$ and reflection probability density function $p_{\Omega',b}(-\vec{\omega}'|\vec{x}, -\vec{\omega}) = \frac{\vec{\omega} \cdot \vec{n}}{\pi}$. To ensure that Chandrasekhar's analytical solution still apply in this configuration the reflection term of the boundary condition will be compensated by the emission (surface source S_b) part. Intensity boundary conditions are stated in Eq. 4 with \mathcal{C}_b the collisional operator of the radiative boundary conditions ($\vec{x} \in \partial G; \vec{\omega} \cdot \vec{n} > 0$):

$$\mathcal{C}_b[I] = \rho \int_{\mathcal{H}'} p_{\Omega',b}(-\vec{\omega}'|\vec{x}, -\vec{\omega}) d\vec{\omega}' I(\vec{x}, \vec{\omega}') \quad (33)$$

and S_b the surface source

$$S_b = \mathcal{L}(\vec{x}, \vec{\omega}) - \mathcal{C}_b[\mathcal{L}(\vec{x}, \vec{\omega})] \quad (34)$$

that will account for the intensity coming out of the sphere surface (Chandrasekhar's solution \mathcal{L}) and the compensation term $\mathcal{C}_b[\mathcal{L}]$. Note that the surface source S_b is supposed to be known and is a function of the analytical solution \mathcal{L} whereas the reflected part of the boundary condition is considered as a function of the unknown incoming intensity.

The intensity spatial derivative is solved by sampling the Monte-Carlo weight $w_{\partial_{1,\vec{\gamma}}I,r}$ (the pseudo-algorithm is not included in the paper at this stage). The results obtained for the spatial derivative of the intensity at $(\vec{x}_{obs}, \vec{\omega}_{obs})$ are presented in Fig. 14 and compared with the analytical solution.

Supplementary informations on the algorithms and the spatial derivative boundary conditions will be found in Appendix. E.2.

Boundary discontinuities The flux density φ and its spatial derivative $\partial_{1,\vec{\gamma}}\varphi$ are estimated at location \vec{x}_{obs} as described in Fig. 11. The geometric configuration is identical to Sec. 4.1 slab configuration. The medium between the two parallel planes is still transparent and the bottom plane surface is still a black body at cold temperature. However, this time the top plane is an emissive and reflective (diffuse) surface at temperature T_{hot} in a square surface \mathcal{S}_{hot} and T_{cold} outside the square surface. The reflection coefficient and the reflection probability density function are homogeneous along the plane and stated as $\rho = 0.6$ and $p_{\Omega',b}(-\vec{\omega}'|\vec{x}, -\vec{\omega}) = \frac{\vec{\omega}' \cdot \vec{n}_{top}}{\pi}$.

The flux density is solved by sampling $w_{\varphi,r}$ (the algorithm is not included in the paper at this stage) and results are compared to analytical solution in Fig. 15 and table (the table is not included in the current state of the paper). The flux density spatial derivative is solved by sampling $w_{\partial_{1,\vec{\gamma}}\varphi,r}$ (pseudo-algorithm is not included in the current state of the paper). Results of the flux density (and its spatial derivative) estimations are presented in Fig. 15 and compared with the analytical solution.

Supplementary informations on the algorithms and the spatial derivative boundary conditions will be found in Appendix. E.2.

4.3 Emissive surfaces, no reflection, non-uniform scattering, non-uniform volume absorption, non-uniform volume emission

Convex domain with differentiable boundaries The intensity I and its derivative $\partial_{1,\vec{\gamma}}I$ are estimated at location \vec{x}_{obs} and direction $\vec{\omega}_{obs}$ as described in Fig. 11. The geometrical and radiative configurations are identical to Sec. 4.1: a sphere which surface is considered as a black body with the Chandrasekhar solution \mathcal{L} as emitted intensity. The only difference here is that the scattering properties of the infinite medium and sphere volume change: the scattering coefficient field is now non-uniform and is stated as $k_s = k_0 \exp(k_1 \vec{x} \cdot \vec{e}_3)$. The optical thickness is then $\tau = \frac{k_0}{k_1} (\exp(k_1 \vec{x} \cdot \vec{e}_1) - 1)$. Volume emission and absorption are not considered in the current state of the paper. With this example we illustrate how non-uniform scattering will impact the Monte-Carlo algorithm used to solve the spatial derivative.

The results of spatial gradient estimation at $(\vec{x}_{obs}, \vec{\omega}_{obs})$ are presented in Fig. 16 and compared with the analytical solution.

Supplementary informations on the algorithms and the spatial derivative boundary conditions will be found in Appendix. E.3.

Boundary discontinuities In the present state of the paper this configuration is not described.

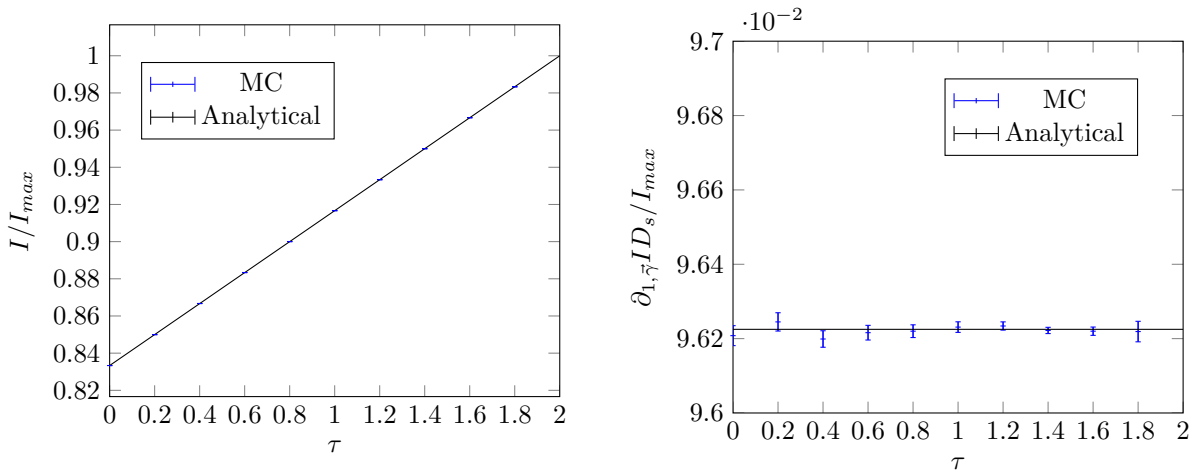


Figure 12: Monte-Carlo estimations and analytical solutions for the intensity (*left*) and its spatial derivative in the direction $\vec{\gamma} = (\frac{1}{\sqrt{3}}, \frac{1}{\sqrt{3}}, \frac{1}{\sqrt{3}})$ (*right*). The corresponding configuration is described in Sec. 4.1: a convex domain with differentiable boundaries (the sphere in Fig. 11) and emissive surfaces. Intensity and its derivative are estimated at optical thickness $\tau = k_s \vec{x}_{obs} \cdot \vec{e}_1$ and in the direction $\vec{\omega}_{obs} = (0, 0, 1)$. Monte-Carlo number of sampling is $N = 10^8$, the sphere diameter $D_s = 1\text{m}$.

Algorithm 1: Sample the Monte Carlo weight w_I for domains of any shape, with emissive surfaces, no reflection, uniform scattering, no volume absorption and no volume emission.

```

1 Initialize  $\vec{x}$  and  $\vec{\omega}$ ;
2 Reverse the direction:  $\vec{\omega} \leftarrow -\vec{\omega}$ ;
3 Set intersection to False;
4 while intersection = False do
5   Sample a scattering free path  $\ell$  according to  $p(\ell) = k_s \exp(-k_s \ell)$ ;
6   Find the distance  $\ell_b$  to the boundary from  $\vec{x}$  in direction  $\vec{\omega}$ ;
7   if  $\ell < \ell_b$  then
8      $\vec{x} \leftarrow \vec{x} + \ell \vec{\omega}$ ;
9     Sample  $\vec{\omega}_s$  according to  $p_\Omega(\vec{\omega}_s | \vec{x}, \vec{\omega})$ ;
10     $\vec{\omega} \leftarrow \vec{\omega}_s$ ;
11  else
12     $\vec{x} \leftarrow \vec{x} + \ell_b \vec{\omega}$ ;
13    intersection  $\leftarrow$  True;
14     $w_I \leftarrow S_b(\vec{x}, -\vec{\omega})$ ;
15  end
16 end

```

Algorithm 2: Sample the Monte Carlo weight $w_{\partial_1, \vec{\gamma} I}$ for a convex domain with differentiable boundaries, emissive surfaces, no reflection, uniform scattering, no volume absorption and no volume emission.

```

1 Initialize  $\vec{x}$  and  $\vec{\omega}$ ;
2 Reverse the direction:  $\vec{\omega} \leftarrow -\vec{\omega}$ ;
3 Set intersection to False;
4 while intersection = False do
5   Sample a scattering free path  $\ell$  according to  $p(\ell) = k_s \exp(-k_s \ell)$ ;
6   Find the distance  $\ell_b$  to the boundary from  $\vec{x}$  in direction  $\vec{\omega}$ ;
7   if  $\ell < \ell_b$  then
8      $\vec{x} \leftarrow \vec{x} + \ell \vec{\omega}$ ;
9     Sample  $\vec{\omega}_s$  according to  $p_\Omega(\vec{\omega}_s | \vec{x}, \vec{\omega})$ ;
10     $\vec{\omega} \leftarrow \vec{\omega}_s$ ;
11  else
12     $\vec{x} \leftarrow \vec{x} + \ell_b \vec{\omega}$ ;
13    intersection  $\leftarrow$  True;
14    Compute  $\alpha$ ,  $\beta$  and  $\vec{u}$  for the transport direction  $-\vec{\omega}$ ;
15    Sample  $\vec{\omega}_s$  according to  $p_\Omega(\vec{\omega}_s | \vec{x}, \vec{\omega})$ ;
16    if  $\vec{\omega}_s \cdot \vec{n} < 0$  then
17       $w_{\partial_1, \vec{\gamma} I} \leftarrow \alpha(S_b(\vec{x}, -\vec{\omega}_s) - S_b(\vec{x}, -\vec{\omega})) + \beta \partial_{1, \vec{u}} S_b(\vec{x}, -\vec{\omega})$ ;
18    else
19      Sample  $w_I$  for  $\vec{x}$  and  $-\vec{\omega}_s$  using Algorithm 1;
20       $w_{\partial_1, \vec{\gamma} I} \leftarrow \alpha(w_I - S_b(\vec{x}, -\vec{\omega})) + \beta \partial_{1, \vec{u}} S_b(\vec{x}, -\vec{\omega})$ ;
21    end
22  end
23 end

```

Algorithm 3: Sample the Monte Carlo weight w_φ for a convex domain with differentiable boundaries, emissive surfaces, no reflection, uniform scattering, no volume absorption and no volume emission.

```

1 Initialize  $\vec{x}$  and  $\vec{n}$ ;
2 sample  $\vec{\omega}$  according to a Lambert distribution around  $\vec{n}$  (i.e.  $p(\vec{\omega}) = \frac{\vec{\omega} \cdot \vec{n}}{\pi}$ );
3 Sample  $w_I$  for  $\vec{x}$  and  $-\vec{\omega}$  using Algorithm 16;
4  $w_\varphi \leftarrow \pi w_I$ ;

```

Algorithm 4: Sample the Monte Carlo weight $w_{\partial_{\vec{\gamma}}\varphi}$ for a convex domain with differentiable boundaries, emissive surfaces, no reflection, uniform scattering, no volume absorption and no volume emission.

- 1 Initialize \vec{x} and \vec{n} ;
 - 2 sample $\vec{\omega}$ according to a Lambert distribution around \vec{n} (i.e. $p(\vec{\omega}) = \frac{\vec{\omega} \cdot \vec{n}}{\pi}$);
 - 3 Sample $w_{\partial_{1,\vec{\gamma}}I}$ for \vec{x} and $-\vec{\omega}$ using Algorithm 2;
 - 4 $w_{\partial_{\vec{\gamma}}\varphi} \leftarrow \pi w_{\partial_{1,\vec{\gamma}}I}$;
-

Algorithm 5: Sample the Monte Carlo weight $w_{\partial_{1,\vec{\gamma}}I}$ for a closed cavity composed of adjacent plane surfaces with emissive surfaces, no reflection, uniform scattering, no volume absorption and no volume emission.

- 1 Initialize \vec{x} and $\vec{\omega}$;
 - 2 Reverse the direction: $\vec{\omega} \leftarrow -\vec{\omega}$;
 - 3 Set *intersection* to *False*;
 - 4 Set $w_{\partial_{1,\vec{\gamma}}I}$ to 0;
 - 5 **while** *intersection* = *False* **do**
 - 6 Sample a scattering free path ℓ according to $p(\ell) = k_s \exp(-k_s \ell)$;
 - 7 Find the distance ℓ_b to the boundary from \vec{x} in direction $\vec{\omega}$;
 - 8 **if** $\ell < \ell_b$ **then**
 - 9 $\vec{x} \leftarrow \vec{x} + \ell \vec{\omega}$;
 - 10 Uniformly sample a location \vec{y} on the edges of total length L_{edges} ;
 - 11 Trace a ray from \vec{x} to \vec{y} and check if there is an intermediate surface is intersected;
 - 12 **if** No intermediate surface is detected **then**
 - 13 Compute the unit vector \vec{t} tangent to the edge at \vec{y} (its orientation defines which of the two adjacent surfaces is labeled \mathcal{S}_1 and \mathcal{S}_2);
 - 14 Compute the unit vector $\vec{\omega}_s$ from \vec{x} to \vec{y} ;
 - 15 Compute the distance r from \vec{x} to \vec{y} ;
 - 16 Get $S_b(\vec{y}, -\vec{\omega}_s)$ for each of the two adjacent surfaces ($S_{b,1}(\vec{y}, -\vec{\omega}_s)$ for \mathcal{S}_1 and $S_{b,2}(\vec{y}, -\vec{\omega}_s)$ for \mathcal{S}_2);
 - 17 $w_{\partial_{1,\vec{\gamma}}I} \leftarrow w_{\partial_{1,\vec{\gamma}}I} + L_{edges} p_{\Omega}(\vec{\omega}_s | \vec{x}, \vec{\omega}) \frac{(\vec{\omega} \wedge \vec{\gamma}) \cdot \vec{t}}{r^2} [S_{b,1}(\vec{y}, -\vec{\omega}_s) - S_{b,2}(\vec{y}, -\vec{\omega}_s)] \exp(-k_s r)$;
 - 18 **end**
 - 19 Sample $\vec{\omega}_s$ according to $p_{\Omega}(\vec{\omega}_s | \vec{x}, \vec{\omega})$;
 - 20 $\vec{\omega} \leftarrow \vec{\omega}_s$;
 - 21 **else**
 - 22 $\vec{x} \leftarrow \vec{x} + \ell_b \vec{\omega}$;
 - 23 *intersection* $\leftarrow True$;
 - 24 Compute α , β and \vec{u} for the transport direction $-\vec{\omega}$;
 - 25 Sample $\vec{\omega}_s$ according to $p_{\Omega}(\vec{\omega}_s | \vec{x}, \vec{\omega})$;
 - 26 **if** $\vec{\omega}_s \cdot \vec{n} < 0$ **then**
 - 27 $w_{\partial_{1,\vec{\gamma}}I} \leftarrow w_{\partial_{1,\vec{\gamma}}I} + \alpha k_s (S_b(\vec{x}, -\vec{\omega}_s) - S_b(\vec{x}, -\vec{\omega})) + \beta \partial_{1,\vec{u}} S_b(\vec{x}, -\vec{\omega})$;
 - 28 **else**
 - 29 Sample w_I for \vec{x} and $-\vec{\omega}_s$ using Algorithm 1;
 - 30 $w_{\partial_{1,\vec{\gamma}}I} \leftarrow w_{\partial_{1,\vec{\gamma}}I} + \alpha k_s (w_I - S_b(\vec{x}, -\vec{\omega})) + \beta \partial_{1,\vec{u}} S_b(\vec{x}, -\vec{\omega})$;
 - 31 **end**
 - 32 **end**
 - 33 **end**
-

Algorithm 6: Sample the Monte Carlo weight $w_{\partial_{\vec{\gamma}}\varphi}$ for a closed cavity composed of adjacent plane surfaces with emissive surfaces, no reflection, uniform scattering, no volume absorption and no volume emission.

```

1 Initialize  $\vec{x}$  and  $\vec{n}$ ;
2 set  $w_{\partial_{\vec{\gamma}}\varphi}$  to 0;
3 Find the edges potentially visible from  $\vec{x}$  and compute their total length  $L_{edges}$ ;
4 Uniformly sample a location  $\vec{y}$  on the edges;
5 Trace a ray from  $\vec{x}$  to  $\vec{y}$  and check if there is an intermediate surface is intersected;
6 if No intermediate surface is detected then
7   Compute the unit vector  $\vec{t}$  tangent to the edge at  $\vec{y}$  (its orientation defines which of the two adjacent
   surfaces is labeled  $\mathcal{S}_1$  and  $\mathcal{S}_2$ );
8   Compute the unit vector  $\vec{\omega}_s$  from  $\vec{x}$  to  $\vec{y}$ ;
9   Compute the distance  $r$  from  $\vec{x}$  to  $\vec{y}$ ;
10  Get  $S_b(\vec{y}, -\vec{\omega}_s)$  for each of the two adjacent surfaces ( $S_{b,1}(\vec{y}, -\vec{\omega}_s)$  for  $\mathcal{S}_1$  and  $S_{b,2}(\vec{y}, -\vec{\omega}_s)$  for  $\mathcal{S}_2$ );
11   $w_{\partial_{\vec{\gamma}}\varphi} \leftarrow w_{\partial_{\vec{\gamma}}\varphi} + L_{edge}(\vec{\omega} \cdot \vec{n}) \frac{(\vec{\omega} \wedge \vec{\gamma}) \cdot \vec{t}}{r^2} [S_{b,1}(\vec{y}, -\vec{\omega}_s) - S_{b,2}(\vec{y}, -\vec{\omega}_s)] \exp(-k_s r)$ ;
12 end
13 sample  $\vec{\omega}$  according to a Lambert distribution around  $\vec{n}$  (i.e.  $p(\vec{\omega}) = \frac{\vec{\omega} \cdot \vec{n}}{\pi}$ );
14 Sample  $w_{\partial_{1,\vec{\gamma}}I}$  for  $\vec{x}$  and  $-\vec{\omega}$  using Algorithm 5;
15  $w_{\partial_{\vec{\gamma}}\varphi} \leftarrow w_{\partial_{\vec{\gamma}}\varphi} + \pi w_{\partial_{1,\vec{\gamma}}I}$ ;

```

Algorithm 7: Sample the Monte Carlo weight $w_{I,r}$ for domains of any shape, with diffuse surfaces (emission and diffuse reflection), uniform scattering, no volume absorption and no volume emission.

```

1 Initialize  $\vec{x}$  and  $\vec{\omega}$ ;
2 Reverse the direction:  $\vec{\omega} \leftarrow -\vec{\omega}$ ;
3 Set stop_criterion to 1;
4 Set  $w_{I,r}$  to 0;
5 while stop_criterion > 0.1 do
6   Set intersection to False;
7   while intersection = False do
8     Sample a scattering free path  $\ell$  according to  $p(\ell) = k_s \exp(-k_s \ell)$ ;
9     Find the distance  $\ell_b$  to the boundary from  $\vec{x}$  in direction  $\vec{\omega}$ ;
10    if  $\ell < \ell_b$  then
11       $\vec{x} \leftarrow \vec{x} + \ell \vec{\omega}$ ;
12      Sample  $\vec{\omega}_s$  according to  $p_{\Omega}(\vec{\omega}_s | \vec{x}, \vec{\omega})$ ;
13       $\vec{\omega} \leftarrow \vec{\omega}_s$ ;
14    else
15       $\vec{x} \leftarrow \vec{x} + \ell_b \vec{\omega}$ ;
16      intersection  $\leftarrow$  True;
17       $w_{I,r} \leftarrow w_{I,r} + \text{stop\_criterion} \times S_b(\vec{x}, -\vec{\omega})$ ;
18      stop_criterion  $\leftarrow$  stop_criterion  $\times \rho$ ;
19      Sample  $\vec{\omega}$  according to  $p_{\Omega,b}(-\vec{\omega} | \vec{x}, -\vec{\omega}_s)$ ;
20    end
21  end
22 end

```

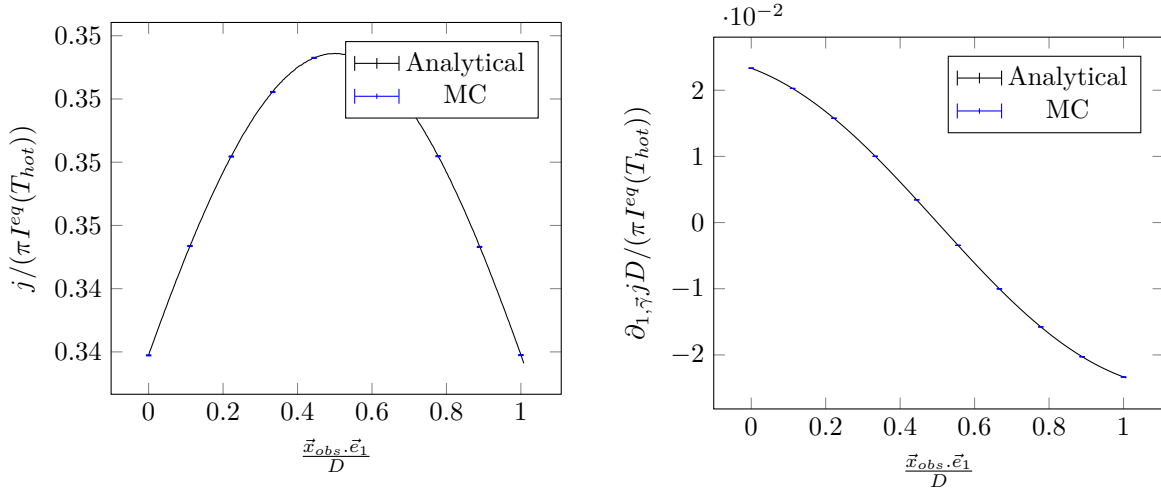


Figure 13: Monte-Carlo estimations and analytical solutions for the radiative flux j (left) and its spatial derivative $\partial_{1,\vec{\gamma}}j$ in the direction $\vec{\gamma} = (\frac{1}{\sqrt{2}}, \frac{1}{\sqrt{2}}, 0)$ (right). The corresponding configuration is described in Sec. 4.1: a convex domain with boundary discontinuity between emissive surfaces at different temperatures (top plane of the slab geometry described in Fig. 11). The radiative flux and its derivative are estimated at the position \vec{x}_{obs} such as $\frac{\vec{x}_{obs} \cdot \vec{e}_1}{D} = \frac{\vec{x}_{obs} \cdot \vec{e}_2}{D}$ and $\vec{x}_{obs} \cdot \vec{e}_3 = 0$. Monte-Carlo number of samplings is $N = 10^9$, the top hot square dimensions are $D \times D$ with $D = 2m$.

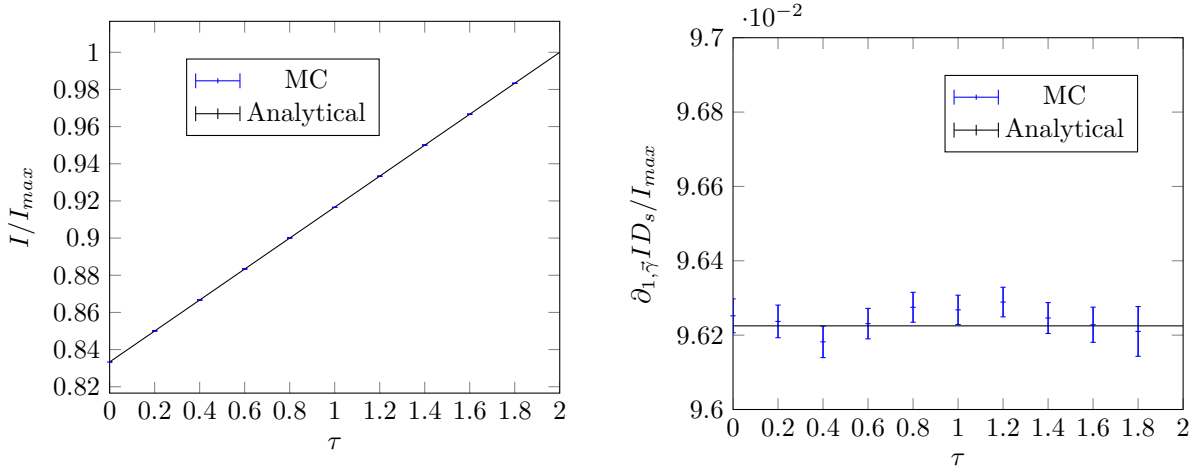


Figure 14: Monte-Carlo estimations and analytical solutions for the intensity (left) and its spatial derivative in the direction $\vec{\gamma} = (\frac{1}{\sqrt{3}}, \frac{1}{\sqrt{3}}, \frac{1}{\sqrt{3}})$ (right). The corresponding configuration is described in Sec. 4.2: a convex domain with differentiable boundaries (the sphere described in Fig. 11) and diffuse and emissive surfaces. The intensity and its spatial derivative are estimated at optical thickness $\tau = k_s \vec{x}_{obs} \cdot \vec{e}_1$ and in the direction $\vec{\omega}_{obs} = (0, 0, 1)$. Monte-Carlo number of samplings is $N = 10^8$, the sphere diameter $D_s = 1m$.

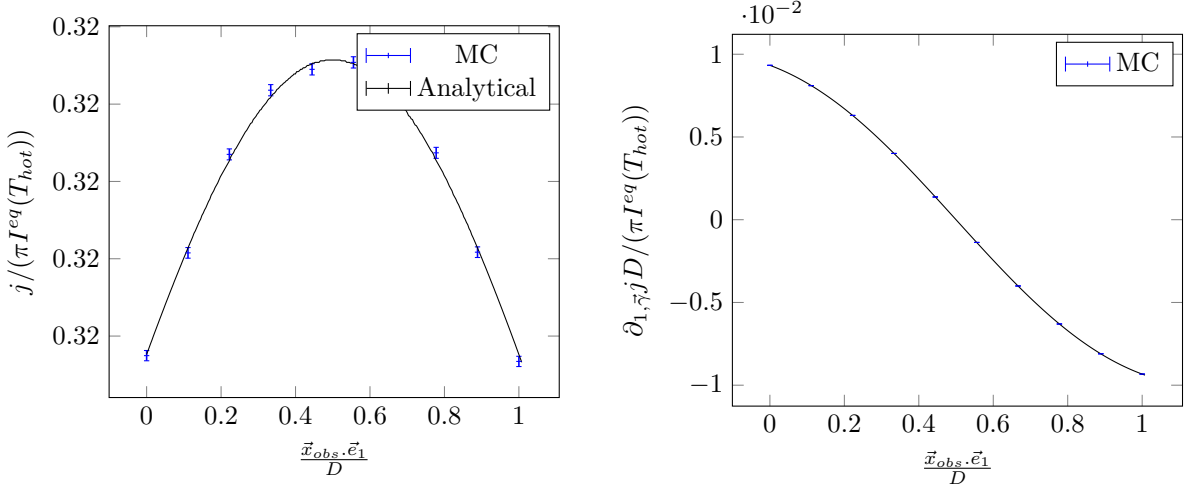


Figure 15: Monte-Carlo estimations and analytical solutions for the radiative flux j (left) and its spatial derivative $\partial_{1,\vec{\gamma}}j$ in the direction $\vec{\gamma} = (\frac{1}{\sqrt{2}}, \frac{1}{\sqrt{2}}, 0)$ (right). The configuration is described in Sec. 4.2: a convex domain with boundary discontinuities between adjacent diffuse surfaces at different temperatures (top plane of the slab geometry described in Fig. 11). The radiative flux and its derivative are estimated at the position \vec{x}_{obs} such as $\frac{\vec{x}_{obs} \cdot \vec{e}_1}{D} = \frac{\vec{x}_{obs} \cdot \vec{e}_2}{D}$ and $\vec{x}_{obs} \cdot \vec{e}_3 = 0$. Monte-Carlo number of samplings is $N = 10^9$, the top hot square dimensions are $D \times D$ with $D = 2m$.

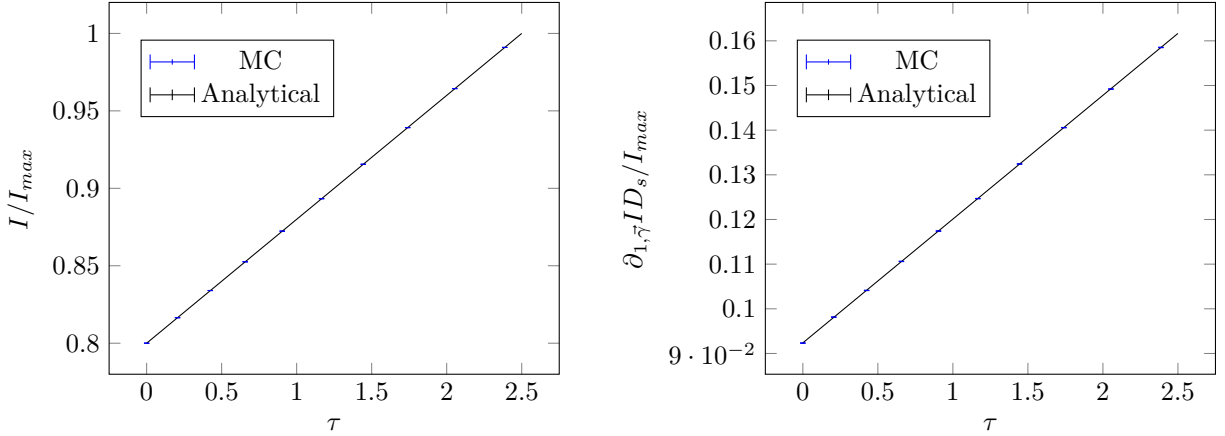


Figure 16: Monte-Carlo estimations and analytical solutions for the intensity (left) and its spatial derivative in the direction $\vec{\gamma} = (\frac{1}{\sqrt{3}}, \frac{1}{\sqrt{3}}, \frac{1}{\sqrt{3}})$ (right). The corresponding configuration is described in Sec. 4.3: a convex domain with differentiable boundaries (the sphere described in Fig. 11), emissive surfaces and non-homogeneous scattering coefficient. The intensity and its spatial derivative are estimated at optical thickness $\tau = \frac{k_0}{k_1} (\exp(k_1 \vec{x}_{obs} \cdot \vec{e}_1) - 1)$ and in the direction $\vec{\omega}_{obs} = (0, 0, 1)$. Monte-Carlo number of samplings is $N = 10^8$, the sphere diameter $D_s = 1m$.

A Projection on the surface

Omitting the index 1, we make use of the same direct orthonormal basis $(\vec{m}, \vec{t}, \vec{n})$ as for \mathcal{S}_1 in Figure 8. $\vec{\gamma}$ is decomposed using the non-orthogonal basis $(\vec{\omega}, \vec{m}, \vec{t})$:

$$\vec{\gamma} = \alpha \vec{\omega} + \zeta \vec{m} + \chi \vec{t} \quad (35)$$

Taking the scalar product of $\vec{\gamma}$ with \vec{n} , $\vec{\omega} \wedge \vec{t}$ and $\vec{\omega} \wedge \vec{m}$ leads to

$$\begin{aligned} \alpha &= \frac{\vec{\gamma} \cdot \vec{n}}{\vec{\omega} \cdot \vec{n}} \\ \zeta &= \frac{\vec{\gamma} \cdot (\vec{\omega} \wedge \vec{t})}{\vec{m} \cdot (\vec{\omega} \wedge \vec{t})} \\ \chi &= \frac{\vec{\gamma} \cdot (\vec{\omega} \wedge \vec{m})}{\vec{t} \cdot (\vec{\omega} \wedge \vec{m})} \end{aligned} \quad (36)$$

Replacing \vec{m} with $\vec{t} \wedge \vec{n}$ and using standard algebra (line 2: circulation property of triple products; line 3: development of double vectorial products; line 4: $\vec{t} \cdot \vec{n} = 0$ and $\vec{t} \cdot \vec{t} = 1$),

$$\begin{aligned} \vec{m} \cdot (\vec{\omega} \wedge \vec{t}) &= (\vec{t} \wedge \vec{n}) \cdot (\vec{\omega} \wedge \vec{t}) \\ &= ((\vec{\omega} \wedge \vec{t}) \wedge \vec{t}) \cdot \vec{n} \\ &= (-\vec{t} \cdot \vec{t}) \vec{\omega} + (\vec{\omega} \cdot \vec{t}) \vec{t} \cdot \vec{n} \\ &= -\vec{\omega} \cdot \vec{n} \end{aligned} \quad (37)$$

Similarly $\vec{t} \cdot (\vec{\omega} \wedge \vec{m}) = \vec{\omega} \cdot \vec{n}$ and we get

$$\begin{aligned} \alpha &= \frac{\vec{\gamma} \cdot \vec{n}}{\vec{\omega} \cdot \vec{n}} \\ \zeta &= -\frac{\vec{\gamma} \cdot (\vec{\omega} \wedge \vec{t})}{\vec{\omega} \cdot \vec{n}} \\ \chi &= \frac{\vec{\gamma} \cdot (\vec{\omega} \wedge \vec{m})}{\vec{\omega} \cdot \vec{n}} \end{aligned} \quad (38)$$

By definition, $\beta \vec{u} = \zeta \vec{m} + \chi \vec{t}$ and observing (line 1: development of double vectorial products; line 2: replacement of $\vec{\gamma}$ with its development; line 3: $\alpha = \frac{\vec{\gamma} \cdot \vec{n}}{\vec{\omega} \cdot \vec{n}}$)

$$\begin{aligned} (\vec{\gamma} \wedge \vec{\omega}) \wedge \vec{n} &= -(\vec{\omega} \cdot \vec{n}) \vec{\gamma} + (\vec{\gamma} \cdot \vec{n}) \vec{\omega} \\ &= -(\vec{\omega} \cdot \vec{n}) (\alpha \vec{\omega} + \zeta \vec{m} + \chi \vec{t}) + (\vec{\gamma} \cdot \vec{n}) \vec{\omega} \\ &= -(\vec{\omega} \cdot \vec{n}) (\zeta \vec{m} + \chi \vec{t}) \end{aligned} \quad (39)$$

we get

$$\beta \vec{u} = \frac{(\vec{\omega} \wedge \vec{\gamma}) \wedge \vec{n}}{\vec{\omega} \cdot \vec{n}} \quad (40)$$

B Linear emission

For any location $\vec{x} \in \mathcal{S}_1$, we note (y, ℓ) the coordinates of \vec{x} in a two dimension Cartesian system of basis (\vec{m}_1, \vec{t}) . Therefore y is also the distance from \vec{x} to the edge \mathcal{L}_{12} . Remembering that $\beta \vec{u} = \zeta \vec{m}_1 + \chi \vec{t}$, when intensity is discontinuous at the edge (I_1 on \mathcal{S}_1 , I_2 on \mathcal{S}_2), the term $\beta \partial_{1,\vec{u}} I = \beta \vec{u} \cdot \vec{grad}(I)$ in Eq. 10 induces a Dirac in the coordinate y normal to the edge:

$$\zeta \vec{m}_1 \cdot \vec{grad}(I) = \zeta \delta(y) (I_1 - I_2) \quad (41)$$

When this Dirac is multiplied by $\vec{\omega} \cdot \vec{n}_1$ to get a flux density, and then integrated over the surface (including the edge), writing the differential surface $d\sigma = dy d\ell$, the integral over y vanishes to give

$$\int_{\mathcal{S}_1} (\vec{\omega} \cdot \vec{n}_1) \zeta \delta(y) (I_1 - I_2) d\sigma = \int_{\mathcal{L}_{12}} (\vec{\omega} \cdot \vec{n}_1) \zeta (I_1 - I_2) d\ell \quad (42)$$

Reporting the expression of ζ and using the circulation property of triple products:

$$\int_{\mathcal{S}_1} (\vec{\omega} \cdot \vec{n}_1) \zeta \delta(y) (I_1 - I_2) d\sigma = - \int_{\mathcal{L}_{12}} \vec{\gamma} \cdot (\vec{\omega} \wedge \vec{t}) d\ell = \int_{\mathcal{L}_{12}} (\vec{\omega} \wedge \vec{\gamma}) \cdot \vec{t} (I_1 - I_2) d\ell \quad (43)$$

The linear emission associated to each differential length $d\ell$ is therefore $(\vec{\omega} \wedge \vec{\gamma}) \cdot \vec{t} (I_1 - I_2) d\ell$.

C Chandrasekhar's exact solution for heterogeneous multiple-scattering atmospheres

In a heterogeneous, purely scattering and infinite medium, with plane parallel stratified intensity field, the radiative transfer equation has an analytical solution $I(\tau, \mu)$ ([15]):

$$I(\tau, \mu) = \frac{\eta(0)}{4\pi} + \frac{3}{4\pi}j[(g-1)\tau + \mu] \quad (44)$$

with $\eta(0)$ and j being constants, g is the asymmetric coefficient, τ is the optical thickness normal to the plane of stratification and μ the direction cosine. \vec{e}_3 being the plane normal unit vector and a vector of the Cartesian coordinate system ($\vec{e}_1, \vec{e}_2, \vec{e}_3$) we state the normal optical thickness as:

$$\tau = \int_0^{\vec{x} \cdot \vec{e}_3} k_s(l) dl \quad (45)$$

with \vec{x} the position in the infinite medium. The cosine $\mu = \vec{\omega} \cdot \vec{e}_3$ with $\vec{\omega}$ the transport direction. We state the analytical intensity \mathcal{L} as $\mathcal{L}(\vec{x}, \vec{\omega}) = I(\tau, \mu)$.

The analytical spatial derivative $\partial_{1,\vec{\gamma}}\mathcal{L}$ is obtain by differentiating $I(\tau(\vec{x}), \mu)$:

$$\partial_{1,\vec{\gamma}}\mathcal{L}(\vec{x}, \vec{\omega}) = \partial_{1,\vec{\gamma}}I(\tau(\vec{x}), \mu) = \frac{3}{4\pi}j(g-1)\partial_{1,\vec{\gamma}}\tau(\vec{x}) \quad (46)$$

with

$$\partial_{1,\vec{\gamma}}\tau(\vec{x}) = \int_0^{\vec{x} \cdot \vec{e}_3} \partial_{1,\vec{\gamma}}k_s(l) dl + (\vec{\gamma} \cdot \vec{e}_3) k_s(\vec{x} \cdot \vec{e}_3) \quad (47)$$

D The slab

The black surface is at $x_3 = 0$. Its temperature is T_{hot} . The emissive/reflective diffuse surface is at $x_3 = c$. Its temperature is $T_{hot} \forall x_1 \in [0, a], x_2 \in [0, a]$ and T_{cold} elsewhere. Its emissivity ϵ is uniform. The observation location is at $x_1 \in [0, a], x_2 \in [0, a]$ and $x_3 = 0$ (on the black surface, facing the square). The flux density is

$$\varphi = \pi\epsilon FI^{eq}(T_{hot}) + \pi(1-\epsilon)FI^{eq}(T_{cold}) + \pi(1-F)I^{eq}(T_{cold}) \quad (48)$$

with

$$\begin{aligned} F = & \frac{\mathcal{X}_1}{2\pi\sqrt{1+\mathcal{X}_1^2}} \tan^{-1} \frac{\mathcal{X}_2}{\sqrt{1+\mathcal{X}_1^2}} + \frac{\mathcal{X}_2}{2\pi\sqrt{1+\mathcal{X}_2^2}} \tan^{-1} \frac{\mathcal{X}_1}{\sqrt{1+\mathcal{X}_2^2}} \\ & + \frac{\mathcal{A}-\mathcal{X}_1}{2\pi\sqrt{1+(\mathcal{A}-\mathcal{X}_1)^2}} \tan^{-1} \frac{\mathcal{X}_2}{\sqrt{1+(\mathcal{A}-\mathcal{X}_1)^2}} + \frac{\mathcal{X}_2}{2\pi\sqrt{1+\mathcal{X}_2^2}} \tan^{-1} \frac{\mathcal{A}-\mathcal{X}_1}{\sqrt{1+\mathcal{X}_2^2}} \\ & + \frac{\mathcal{X}_1}{2\pi\sqrt{1+\mathcal{X}_1^2}} \tan^{-1} \frac{\mathcal{A}-\mathcal{X}_2}{\sqrt{1+\mathcal{X}_1^2}} + \frac{\mathcal{A}-\mathcal{X}_2}{2\pi\sqrt{1+(\mathcal{A}-\mathcal{X}_2)^2}} \tan^{-1} \frac{\mathcal{X}_1}{\sqrt{1+(\mathcal{A}-\mathcal{X}_2)^2}} \\ & + \frac{\mathcal{A}-\mathcal{X}_1}{2\pi\sqrt{1+(\mathcal{A}-\mathcal{X}_1)^2}} \tan^{-1} \frac{\mathcal{A}-\mathcal{X}_2}{\sqrt{1+(\mathcal{A}-\mathcal{X}_1)^2}} + \frac{\mathcal{A}-\mathcal{X}_2}{2\pi\sqrt{1+(\mathcal{A}-\mathcal{X}_2)^2}} \tan^{-1} \frac{\mathcal{A}-\mathcal{X}_1}{\sqrt{1+(\mathcal{A}-\mathcal{X}_2)^2}} \end{aligned} \quad (49)$$

$\mathcal{X}_1 = x_1/c$, $\mathcal{X}_2 = x_2/c$ and $\mathcal{A} = a/c$.

E Examples supplementary information

E.1 Emissive surfaces, no reflection, uniform scattering, no volume absorption, no volume emission

Convex domain with differentiable boundaries Solving the intensity using a Monte-Carlo algorithm falls down to sample a scattered radiative path in the medium until it reaches the sphere boundary. The Monte-Carlo weight is then implemented with the sphere surface emission, that is $\mathcal{L}(\vec{x}, \vec{\omega})$.

The spatial derivative $\partial_{1,\vec{\gamma}}I$ transport equation is identical to the radiative transfer equation in this configuration. In term of Monte-Carlo algorithm it implies that the spatial derivative scattering paths sampling will

be identical to radiative paths sampling until paths reach the sphere boundary. At the boundary the spatial derivative $\partial_{1,\vec{\gamma}}I$ is derived from Eq. 14 and Eq. 32:

$$\partial_{1,\vec{\gamma}}I = -\alpha k_s \left(\mathcal{L}(\vec{x}, \vec{\omega}) - \int_{4\pi} p_{\Omega'}(-\vec{\omega}'|\vec{x}, -\vec{\omega}) d\vec{\omega}' I(\vec{x}, \vec{\omega}') \right) + \beta \partial_{1,\vec{\gamma}}\mathcal{L}(\vec{x}, \vec{\omega}) \quad \vec{x} \in \partial G; \vec{\omega} \cdot \vec{n} > 0 \quad (50)$$

With \mathcal{L} and $\partial_{1,\vec{\gamma}}\mathcal{L}$ derived in Appendix. C. At the boundary the spatial derivative is coupled with the intensity $I(\vec{x}, \vec{\omega}')$ so that sampling a spatial derivative path comes down to sample a scattering path until it reaches the sphere boundary, sample a direction $-\vec{\omega}'$, and sample w_I from $(\vec{x}, \vec{\omega}')$.

Boundary discontinuities The medium is transparent so that the radiative paths between the surfaces will only be strait lines whether it be for the intensity or for its spatial gradient. For the intensity boundary conditions we refer to Eq. 4 with:

$$S_b = I^{eq}(T_{hot})H(\vec{x} \in \mathcal{S}_{hot}) + I^{eq}(T_{cold})H(\vec{x} \notin \mathcal{S}_{hot})\vec{x} \in \partial G_{top} \quad (51)$$

The flux density is solved by sampling w_φ (see Algorithm 4) and results are compared to analytical solution in Fig. 13 and table (the table is not included in the current state of the paper) .

The flux density spatial gradient is estimated by solving:

$$\partial_{1,\vec{\gamma}}\varphi = \int_{\mathcal{H}^-} (\vec{\omega} \cdot \vec{n}) \partial_{1,\vec{\gamma}}I d\vec{\omega} = \int_{\partial G_{top}} (\vec{\omega} \cdot \vec{n}) \frac{\vec{\omega} \cdot \vec{n}_{top}}{r^2} (\beta \mathcal{C}_b[\partial_{1,\vec{u}}I] + S_{b,\vec{\gamma}}[I]) dS_{top} + \int_{\mathcal{L}_{top}} (\vec{\omega} \cdot \vec{n}) \frac{\vec{\omega} \wedge \vec{\gamma}}{r^2} (I_1 - I_2) d\ell_{top} \quad (52)$$

which is the direct application of Eq. 31 for this configuration. Here:

$$\mathcal{C}_b[\partial_{1,\vec{u}}I] = 0 \text{ and } S_{b,\vec{\gamma}}[I] = 0 \quad (53)$$

The intensities I_1 and I_2 are stated as $I_1 = S_{b,1}$ and $I_2 = S_{b,2}$ (see Eq. 29 and 30). According to \vec{m}_1 and \vec{m}_2 the sources $S_{b,1}$ and $S_{b,2}$ can take the values of $I^{eq}(T_{hot})$ or $I^{eq}(T_{cold})$. In the Monte-Carlo algorithm the discontinuity sources are sampled uniformly from $p_{L_{edges}}$ along the square edges, I_1 and I_2 are evaluated and the Monte-Carlo weight $(\vec{\omega} \cdot \vec{n}_{bottom}) \frac{1}{p_{L_{edges}}} \frac{\vec{\omega} \wedge \vec{\gamma}}{r^2} (I_1 - I_2)$ is computed.

E.2 Emitting and reflective surfaces, uniform scattering, no volume absorption, no volume emission

Convex domain with differentiable boundaries Solving numerically the intensity at $(\vec{x}_{obs}, \vec{\omega}_{obs})$ comes down to sample a radiative path that will be scattered in the medium (according to the medium scattering properties in Eq. 2) and reflected at the boundary (according to the reflection properties in Eq. 33). As we usually do in the case of reflective surfaces, the Monte-Carlo weight will account for the source accumulation of each radiative path encounter with the boundary. The results obtained for the intensity at $(\vec{x}_{obs}, \vec{\omega}_{obs})$ are presented in Fig. 14 and compared with the analytical solution $\mathcal{L}(\vec{x}_{obs}, \vec{\omega}_{obs})$.

The spatial derivative $\partial_{1,\vec{\gamma}}I$ is estimated at the same observation location as the intensity and the spatial derivative transport equation (Eq. 6) is identical to the intensity radiative transfer equation. For the boundary conditions we refer to Eq. 13 with ρ and $p_{\Omega',b}$ being constant along the sphere surface:

$$\mathcal{C}_b[\partial_{1,\vec{u}}I] = \rho \int_{\mathcal{H}'} p_{\Omega',b}(-\vec{\omega}'|\vec{x}, -\vec{\omega}) d\vec{\omega}' \partial_{1,\vec{u}}I(\vec{x}, \vec{\omega}') \quad (54)$$

$$S_{b,\vec{\gamma}}[I] = \alpha \mathcal{C}[I] + \beta \partial_{1,\vec{u}}\mathcal{L}(\vec{x}, \vec{\omega}) - \beta \mathcal{C}_b[\partial_{1,\vec{u}}\mathcal{L}(\vec{x}, \vec{\omega})] \quad (55)$$

with

$$\mathcal{C}[I] = -k_s \mathcal{L}(\vec{x}, \vec{\omega}) + k_s \int_{\Omega'} p_{\Omega'}(-\vec{\omega}'|\vec{x}, \vec{\omega}) I(\vec{x}, \vec{\omega}') \quad (56)$$

Boundary discontinuities The medium is transparent so that the radiative paths between the surfaces will only be strait lines whether it be for the intensity or for its spatial gradient. For the intensity boundary conditions we refer to Eq. 4 with:

$$S_b = \varepsilon I^{eq}(T_{hot})H(\vec{x} \in \mathcal{S}_{hot}) + \varepsilon I^{eq}(T_{cold})H(\vec{x} \notin \mathcal{S}_{hot})\vec{x} \in \partial G_{top} \quad (57)$$

The flux density spatial gradient is estimated by solving:

$$\partial_{1,\vec{\gamma}}\varphi = \int_{\mathcal{H}^-} (\vec{\omega}\cdot\vec{n})\partial_{1,\vec{\gamma}}I d\vec{\omega} = \int_{\partial G_{top}} (\vec{\omega}\cdot\vec{n})\frac{\vec{\omega}\cdot\vec{n}_{top}}{r^2}(\beta\mathcal{C}_b[\partial_{1,\vec{u}}I] + S_{b,\vec{\gamma}}[I])dS_{top} + \int_{\mathcal{L}_{top}} (\vec{\omega}\cdot\vec{n})\frac{\vec{\omega}\wedge\vec{\gamma}}{r^2}(I_1 - I_2)d\ell_{top} \quad (58)$$

which is the direct application of Eq. ref for this configuration. Here:

$$\mathcal{C}_b[\partial_{1,\vec{u}}I] = \rho \int_{\mathcal{H}'} p_{\Omega',b}(-\vec{\omega}'|\vec{x}, -\vec{\omega})d\vec{\omega}'\partial_{1,\vec{u}}I(\vec{x}, \vec{\omega}') \quad (59)$$

and

$$S_{b,\vec{\gamma}}[I] = 0 \quad (60)$$

A realization of the Monte-Carlo weight consist on sampling a direction $\vec{\omega}$ from Lambert distribution, sample a path in the $-\vec{\omega}$ direction. If the path reaches the hot square part of the top surface then $\mathcal{C}_b[\partial_{1,\vec{u}}I]$ is evaluated by sampling a direction $\vec{\omega}'$ from $p_{\Omega',b}$ and sampling a path in that direction. $\partial_{1,\vec{\gamma}}I(x, \vec{\omega}')$ depends on the intensity gradient at the bottom surface since in a transparent medium a path leaving the top surface will only reach the bottom surface. If the boundary condition at the bottom is homogeneous, as it is the case here, then $\partial_{1,\vec{u}}I_{bottom}$ is null and $\mathcal{C}_b[\partial_{1,\vec{u}}I]$ is null.

The intensities I_1 and I_2 are stated in Eq. 29 and 30. The discontinuities sources are sampled uniformly from $p_{L_{edges}}$ along the square edges, I_1 and I_2 are evaluated and the Monte-Carlo weight $(\vec{\omega}\cdot\vec{n}_{bottom})p_{L_{edges}}\frac{\vec{\omega}\wedge\vec{\gamma}}{r^2}(I_1 - I_2)$ is computed. The only difference with example Sec. 4.1 at that stage is the evaluation of I_1 and I_2 . In the previous example the top boundary was a black body so that only $S_{b,1}$ and $S_{b,2}$ were used. Here the top surface is diffuse so that the incoming intensity also has to be evaluated at the edges to evaluate I_1 and I_2 .

E.3 Emissive surfaces, no reflection, non-uniform scattering, non-uniform volume absorption, non-uniform volume emission

Convex domain with differentiable boundaries The radiative transfer model in the medium G is stated by Eq. 2 with the collisional operator \mathcal{C} containing only the scattering terms, the volume source being $S = 0$. The intensity is solved by sampling the Monte-Carlo weight w_{I,k_s} (the pseudo-algorithm is not present in the paper at its current state). The only difference with Algorithm 16 is in the non-uniform scattering coefficient sampling. Other than that the algorithm remain identical.

The spatial derivative is estimated at the same observation location and its boundary conditions are stated in the first example Eq. 32. The model in the medium G is stated in Eq. 7 with S_γ being:

$$S_\gamma = -\partial_{1,\vec{\gamma}}k_s I(\vec{x}, \vec{\omega}) + \partial_{1,\vec{\gamma}}k_s \int_{4\pi} p_{\Omega'}(-\vec{\omega}'|\vec{x}, -\vec{\omega})d\vec{\omega}'I(\vec{x}, \vec{\omega}') \quad (61)$$

with $\partial_{1,\vec{\gamma}}k_s = (\vec{\gamma}\cdot\vec{e}_x)(-k_1k_0 \exp(-k_1x))$. The source S_γ is regarded as a volume source in the spatial gradient model. To estimate the spatial gradient numerically this source will be stored along the sampled path, as any usual Monte-Carlo algorithm that estimate the intensity in presence of thermal emission. The only difference with such algorithm is that the source S_γ is here a function of the intensity in the medium and will be estimated by sampling w_I (Algorithm 16) in the double-randomization process. The spatial gradient is then solved by sampling $w_{\partial_{1,\vec{\gamma}}I,k_s}$ (pseudo-algorithm is not present in the paper at its current state): it starts by sampling a scattering path until it reaches the sphere boundary and then sampling S_γ uniformly along the path. To evaluate S_γ at $(\vec{x}, \vec{\omega})$ a direction $\vec{\omega}'$ is sampled from the phase function and the Monte-Carlo weight w_I is sampled twice: from $(\vec{x}, \vec{\omega}')$ and $(\vec{x}, \vec{\omega})$; then both contributions are added as in Eq. 61 and counted in the Monte-Carlo $w_{\partial_{1,\vec{\gamma}}I,k_s}$ as well as the boundary condition weight (from Eq. 50).

Boundary discontinuities In the present state of the paper this configuration is not described.

PART 2: A physical model and a Monte Carlo estimate for the angular derivative of the specific intensity

Abstract

Starting from the radiative transfer equation and its usual boundary conditions, the objective of the present article is to design a Monte Carlo algorithm estimating the angular derivative of the specific intensity. There are two common ways to address this question. The first consists in using two independent Monte Carlo estimates for the specific intensity in two directions and using a finite difference to approximate the angular derivative; the associated uncertainties are difficult to handle. The second consists in considering any Monte Carlo algorithm for the specific intensity, writing down its associated integral formulation, angular differentiating this integral, and reformulating it so that it defines a new Monte Carlo algorithm directly estimating the angular derivative of the specific intensity; the corresponding formal developments are very demanding [1]. We here explore an alternative approach in which we derivate both the radiative transfer equation and its boundary conditions to set up a physical model for the angular derivative of the specific intensity. Then a standard path integral translation is made to design a Monte Carlo algorithm solving this model. The only subtlety at this stage is that the model for the angular derivative is coupled to the specific intensity itself, as well as the spatial derivative of the specific intensity. The paths associated to the angular derivative of the specific intensity give birth to paths associated to specific intensity (standard radiative transfer paths) and paths associated to the spatial derivative PART 1. When designing a Monte Carlo algorithm for the coupled problem a double randomization approach is therefore required.

1 Introduction

We address the question of modeling and numerically simulating the angular derivative $\partial_{2,\vec{\gamma}}I \equiv \partial_{2,\vec{\gamma}}I(\vec{x},\vec{\omega})$ of the specific intensity $I \equiv I(\vec{x},\vec{\omega})$ at location \vec{x} in direction $\vec{\omega}$. This angular derivative corresponds to a rotation around the direction of the unit vector $\vec{\gamma}$, which means that

$$\partial_{2,\vec{\gamma}}I = \lim_{\delta\varphi \rightarrow 0} \frac{I(\vec{x},\vec{\omega}_{\delta\varphi}^{\vec{\gamma}}) - I(\vec{x},\vec{\omega})}{\delta\varphi} \quad (1)$$

where $\vec{\omega}_{\delta\varphi}^{\vec{\gamma}}$ is the unit vector obtained by rotating $\vec{\omega}$ of $\delta\varphi$ around $\vec{\gamma}$. Intensity I has two independent variables $(\vec{x},\vec{\omega})$; the angular derivative $\partial_{2,\vec{\gamma}}I$ has three independent variables $(\vec{x},\vec{\omega},\vec{\gamma})$. As two of these variables are directions (vectors in the unit sphere), they will be distinguished by specifying the transport direction for $\vec{\omega}$ and the rotation direction for $\vec{\gamma}$ (see Figure 1).

The reason why we address $\partial_{2,\vec{\gamma}}I$, a scalar quantity defined for only one given direction, instead of addressing a more general vector quantity, is the attempt to make explicit connections between the modeling of angular derivatives and standard radiative transfer modeling. We make the very same choice in PART 1 as far as spatial derivatives are concerned (considering only one spatial direction instead of the gradient). Starting from the available transport physics for I , our main objective is to introduce a new, very similar transport physics for $\partial_{2,\vec{\gamma}}I$. Then all the standard practice of analysing and numerically simulating I can be straightforward translated into new tools for analysing and numerically simulating angular derivatives.

Standard radiative transfer physics can be gathered into two equations: the partial differential equation governing I at any location inside the field G (the radiative transfer equation) and an integral constraint at the boundary ∂G (the incoming radiation equation), relating I in any direction toward the field to I in all the directions exiting the field. Recognizing, in the writing of these equations, the processes of volume emission/absorption/scattering and surface emission/absorption/reflection, translating them into path statistics, is quite straightforward. We will do the same with $\partial_{2,\vec{\gamma}}I$:

- Two equations will be constructed for $\partial_{2,\vec{\gamma}}I$ by differentiating the radiative transfer equation and the incoming radiation equation (differentiating the equations of the I model).

* plapeyre@uwaterloo.ca

- The resulting equations will be physically interpreted using transport physics processes, defining volume emission/absorption and surface emission/absorption processes for the angular derivative. We will observe that there is no scattering/reflection processes. A particular attention will be devoted to the identifications of the sources of the angular derivative.
- Statistical paths will then be defined for $\partial_{2,\vec{\gamma}}I$, from the sources to the location and direction of observation.

Numerically estimating $\partial_{2,\vec{\gamma}}I$ will then be simply achieved using a Monte Carlo approach, i.e. sampling large numbers of paths. We will display the observed variance of the resulting Monte Carlo estimate but no attempt will be made to optimize convergence in the frame of the present article. Configurations for which $\partial_{2,\vec{\gamma}}I$ is known analytically will be used both to validate the formal developments and to illustrate the physical meaning of each of the identified processes of emission and absorption as far as angular derivatives are concerned.

Even if the presentation of the mathematical developments remains strictly formal, we will try to stick to the spirit of radiative transfer: trying to write down the physics of angular derivatives by maintaining a parallel, as strict as possible, with the physics of photon transport. This parallel will not be complete. Beer-Lambert will be entirely recovered, but volume scattering and surface reflection will vanish. The physics of photon scattering and photon reflection will only impact the angular derivative via the fact that the sources of angular derivatives are functions of both intensity and spatial derivative PART 1 (these two quantities depending on scattering and reflection). It is therefore meaningful to view the angular derivative as a physical quantity propagated along straight lines: extinction along the lines is strictly the same as photon extinction; volume/surface emission requires the knowledge of both intensity and spatial derivative. In PART 1 we showed that the model of spatial derivative was coupled with the model of intensity. Here we show that angular derivative is coupled with both intensity and spatial derivative. We will devote some attention to the particular case of specular reflection for which one of the sources of angular derivation, at the boundary, can be interpreted as a standard specular reflection process, changing only the rotation direction. For spatial derivatives in PART 1, all types of reflections were recovered and the derivation directions were modified by the reflection process. Here this is only true for specular reflections.

The text is essentially a short note with three sections:

- Section 2 provides the model in its differential form for boundary surfaces without any discontinuity.
- Section 3 deals with the specific case of discontinuities at the junction between two plane surfaces.
- Section 4 provides the associated statistical paths and illustrates how a standard Monte Carlo approach can be used to estimate $\partial_{2,\vec{\gamma}}I$ (or any radiative transfer observable defined as an integral of $\partial_{2,\vec{\gamma}}I$).

2 Convex domain with differentiable boundaries

Noting \mathcal{C} the collision operator, the stationary monochromatic radiative transfer equation is

$$\vec{\nabla}I \cdot \vec{\omega} = \mathcal{C}[I] + S \quad \vec{x} \in G \quad (2)$$

with

$$\mathcal{C}[I(\vec{x}, \vec{\omega})] = -k_a(\vec{x})I(\vec{x}, \vec{\omega}) - k_s(\vec{x})I(\vec{x}, \vec{\omega}) + k_s(\vec{x}) \int_{4\pi} p_{\Omega'}(-\vec{\omega}'|\vec{x}, -\vec{\omega})d\vec{\omega}' I(\vec{x}, \vec{\omega}') \quad (3)$$

where k_a is the absorption coefficient, k_s the scattering coefficient and $p_{\Omega'}(-\vec{\omega}'|\vec{x}, \vec{\omega})$ is the probability density that the scattering direction is $-\vec{\omega}'$ for a photon scattered at \vec{x} coming from direction $-\vec{\omega}$ (the single scattering phase function, see Figure 2 for a single collision and Figure 3 for a multiple-scattering photon trajectory). $S \equiv S(\vec{x}, \vec{\omega})$ is the volumic source. When this source is due to thermal emission, under the assumption that the matter is in a state of local thermal equilibrium, then it is isotropic and $S = k_a I^{eq}(T)$ where T is the local temperature and I^{eq} is the specific intensity at equilibrium (following Planck function).

At the boundary, noting \mathcal{C}_b the reflection operator, the incoming radiation equation is

$$I = \mathcal{C}_b[I] + S_b \quad \vec{x} \in \partial G ; \vec{\omega} \cdot \vec{n} > 0 \quad (4)$$

with

$$\mathcal{C}_b[I] = \rho(\vec{x}, -\vec{\omega}) \int_{\mathcal{H}'} p_{\Omega',b}(-\vec{\omega}'|\vec{x}, -\vec{\omega})d\vec{\omega}' I(\vec{x}, \vec{\omega}') \quad (5)$$

where \vec{n} is the normal to the boundary at \vec{x} , oriented toward the inside, $\vec{\omega}$ is a direction within the inside hemisphere \mathcal{H} , $\vec{\omega}'$ is any direction within the outside hemisphere \mathcal{H}' , $\rho(\vec{x}, -\vec{\omega})$ is the surface reflectivity for a photon impacting the boundary in direction $-\vec{\omega}$, and $p_{\Omega',b}(-\vec{\omega}'|\vec{x}, -\vec{\omega})$ is the probability density that the reflection direction is $-\vec{\omega}'$ for a photon reflected at \vec{x} coming from direction $-\vec{\omega}$ (the product $\rho p_{\Omega',b}$ is the bidirectional reflectivity density function, see Figure 4 collision at the boundary and Figure 5 for a multiple-reflection photon trajectory). When the surfacic source $S_b \equiv S_b(\vec{x}, \vec{\omega})$ is due to the thermal emission of an opaque surface, under the assumption that the matter at this surface is in a state of local thermal equilibrium, then $S_b = (1 - \rho(\vec{x}, -\vec{\omega})) I^{eq}(T_b)$ where T_b is the local surface temperature.

Angularly differentiating equation 2 provides a transport model for $\partial_{2,\vec{\gamma}}I$. The collision operator involved in this model includes only extinction (no inward scattering) and the source term depends on both intensity I and the spatial derivative of intensity in direction $\vec{\gamma} \wedge \vec{\omega}$, i.e. $\partial_{1,\vec{\gamma} \wedge \vec{\omega}}I = (\vec{\gamma} \wedge \vec{\omega}) \cdot \vec{\nabla}I$:

$$\vec{\nabla}(\partial_{2,\vec{\gamma}}I) \cdot \vec{\omega} = \mathcal{C}[\partial_{2,\vec{\gamma}}I] + S_{\vec{\gamma}} \quad \vec{x} \in G \quad (6)$$

with

$$\mathcal{C}[\partial_{2,\vec{\gamma}}I] = -k_a(\vec{x})\partial_{2,\vec{\gamma}}I - k_s(\vec{x})\partial_{2,\vec{\gamma}}I \quad (7)$$

and $S_{\vec{\gamma}} = \partial_{2,\vec{\gamma}}\mathcal{C}[I] + \partial_{2,\vec{\gamma}}S - \mathcal{C}[I]$, leading to

$$\begin{aligned} S_{\vec{\gamma}} &= -\partial_{1,\vec{\gamma} \wedge \vec{\omega}}I \\ &+ k_s \int_{4\pi} \partial_{2,\vec{\gamma}} p_{\Omega'}(-\vec{\omega}'|\vec{x}, -\vec{\omega}) d\vec{\omega}' I(\vec{x}, \vec{\omega}') \\ &+ \partial_{2,\vec{\gamma}}S \end{aligned} \quad (8)$$

Angularly differentiating equation 4 closes the model of $\partial_{2,\vec{\gamma}}I$ by providing a boundary condition for equation 6. There is no collision operator (no reflection of $\partial_{2,\vec{\gamma}}I$ in incident directions) and the source term depends on intensity I :

$$\partial_{2,\vec{\gamma}}I = S_{b,\vec{\gamma}} \quad \vec{x} \in \partial G ; \vec{\omega} \cdot \vec{n} > 0 \quad (9)$$

with

$$\begin{aligned} S_{b,\vec{\gamma}} &= \partial_{2,\vec{\gamma}}S_b \\ &+ \partial_{2,\vec{\gamma}}\rho(\vec{x}, -\vec{\omega}) \int_{\mathcal{H}'} p_{\Omega',b}(-\vec{\omega}'|\vec{x}, -\vec{\omega}) d\vec{\omega}' I(\vec{x}, \vec{\omega}') \\ &+ \rho(\vec{x}, -\vec{\omega}) \int_{\mathcal{H}'} \partial_{2,\vec{\gamma}} p_{\Omega',b}(-\vec{\omega}'|\vec{x}, -\vec{\omega}) d\vec{\omega}' I(\vec{x}, \vec{\omega}') \end{aligned} \quad (10)$$

The model for I was (see Eq. 2 and Eq. 4)

$$\begin{cases} \vec{\nabla}I \cdot \vec{\omega} = \mathcal{C}[I] + S & \vec{x} \in G \\ I = \mathcal{C}_b[I] + S_b & \vec{x} \in \partial G ; \vec{\omega} \cdot \vec{n} > 0 \end{cases} \quad (11)$$

The model for $\partial_{2,\vec{\gamma}}I$ is (see Eq. 6 and Eq. 9)

$$\begin{cases} \vec{\nabla}(\partial_{2,\vec{\gamma}}I) \cdot \vec{\omega} = \mathcal{C}[\partial_{2,\vec{\gamma}}I] + S_{\vec{\gamma}} & \vec{x} \in G \\ \partial_{2,\vec{\gamma}}I = S_{b,\vec{\gamma}} & \vec{x} \in \partial G ; \vec{\omega} \cdot \vec{n} > 0 \end{cases} \quad (12)$$

The main differences are the following:

- In the field, the collision operator is changed: there is no incoming scattering. Volume collision is restricted to pure extinction according to the extinction coefficient $k_e = k_a + k_s$. Although the scattering coefficient k_s (that of the I model) appears in this extinction, along a line of sight $\partial_{2,\vec{\gamma}}I$ is not reinforced by any inward scattering of $\partial_{2,\vec{\gamma}}I$ in other directions. The physical picture is therefore that of angular derivatives being "absorbed" along the line of sight according to an exponential Beer extinction, the coefficient of this exponential "absorption" of $\partial_{2,\vec{\gamma}}I$ being that of the total extinction of I (i.e. that of the extinction of I by both absorption and scattering).
- At the boundary there is no reflection. There is indeed no collision operator: $\partial_{2,\vec{\gamma}}I$ for directions exciting the boundary is not impacted by $\partial_{2,\vec{\gamma}}I$ in any incoming direction.
- In the standard radiative transfer model, the sources S and S_b are given quantities (functions of the volume and surface properties), but in the model for $\partial_{2,\vec{\gamma}}I$, the sources $S_{\vec{\gamma}}$ and $S_{b,\vec{\gamma}}$ depend on I and $\partial_{1,\vec{\gamma} \wedge \vec{\omega}}I$. In pure mathematical terms, they are sources in the model for $\partial_{2,\vec{\gamma}}I$ only if this model is decoupled from both the radiative transfer model and the model of the spatial derivative. But the complete physics implies that the models are coupled: $S_{b,\vec{\gamma}}$ expresses part of this coupling via I , and $S_{\vec{\gamma}}$ expresses the rest of this coupling via both I and $\partial_{1,\vec{\gamma} \wedge \vec{\omega}}I$.

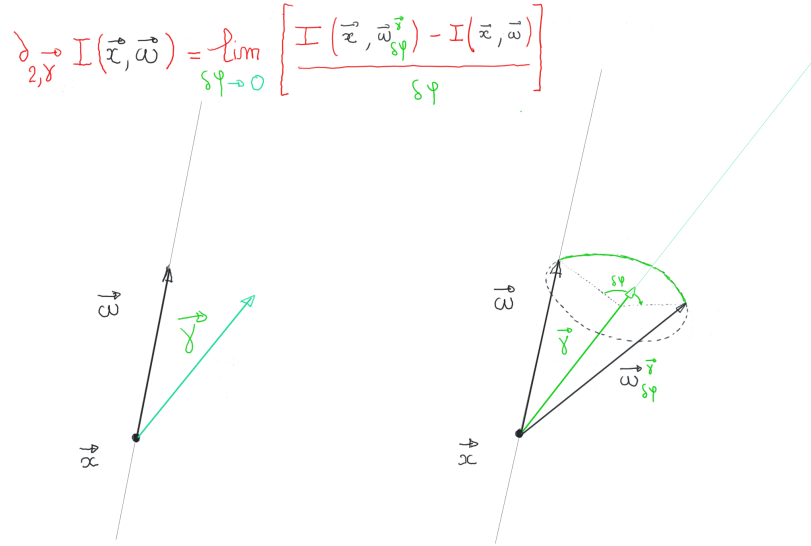


Figure 1: The angular derivative $\partial_{2,\vec{\gamma}} I$ pictured as an elementary rotation around the rotation direction $\vec{\gamma}$ according to $\partial_{2,\vec{\gamma}} I = \lim_{\delta\varphi \rightarrow 0} \frac{I(\vec{x}, \vec{\omega}_{\delta\varphi}) - I(\vec{x}, \vec{\omega})}{\delta\varphi}$ where $\vec{\omega}_{\delta\varphi}$ is the unit vector obtained by rotating $\vec{\omega}$ of $\delta\varphi$ around $\vec{\gamma}$. When picturing photon transport, we need to draw the location \vec{x} and the line of sight, i.e. the transport direction $\vec{\omega}$. When picturing the physics of spatial derivatives, we will need to draw the location \vec{x} and two vectors: $\vec{\omega}$ for the transport direction and $\vec{\gamma}$ for the rotation direction.

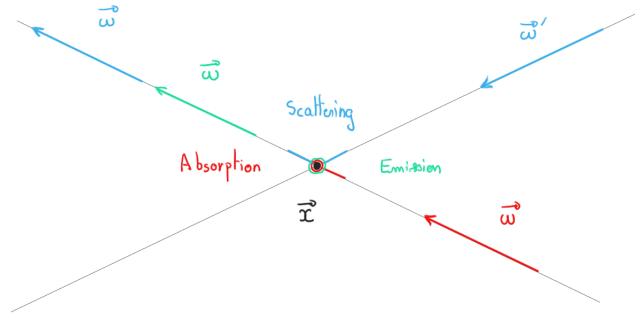


Figure 2: Sources (emission) and collisions (absorption and scattering) within the volume. The formulation of Eq. 3 favors a reciprocal/adjoint interpretation thanks to the micro-reversibility relation $p_{\Omega'}(-\vec{\omega}'|\vec{x}, -\vec{\omega}) = p_{\Omega}(\vec{\omega}|\vec{x}, \vec{\omega}')$. The physical picture then becomes that of a photon initially in direction $-\vec{\omega}$ scattered in direction $-\vec{\omega}'$.

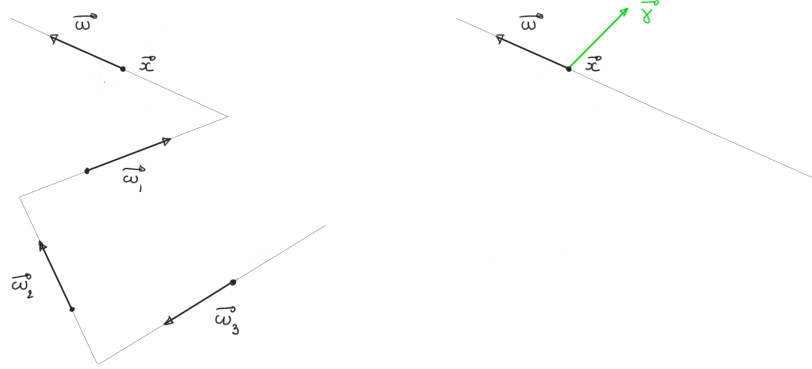


Figure 3: Left: a multiple-scattering photon trajectory leading to location \vec{x} and transport direction $\vec{\omega}$. Right: its correspondence for angular derivatives (rotation direction $\vec{\gamma}$). Scattering vanishes. The physics of angular derivatives involves absorption and sources along the line of sight but this line of sight is uninterrupted from the surface to the observation location \vec{x} in direction $\vec{\omega}$.

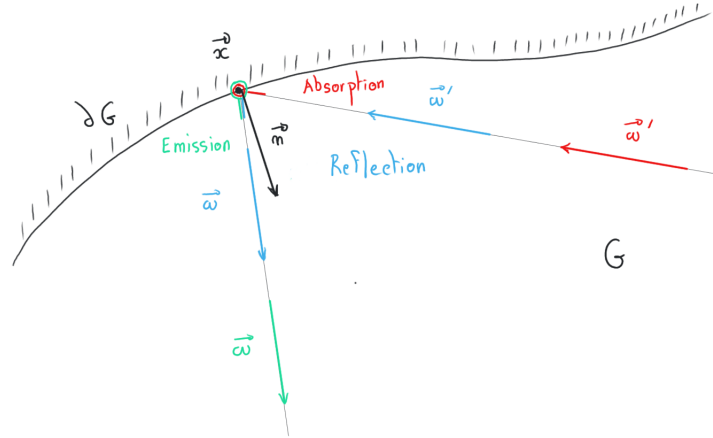


Figure 4: Sources (emission) and collisions (absorption and reflection) at the boundary. The formulation of Eq. 4 favors a reciprocal/adjoint interpretation thanks to the micro-reversibility relation $(\vec{\omega} \cdot \vec{n})\rho(\vec{x}, -\vec{\omega})p_{\Omega',b}(-\vec{\omega}'|\vec{x}, -\vec{\omega}) = -(\vec{\omega}' \cdot \vec{n})\rho(\vec{x}, \vec{\omega}')p_{\Omega,b}(\vec{\omega}|\vec{x}, \vec{\omega}')$. The physical picture then becomes that of a photon initially in direction $-\vec{\omega}$ reflected in direction $-\vec{\omega}'$.

- The physical meaning of $S_{b,\vec{\gamma}}$ is quite simple, with nothing else than the angular derivative of S_b and of the product $\rho p_{\Omega',b}$ (i.e. the bi-directional reflectivity function). Similar derivatives appear in $S_{\vec{\gamma}}$ (the angular derivative of S_b and $p_{\Omega'}$, i.e. the single scattering phase function), but there is an additional term: $-\partial_{1,\vec{\gamma}\wedge\vec{\omega}}I$. This term is simply due to the fact that when rotating the line of sight of an elementary angle $\delta\varphi$, any target location at distance r is moved along the arc of a distance $r\delta\varphi$, which introduces a spatial derivative (see Fig. 6).

The sources $S_{\vec{\gamma}}$ and $S_{b,\vec{\gamma}}$ can be reformulated, depending on the configuration and the addressed question, in order to highlight a chosen set of features of angular derivatives. Hereafter, as an example, we put forward the fact that when reaching a state of radiative equilibrium, intensity is isotropic and therefore $\partial_{2,\vec{\gamma}}I$ is null whatever the rotation direction $\vec{\gamma}$: there must be no sources for $\partial_{2,\vec{\gamma}}I$. Equations 8 and 10 can be transformed the following way to help picturing this equilibrium limit:

$$S_{\vec{\gamma}} = \partial_{2,\vec{\gamma}}S - \partial_{1,\vec{\gamma}\wedge\vec{\omega}}I + k_s \int_{4\pi} \partial_{2,\vec{\gamma}} p_{\Omega'}(-\vec{\omega}'|\vec{x}, -\vec{\omega})d\vec{\omega}' (I(\vec{x}, \vec{\omega}') - I) \quad (13)$$

$$S_{b,\vec{\gamma}} = \partial_{2,\vec{\gamma}}S_b + \partial_{2,\vec{\gamma}}\rho(\vec{x}, -\vec{\omega})I + \partial_{2,\vec{\gamma}}\rho(\vec{x}, -\vec{\omega}) \int_{\mathcal{H}'} p_{\Omega',b}(-\vec{\omega}'|\vec{x}, -\vec{\omega})d\vec{\omega}' (I(\vec{x}, \vec{\omega}') - I) + \rho(\vec{x}, -\vec{\omega}) \int_{\mathcal{H}'} \partial_{2,\vec{\gamma}}p_{\Omega',b}(-\vec{\omega}'|\vec{x}, -\vec{\omega})d\vec{\omega}' (I(\vec{x}, \vec{\omega}') - I) \quad (14)$$

This leaves us with two terms for $S_{\vec{\gamma}}$ and three terms for $S_{b,\vec{\gamma}}$:

- The first term of $S_{\vec{\gamma}}$ is the difference of two terms, $\partial_{2,\vec{\gamma}}S$ and $\partial_{1,\vec{\gamma}\wedge\vec{\omega}}I$, that are both null at equilibrium. When the radiative transfer problem is compatible with equilibrium, $S = k_a I^{eq}(T)$ is isotropic and its angular derivative is null. At equilibrium $I = I^{eq}(T)$ is uniform and its spatial derivative is null.
- The second term of $S_{\vec{\gamma}}$ is null at equilibrium because $I(\vec{x}, \vec{\omega}') = I = I^{eq}(T)$. It is obtained by noticing that

$$\int_{4\pi} \partial_{2,\vec{\gamma}} p_{\Omega'}(-\vec{\omega}'|\vec{x}, -\vec{\omega})d\vec{\omega}' I = I \int_{4\pi} \partial_{2,\vec{\gamma}} p_{\Omega'}(-\vec{\omega}'|\vec{x}, -\vec{\omega})d\vec{\omega}' = I \partial_{2,\vec{\gamma}} \int_{4\pi} p_{\Omega'}(-\vec{\omega}'|\vec{x}, -\vec{\omega})d\vec{\omega}' = I \partial_{2,\vec{\gamma}} 1 = 0 \quad (15)$$

- The first term of $S_{b,\vec{\gamma}}$ is the sum of two terms, $\partial_{2,\vec{\gamma}}S_b$ and $\partial_{2,\vec{\gamma}}\rho(\vec{x}, -\vec{\omega})I$, that compensate each other exactly at equilibrium. Indeed when the radiative transfer problem is compatible with equilibrium, $S_b = (1 - \rho(\vec{x}, -\vec{\omega}))I^{eq}(T)$ and $I^{eq}(T)$ is isotropic. Therefore

$$\partial_{2,\vec{\gamma}}S_b = -\partial_{2,\vec{\gamma}}\rho(\vec{x}, -\vec{\omega})I^{eq}(T) \quad (16)$$

As $I = I^{eq}(T)$ at equilibrium

$$\partial_{2,\vec{\gamma}}\rho(\vec{x}, -\vec{\omega})I = \partial_{2,\vec{\gamma}}\rho(\vec{x}, -\vec{\omega})I^{eq}(T) \quad (17)$$

and the sum $\partial_{2,\vec{\gamma}}S_b + \partial_{2,\vec{\gamma}}\rho(\vec{x}, -\vec{\omega})I$ is null.

- The second term of $S_{b,\vec{\gamma}}$ is obtained by noting that

$$\partial_{2,\vec{\gamma}}\rho(\vec{x}, -\vec{\omega}) \int_{\mathcal{H}'} p_{\Omega',b}(-\vec{\omega}'|\vec{x}, -\vec{\omega})d\vec{\omega}' I = \partial_{2,\vec{\gamma}}\rho(\vec{x}, -\vec{\omega})I \int_{\mathcal{H}'} p_{\Omega',b}(-\vec{\omega}'|\vec{x}, -\vec{\omega})d\vec{\omega}' = \partial_{2,\vec{\gamma}}\rho(\vec{x}, -\vec{\omega})I \quad (18)$$

which compensates with the second part of the first term. At equilibrium this second term is null because $I(\vec{x}, \vec{\omega}') - I = I^{eq}(T) - I^{eq}(T) = 0$.

- The third term of $S_{b,\vec{\gamma}}$ is obtained by noting that

$$\int_{\mathcal{H}'} \partial_{2,\vec{\gamma}}p_{\Omega',b}(-\vec{\omega}'|\vec{x}, -\vec{\omega})d\vec{\omega}' I = I \partial_{2,\vec{\gamma}} \int_{\mathcal{H}'} p_{\Omega',b}(-\vec{\omega}'|\vec{x}, -\vec{\omega})d\vec{\omega}' = I \partial_{2,\vec{\gamma}} 1 = 0 \quad (19)$$

This third term is null at equilibrium because $I(\vec{x}, \vec{\omega}') - I = I^{eq}(T) - I^{eq}(T) = 0$.

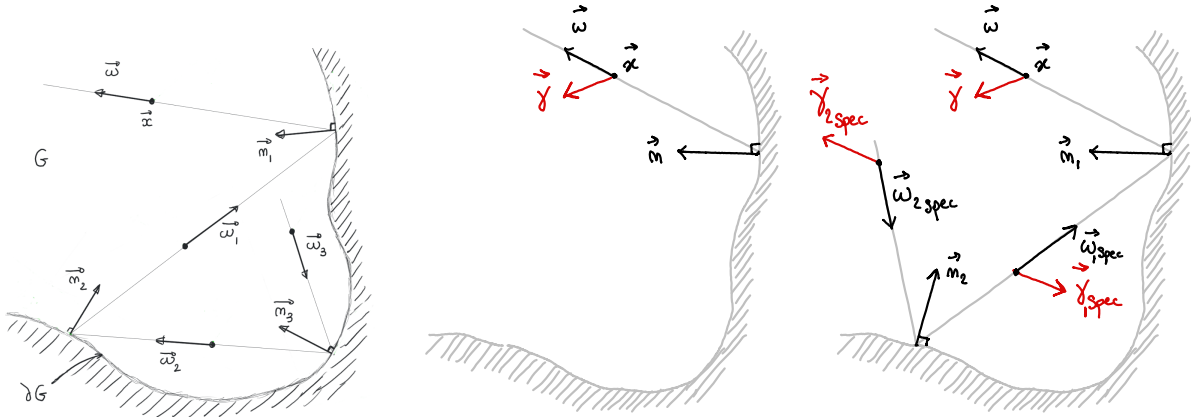


Figure 5: **Left:** a multiple-reflection photon trajectory leading to location \vec{x} and transport direction $\vec{\omega}$ for diffuse surfaces. **Center:** its correspondence for angular derivatives (derivation rotation direction $\vec{\gamma}$). The angular derivative is not reflected on a diffuse surface. **Right:** its correspondence in the case of specular surfaces. The characteristics of usual specular reflection is unchanged, but the derivation direction is modified at each reflection event. Note that once again we favor a reciprocal reading of this transport physics: $\vec{\gamma}$ is transformed into $\vec{\gamma}_{1,spec}$ at the first reflection backward along the line of sight, then $\vec{\gamma}_{1,spec}$ is transformed into $\vec{\gamma}_{2,spec}$ at the second reflection, etc.

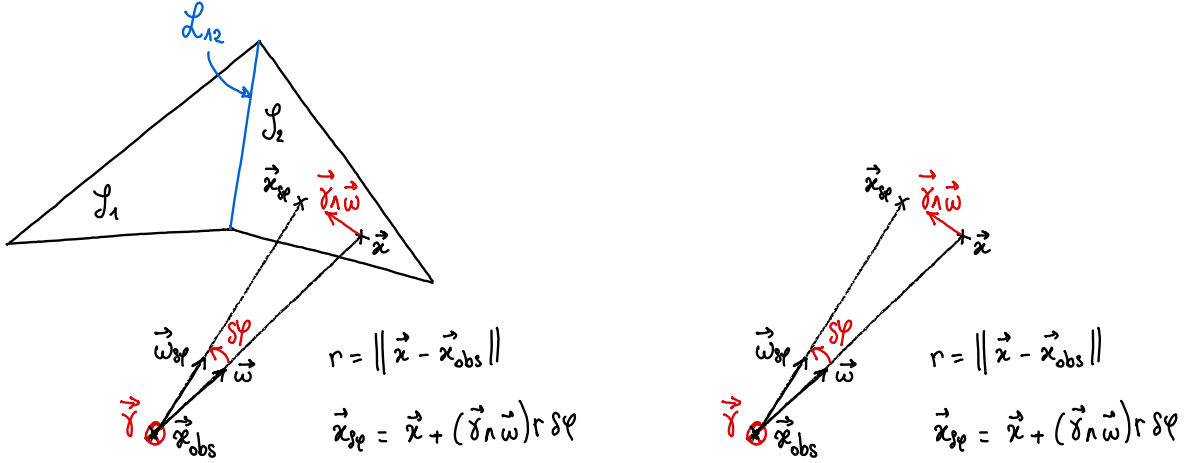


Figure 6: **Left:** In a transparent medium the intensity viewed at the observation point \vec{x}_{obs} in the direction $\vec{\omega}$ is the intensity leaving the surface \mathcal{S}_2 at position \vec{x} . When rotating the direction of an angle $\delta\varphi$ around the rotation axis $\vec{\gamma}$ oriented toward us the surface target location changes to $\vec{x}_{\delta\varphi} = \vec{x} + (\vec{\gamma} \wedge \vec{\omega}) r \delta\varphi$ with r being the length of the line of sight. The angular derivative of the $I(\vec{x}_{obs}, \vec{\omega})$ can therefore be regarded as a spatial derivative along the surface \mathcal{S}_2 in the differentiation direction $\vec{\gamma} \wedge \vec{\omega}$: $\partial_{1, \vec{\gamma} \wedge \vec{\omega}} I(\vec{x}, \vec{\omega})$. **Right:** In presence of a participating medium the angular derivative of the intensity $I(\vec{x}_{obs}, \vec{\omega})$ is influenced by the intensity spatial variation along all the line of sight. This contribution is manifested by the spatial derivative volume source in the angular derivative transport model.

Let us write hereafter Eq. 10 or Eq. 14 at the two limits of purely diffuse and purely specular surfaces. At the diffusive limit $p_{\Omega',b}(-\vec{\omega}'|\vec{x}, -\vec{\omega}) = \frac{|\vec{\omega}' \cdot \vec{n}|}{\pi}$. Equation 10 gives

$$(S_{b,\vec{\gamma}})_{diff} = \partial_{2,\vec{\gamma}} S_b + \partial_{2,\vec{\gamma}} \rho(\vec{x}, -\vec{\omega}) \int_{\mathcal{H}'} \frac{|\vec{\omega}' \cdot \vec{n}|}{\pi} d\vec{\omega}' I(\vec{x}, \vec{\omega}') \quad (20)$$

and Eq. 14 gives

$$(S_{b,\vec{\gamma}})_{diff} = \partial_{2,\vec{\gamma}} S_b + \partial_{2,\vec{\gamma}} \rho(\vec{x}, -\vec{\omega}) I + \partial_{2,\vec{\gamma}} \rho(\vec{x}, -\vec{\omega}) \int_{\mathcal{H}'} \frac{|\vec{\omega}' \cdot \vec{n}|}{\pi} d\vec{\omega}' (I(\vec{x}, \vec{\omega}') - I) \quad (21)$$

At the specular limit $p_{\Omega',b}(-\vec{\omega}'|\vec{x}, -\vec{\omega}) = \delta(\vec{\omega}' - \vec{\omega}_{spec})$ where $\vec{\omega}_{spec} = \vec{\omega} - 2(\vec{\omega} \cdot \vec{n})\vec{n}$. Equation 10 or Eq. 14 give the same following expression:

$$(S_{b,\vec{\gamma}})_{spec} = \partial_{2,\vec{\gamma}} S_b + \partial_{2,\vec{\gamma}} \rho(\vec{x}, -\vec{\omega}) I(\vec{x}, \vec{\omega}_{spec}) - \rho(\vec{x}, -\vec{\omega}) \partial_{2,\vec{\gamma}_{spec}} I(\vec{x}, \vec{\omega}_{spec}) \quad (22)$$

where $\vec{\gamma}_{spec} = \vec{\gamma} - 2(\vec{\gamma} \cdot \vec{n})\vec{n}$.

3 Boundary discontinuities at the junction of two plane surfaces

We have set up a transport model for $\partial_{2,\vec{\gamma}} I$. The corresponding source terms define the emission, in the elementary solid angle $d\vec{\omega}$ around $\vec{\omega}$,

- of any elementary volume $dv \equiv d\vec{x}$ around $\vec{x} \in G$:

$$\text{Volume emission: } S_{\vec{\gamma}}[I] dv d\vec{\omega} \quad (23)$$

- of any elementary surface $d\sigma \equiv d\vec{x}$, of normal \vec{n} , around $\vec{x} \in \partial G$

$$\text{Surface emission: } S_{b,\vec{\gamma}}[I](\vec{\omega} \cdot \vec{n}) d\sigma d\vec{\omega} \quad (24)$$

When the boundary is discrete as an ensemble of plane surfaces, typically an ensemble of triangles, then the intensity in a given direction becomes discontinuous at the edge \mathcal{L}_{12} between adjacent plane surfaces ($\mathcal{S}_1, \mathcal{S}_2$). This discontinuity arise either because the intensity sources are different on the two plane surfaces (different surface temperatures for thermal emission), or because of different reflection properties or different surface orientations. In the angular derivative model this apparent discontinuity is captured by the spatial derivative in the volume source $S_{\vec{\gamma}}$. Indeed, Figure 6 shows that intensity spatial variation impacting the angular derivative translate into a spatial derivative in the model. The spatial derivative will therefore account for the intensity spatial discontinuity on the discrete boundary. It is shown in PART 1 that the boundary discontinuities lead to localized sources along the triangles edges and in the angular derivative model these linear sources will only appear as a result of the coupling with the spatial derivative model in the volume.

Beyond spatial discontinuity, another kind of radiative discontinuity have to be considered at the boundary when the outgoing intensity is angularly discontinuous. A very common example is the solar cone boundary condition designed to simulate solar processes radiative transfers [10, 12]. In these configurations the intensity boundary condition of the processes reflective elements (e.g. heliostats) is a specular reflection of the angularly discontinuous incoming intensity (inside the solar cone the intensity is that of the sun and outside the solar cone the intensity is null). When computing the angular derivative in such configurations the boundary condition described by equation 9 will require an angular Dirac formulation arising from the angular derivative of the discontinuous incoming specular intensity. When integrated (e.g to compute the radiative power collected by the solar processes) the angular Dirac distributions will lead to localized sources along the solar cone boundary.

4 Path statistics and Monte Carlo

Notice: This is a preliminary version of the final paper, consequently, although they have been implemented, the examples and corresponding algorithms are not included in the paper yet. We here only describe what will be soon detailed in this section.

Our main point in this text is that the model of the angular derivative of intensity is so similar to the model of intensity (the radiative transfer model) that the whole radiative transfer literature about path statistics and Monte Carlo simulation can be reinvested in a straightforward manner to numerically estimate angular derivatives. In this last section, we illustrate the practical meaning of this statement. The technical steps that we will highlight with some specificity are the following:

- As already mentioned the angular derivative is not scattered in a participating media and not reflected at reflective surfaces except for specular surfaces. In that case the angular derivative boundary condition depends on the specular angular derivative but with a different rotation axis. In terms of Monte-Carlo algorithm the angular derivative path reaching a specular surface will be reflected but with a special care of changing the rotation direction at each surface encounter.
- Via its volume and surface sources the model of angular derivative is coupled to the radiative transfer model (at the boundaries via $S_{b,\vec{\gamma}}$ and in the medium via $S_{\vec{\gamma}}$) and to the spatial derivative transport model (in the medium via $S_{\vec{\gamma}}$). This couplings can be handled using the very same Monte Carlo techniques as those recently developed for the coupling of radiative transfer with other heat-transfer modes[2, 3, 4, 5], or the coupling of radiative transfer with electromagnetism and photosynthesis[6, 7, 8, 9]. In both cases, the main idea is double randomisation: in standard Monte Carlo algorithms for pure radiative transfer, when a volume source or a surface source is required it is known (typically the temperature is known for infrared radiative transfer); if it is not known but a Monte Carlo algorithm is available to numerically estimate the source as an average of a large number of sampled Monte Carlo weights, then in the coupled problem the source can be replaced by only one sample. The resulting coupled algorithm is rigorously unbiased thanks to the law of expectation (“the expectation of an expectation is an expectation”). In practice, this means that the Monte Carlo algorithms estimating angular derivatives can be designed as if the sources were known, and when a source is required that depends on $I(\vec{x}', \vec{\omega}')$ then one single radiative path is sampled as if estimating the intensity $I(\vec{x}', \vec{\omega}')$ with any available Monte Carlo algorithm. When a source is required that depends on $\partial_{1,\vec{\gamma}\wedge\vec{\omega}}I(\vec{x}', \vec{\omega}')$ then on single spatial derivative path is sampled as if estimating the spatial derivative $\partial_{1,\vec{\gamma}\wedge\vec{\omega}}I(\vec{x}', \vec{\omega}')$ with any available Monte Carlo algorithm. When the boundaries are discrete as in a set of plane triangles solving the spatial derivative requires to sample linear sources as described in PART 1.

We provide hereafter some examples of algorithms that illustrate these three points. They estimate $\partial_{2,\vec{\gamma}}I$ at a location \vec{x} in a direction $\vec{\omega}$. Each example is implemented and tested against exact solutions (see Fig. 7):

- Solution 1: the solution provided by Chandrasekhar for a uniform flux in a stratified heterogeneous scattering atmosphere[15] (see Appendix F). This one-dimension solution is cut by a three-dimension closed boundary (a sphere or a cube) and the boundary conditions are adjusted to insure that Chandrasekhar’s solution is still satisfied. In Chandrasekhar’s solution, there is no volume absorption; when we need to add volume absorption, we compensate it by introducing an adjusted volume emission insuring that Chandrasekhar’s solution is again still satisfied.
- Solution 2: a transparent slab between a black isothermal surface at T_{hot} and an emitting/reflecting diffuse surface of temperature T_{cold} everywhere except for a square subsurface where the temperature is T_{hot} ;

These algorithms sample Monte Carlo weights noted w_Z for each quantity Z , meaning that N samples $w_{Z,1}, w_{Z,2} \dots w_{Z,N}$ are required to estimate Z as $\tilde{Z} = \frac{1}{N} \sum_{i=1}^N w_{Z,i}$,

- w_I for the intensity I when referring to a standard Monte Carlo algorithm estimating the solution of the radiative transfer equation;
- $w_{\partial_{2,\vec{\gamma}}I}$ for the angular derivative of intensity;

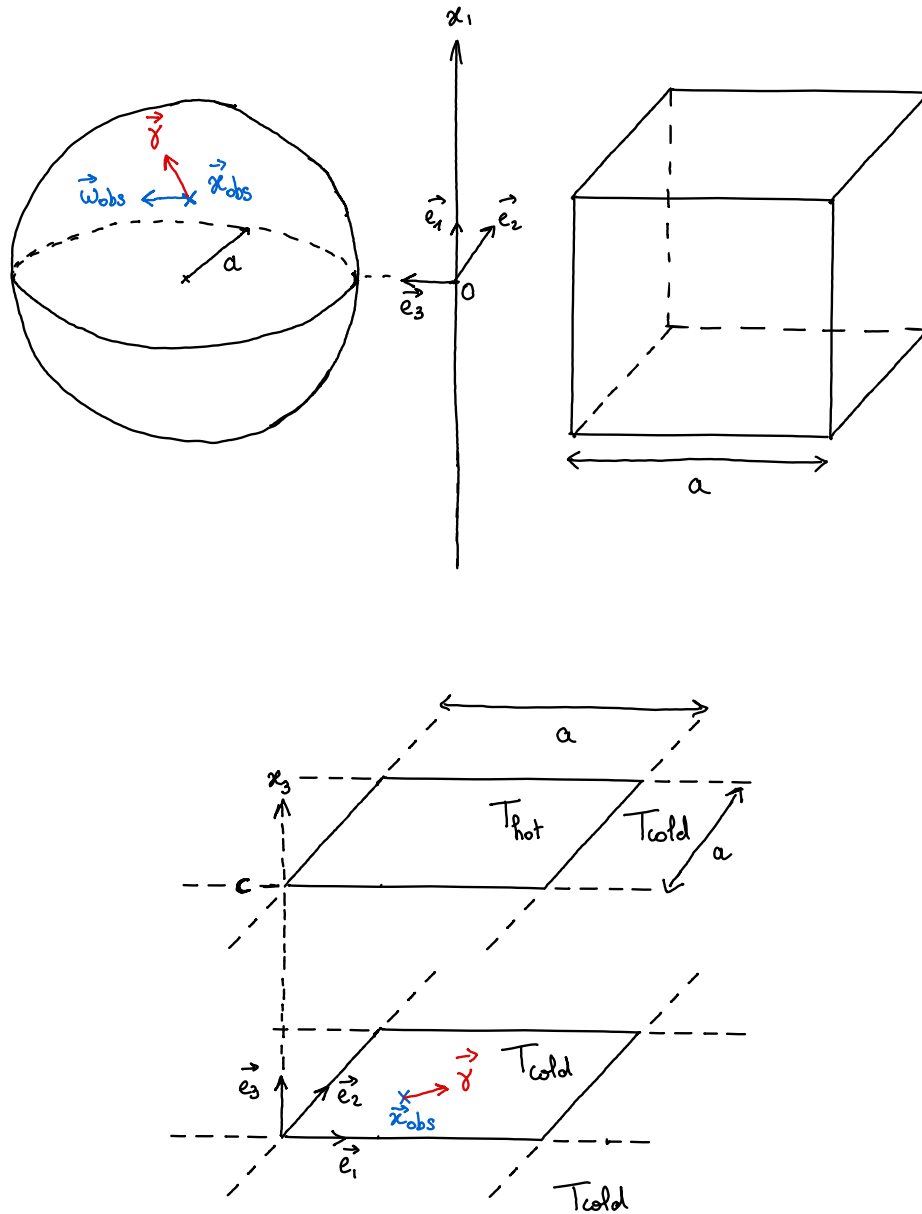


Figure 7: The two configurations used for illustration. Top: the solution provided by Chandrasekhar for a uniform flux in a stratified heterogeneous scattering atmosphere cut by a three-dimension closed boundary (a sphere of radius a or a cube of side a). Bottom: a transparent slab of thickness c between a black isothermal surface at T_{hot} and an emitting/reflecting diffuse surface of temperature T_{cold} everywhere except for a square subsurface of side a where the temperature is T_{hot} . The emissivity ϵ of the emitting/reflecting diffuse surface is uniform.

F Chandrasekhar's exact solution for heterogeneous multiple-scattering atmospheres

In a heterogeneous, purely scattering and infinite medium, with plane parallel stratified intensity field, the radiative transfer equation has an analytical solution $I(\tau, \mu)$ ([15]):

$$I(\tau, \mu) = \frac{\eta(0)}{4\pi} + \frac{3}{4\pi}j[(g-1)\tau + \mu] \quad (25)$$

with $\eta(0)$ and j being constants, g is the asymmetric coefficient, τ is the optical thickness normal to the plane of stratification and μ the direction cosine. \vec{e}_1 being the plane normal unit vector and a vector of the Cartesian coordinate system $(\vec{e}_1, \vec{e}_2, \vec{e}_3)$ we state the normal optical thickness as:

$$\tau = \int_0^{\vec{x} \cdot \vec{e}_1} k_s(l) dl \quad (26)$$

with \vec{x} the position in the infinite medium. The cosine $\mu = \vec{\omega} \cdot \vec{e}_1$ with $\vec{\omega}$ the transport direction. We state the analytical intensity \mathcal{L} as $\mathcal{L}(\vec{x}, \vec{\omega}) = I(\tau, \mu)$.

PART 3: A physical model and a Monte-Carlo estimate for the geometric sensitivity of the specific intensity

Abstract

Starting from the radiative transfer equation and its usual boundary conditions, the objective of the present article is to design a Monte Carlo algorithm estimating the geometric sensitivity of the specific intensity. There are two common ways to address this question. The first consists in using two independent Monte Carlo estimates for the specific intensity in two different geometries and using a finite difference to approximate the geometric sensitivity; the associated uncertainties are difficult to handle. The second consists in considering any Monte Carlo algorithm for the specific intensity, writing down its associated integral formulation, differentiating this integral with regard to a geometrical parameter, and reformulating it so that it defines a new Monte Carlo algorithm directly estimating the geometric sensitivity of the specific intensity; the corresponding formal developments are very demanding [1]. We here explore an alternative approach in which we differentiate both the radiative transfer equation and its boundary conditions to set up a physical model for the geometric sensitivity of the specific intensity. Then a standard path integral translation is made to design a Monte Carlo algorithm solving this model. The only subtlety at this stage is that the model for the geometric sensitivity is coupled to the model for the specific intensity itself and coupled to both models of specific intensity spatial and angular derivatives (see PART 1 and PART 2). The path space associated to the geometric sensitivity of the specific intensity is therefore coupled to the path space associated to specific intensity (standard radiative transfer paths) and to the path space associated to the specific intensity spatial and angular derivative) When designing a Monte Carlo algorithm for the coupled problem a double randomization approach is therefore required.

1 Introduction

We address the question of designing a model and numerically estimating the geometric sensitivity $s \equiv s(\vec{x}, \vec{\omega}, \tilde{\pi})$ of the specific intensity $I \equiv I(\vec{x}, \vec{\omega}, \tilde{\pi})$ at location \vec{x} in the transport direction $\vec{\omega}$ and for a geometry configured by the parameter $\tilde{\pi}$. The intensity has three independent variables:

- The position \vec{x} is a vector of \mathbb{R}^3 that belongs to the set $G \subset \mathbb{R}^3$ of the geometric domain positions. The geometric domain is bounded by ∂G , i.e. the set G includes the interior of the geometric domain and its boundary : $G = \overset{\circ}{G} \cup \partial G$.
- The direction $\vec{\omega}$ is an element of the unit sphere \mathcal{S} .
- The geometric parameter $\tilde{\pi}$ is an element of \mathbb{R} . The intensity is sensitive to a geometry perturbation in every position \vec{x} of G and every direction $\vec{\omega}$ of \mathcal{S} , it will then be referred as $I = I(\vec{x}, \vec{\omega}, \tilde{\pi})$ and the domain $G \equiv G(\tilde{\pi}) = \overset{\circ}{G}(\tilde{\pi}) \cup \partial G(\tilde{\pi})$.

The geometric sensitivity is the intensity derivative with regard to the geometric parameter:

$$s(\vec{x}, \vec{\omega}, \tilde{\pi}) = \partial_{\tilde{\pi}} I(\vec{x}, \vec{\omega}, \tilde{\pi}) = \partial_3 I(\vec{x}, \vec{\omega}, \tilde{\pi}) \quad (1)$$

with $s(\vec{x}, \vec{\omega}, \tilde{\pi})$ a scalar function of three independent variables that quantifies the impact of a boundary perturbation on the intensity at the position $\vec{x} \in G(\tilde{\pi})$ and in the direction $\vec{\omega} \in \mathcal{S}$ (see figure 1).

The reason why we address s as a function of the same independent variables as the intensity I , instead of having position $\vec{x} = \vec{x}(\tilde{\pi})$ and direction $\vec{\omega} = \vec{\omega}(\tilde{\pi})$ following the medium deformation, is in the attempt to draw explicit connections between the standard radiative transfer models and the geometric sensitivity models. We make the very same choice in PART 1 as far as spatial derivatives are concerned (considering only one spatial direction instead of the gradient) and in PART 2 as far as angular derivatives are concerned (considering only one rotation direction instead of an angular gradient). Starting from the available transport physics for I , our main objective is to introduce a new, very similar transport physics for s . Then all the

* plapeyre@uwaterloo.ca

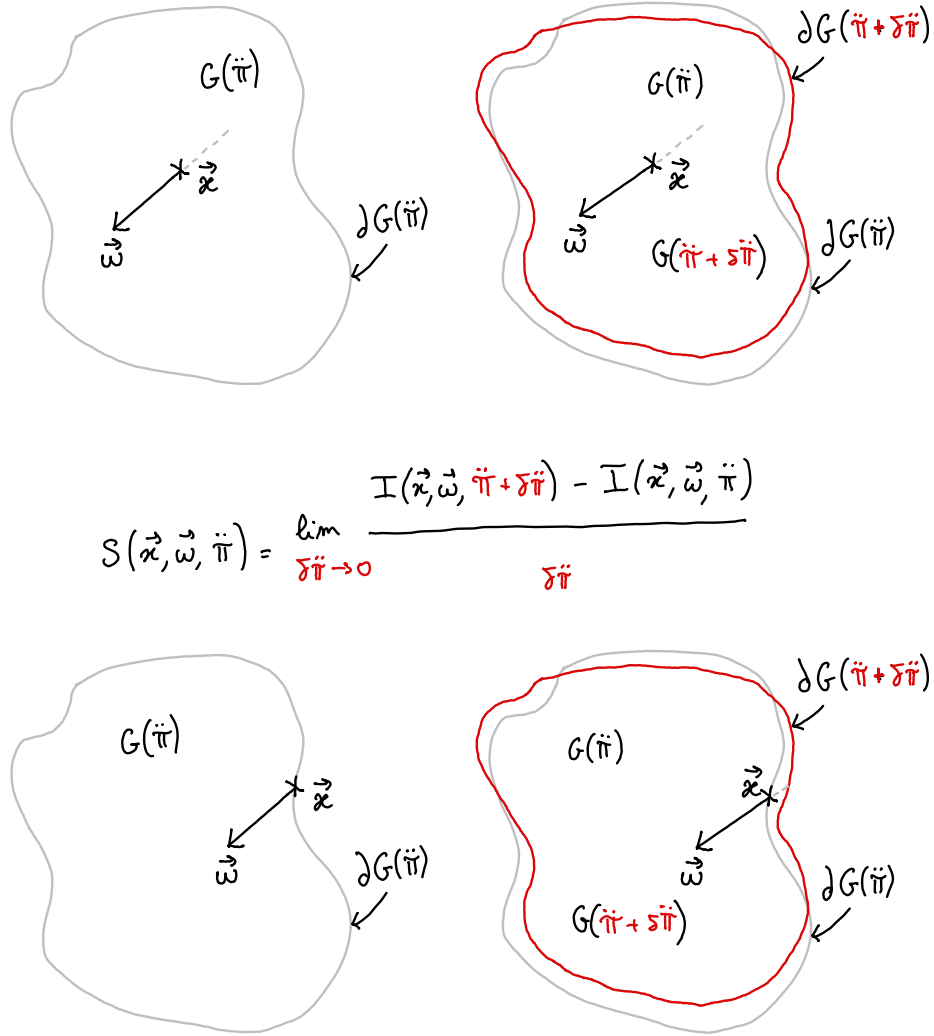


Figure 1: The geometric sensitivity $s(\vec{x}, \vec{w}, \ddot{\pi})$ pictured for a geometry deformation generated by an elementary perturbation of the geometrical parameter $\ddot{\pi}$. Position \vec{x} and transport direction \vec{w} are independent of the geometrical parameter and therefore do not undergo the volume and the boundary deformations. The sensitivity only accounts for the intensity modifications at a given position and direction due to a change of the geometry. **Top:** geometric sensitivity in the volume, **bottom:** geometric sensitivity at the boundary.

standard practice of analysing and numerically simulating I can be directly translated into new tools for analysing and numerically simulating geometric sensitivities.

Standard radiative transfer physics can be gathered into two equations: the partial differential equation governing I at any location inside the domain $\overset{\circ}{G}$ (the radiative transfer equation) and an integral constraint at the boundary ∂G (the incoming radiation equation), relating I in any direction toward the domain to I in all the directions exiting the domain. Recognizing, in the writing of these equations, the processes of volume emission/absorption/scattering and surface emission/absorption/reflection, translating them into path statistics is quite straightforward. We will do the same with s :

- Two equations will be constructed for s by differentiating the radiative transfer equation and the incoming radiation boundary equation (differentiating the equations of the I model).
- The resulting equations will be physically interpreted using transport physics processes, defining volume emission/absorption/scattering and surface emission/absorption/reflection processes for the geometric sensitivity. A particular attention will be devoted to the identifications of the geometric sensitivity sources.
- Path statistics will then be defined for s , from the sources to the location and direction of observation.

Numerically estimating s will then be simply achieved using a Monte Carlo approach, i.e. sampling large numbers of paths. We will display the observed variance of the resulting Monte Carlo estimate but no attempt will be made to optimize convergence in the frame of the present article. Configurations for which s is known analytically will be used both to validate the formal developments and to illustrate the physical meaning of each of the identified processes of emission, absorption, scattering and reflection as far as geometrical sensitivities are concerned.

Even if the presentation of the mathematical developments remains strictly formal, we will try to stick to the spirit of radiative transfer: trying to write down the physics of geometric sensitivities by maintaining a parallel, as strict as possible, with the physics of photon transport. In the case of geometric sensitivity this parallel is complete. Beer-Lambert law will be entirely recovered, volume absorption, scattering and surface reflection of the geometric sensitivity will also be recovered.

The text is essentially a short note with three sections:

- Section 2 provides the model in its differential form for boundary surfaces without any discontinuities.
- Section 3 deals with the specific case of discontinuities at the junction between two plane surfaces.
- Section 4 provides the associated statistical paths and illustrates how a standard Monte Carlo approach can be used to estimate s (or any radiative transfer observable defined as an integral of s).

2 Convex domain with differentiable boundaries

The model for the intensity Noting \mathcal{C} the collision operator, the stationary monochromatic radiative transfer equation is

$$\vec{\nabla} I \cdot \vec{\omega} = \mathcal{C}[I] + S \quad \vec{x} \in G \quad (2)$$

with

$$\mathcal{C}[I(\vec{x}, \vec{\omega})] = -k_a(\vec{x})I(\vec{x}, \vec{\omega}) - k_s(\vec{x})I(\vec{x}, \vec{\omega}) + k_s(\vec{x}) \int_{4\pi} p_{\Omega'}(-\vec{\omega}'|\vec{x}, -\vec{\omega})d\vec{\omega}' I(\vec{x}, \vec{\omega}') \quad (3)$$

where k_a is the absorption coefficient, k_s the scattering coefficient and $p_{\Omega'}(-\vec{\omega}'|\vec{x}, \vec{\omega})$ is the probability density that the scattering direction is $-\vec{\omega}'$ for a photon scattered at \vec{x} coming from direction $-\vec{\omega}$ (the single scattering phase function, see Figure 2 for a single collision and Figure 3 for a multiple-scattering photon trajectory). $S \equiv S(\vec{x}, \vec{\omega})$ is the volumic source. When this source is due to thermal emission, under the assumption that the matter is in a state of local thermal equilibrium, then it is isotropic and $S = k_a I^{eq}(T)$ where T is the local temperature and I^{eq} is the specific intensity at equilibrium (following Planck function).

At the boundary, noting \mathcal{C}_b the reflection operator, the incoming radiation equation is

$$I = \mathcal{C}_b[I] + S_b \quad \vec{x} \in \partial G ; \vec{\omega} \cdot \vec{n} > 0 \quad (4)$$

with

$$\mathcal{C}_b[I] = \rho(\vec{x}, -\vec{\omega}) \int_{\mathcal{H}'} p_{\Omega', b}(-\vec{\omega}'|\vec{x}, -\vec{\omega})d\vec{\omega}' I(\vec{x}, \vec{\omega}') \quad (5)$$

where \vec{n} is the normal to the boundary at \vec{x} , oriented toward the inside, $\vec{\omega}$ is a direction within the inside hemisphere \mathcal{H} , $\vec{\omega}'$ is any direction within the outside hemisphere \mathcal{H}' , $\rho(\vec{x}, -\vec{\omega})$ is the surface reflectivity for a photon impacting the boundary in direction $-\vec{\omega}$, and $p_{\Omega',b}(-\vec{\omega}'|\vec{x}, -\vec{\omega})$ is the probability density that the reflection direction is $-\vec{\omega}'$ for a photon reflected at \vec{x} coming from direction $-\vec{\omega}$ (the product $\rho p_{\Omega',b}$ is the bidirectional reflectivity density function, see Figure 4 collision at the boundary and Figure 5 for a multiple-reflection photon trajectory). When the surfacic source $S_b \equiv S_b(\vec{x}, \vec{\omega})$ is due to the thermal emission of an opaque surface, under the assumption that the matter at this surface is in a state of local thermal equilibrium, then $S_b = (1 - \rho(\vec{x}, -\vec{\omega})) I^{eq}(T_b)$ where T_b is the local surface temperature.

The model for the geometric sensitivity Using the linearity of the collision operator, differentiating equation 2 with regard to $\vec{\pi}$, provides a transport model for s :

$$\vec{\nabla}_s \cdot \vec{\omega} = \mathcal{C}[s] + S_{\vec{\pi}}[I] \quad \vec{x} \in G \quad (6)$$

with $S_{\vec{\pi}}[I] = \partial_{\vec{\pi}} \mathcal{C}[I] + \partial_{\vec{\pi}} S$, leading to

$$\begin{aligned} S_{\vec{\pi}}[I] = & -\partial_{\vec{\pi}} k_a I - \partial_{\vec{\pi}} k_s I \\ & + \partial_{\vec{\pi}} k_s \int_{4\pi} p_{\Omega'}(-\vec{\omega}'|\vec{x}, -\vec{\omega}) d\vec{\omega}' I(\vec{x}, \vec{\omega}') \\ & + k_s \int_{4\pi} \partial_{\vec{\pi}} p_{\Omega'}(-\vec{\omega}'|\vec{x}, -\vec{\omega}) d\vec{\omega}' I(\vec{x}, \vec{\omega}') \\ & + \partial_{\vec{\pi}} S \end{aligned} \quad (7)$$

Establishing the boundary condition for equation 6 is less straightforward because the surface properties are attached to the boundary. Differentiating the intensity boundary conditions with regard to a geometrical parameter therefore relies on:

- Identifying the surface material radiative properties. The material properties will be defined as the surface radiative properties stated in a specific reference domain, also referred as material domain, where the reference geometry is independent of the geometrical parameter. The material domain reference boundary ∂U is mapped to the regular spatial domain geometry boundary $\partial G(\vec{\pi})$ via the application $\mathcal{Z} : \partial U \times \mathbb{R} \rightarrow \partial G(\vec{\pi})$ so that any position in the material domain $\vec{y} \in \partial U$ can be linked to a position in the spatial domain: $\vec{y} = \mathcal{Z}(\vec{y}, \vec{\pi})$ with $\vec{y} \in \partial G(\vec{\pi})$ (see figure 6). In the material domain the surface radiative properties will therefore be functions of the position vector \vec{y} whereas in the spatial domain they will be functions of \vec{y} . In radiative transfer the surface radiative properties are mainly stated with regard to the surface local frame oriented by the surface normal vector (i.e. the reflection coefficient $\rho(\vec{x}, -\vec{\omega})$ or the reflection density probability function $p(-\vec{\omega}'|\vec{x}, -\vec{\omega})$ with $\vec{\omega}$ and $\vec{\omega}'$ referenced in the local frame). Defining the surface radiative properties on the material domain implies stating a material local frame oriented by a material surface normal vector. The material local frame and each emission/absorption/reflection directions $\vec{\omega}$ used to describe the surface material radiative properties will then be mapped to the spatial surface local frame via the application $\Omega : \partial U \times \mathcal{S} \times \mathbb{R} \rightarrow \mathcal{S}$. Therefore any unit vector of the material domain local frame $\vec{\omega}$ (or \vec{n}) can be linked to a unit vector in the spatial domain local frame $\vec{\omega} = \Omega(\vec{y}, \vec{\omega}, \vec{\pi})$ (or $\vec{n} = \Omega(\vec{y}, \vec{n}, \vec{\pi})$) with $\vec{\omega}, \vec{n} \in \mathcal{S}$ (see figure 7). As the geometry deformation can also impact the surface material properties (i.e. changing the micro-structure of the surface and therefore its reflection properties) the material surface radiative properties will be stated as functions of \vec{y} , $\vec{\omega}$ and $\vec{\pi}$ (i.e. $p(-\vec{\omega}'|\vec{y}, -\vec{\omega}, \vec{\pi})$) whereas the corresponding spatial surface properties will be functions of \vec{y} , $\vec{\omega}$ and $\vec{\pi}$ (i.e. $p(-\vec{\omega}'|\vec{y}, -\vec{\omega}, \vec{\pi})$).
- Characterizing the boundary deformation. The geometry boundary deformation is characterized by the boundary deformation vector $\vec{\chi} = \partial_{\vec{\pi}} \mathcal{Z}$ (see figure 8).
- Stating the equivalence between the material and spatial intensities. In the material domain the function $L(\vec{y}, \vec{\omega}, \vec{\pi})$ is the material intensity. The material intensity outgoing the boundary ∂U is equivalent to the specific intensity $I(\vec{y}, \vec{\omega}, \vec{\pi})$ outgoing the spatial domain boundary $\partial G(\vec{\pi})$ which lead to: $I(\vec{y}, \vec{\omega}, \vec{\pi}) = L(\vec{y}, \vec{\omega}, \vec{\pi})$.
- Deriving the geometric sensitivity boundary condition. The mathematical developments leading to the geometric sensitivity boundary condition are detailed in appendix G. They start by differentiating the boundary condition $I(\vec{y}, \vec{\omega}, \vec{\pi})$ with regard to the geometrical parameter. Understanding that \vec{y}

and $\vec{\omega}$ are functions of $\vec{\pi}$ the boundary condition differentiation will automatically lead to spatial and angular derivatives of the intensity revealing couplings of the geometric sensitivity model with the intensity, the intensity spatial derivative and the intensity angular derivative happening at the boundary.

Material and spatial domain formalism (notations $\vec{y}, \vec{y}, \vec{\omega}, \vec{\omega}$) is essential to derive the geometric sensitivity boundary condition (see appendix G). However, once the model for the incoming geometric sensitivity is stated the standard phase space notations are recovered, using \vec{x} for the position and $\vec{\omega}$ for the transport direction. All together, the boundary condition of the transport model for s is

$$s = \mathcal{C}_b[s] + S_{b,\vec{\pi}}[I, \partial_{1,\vec{u}}I, \partial_{1,\vec{\chi}}I, \partial_{2,\vec{\gamma}}I] \quad \vec{x} \in \partial G(\vec{\pi}); \vec{\omega} \cdot \vec{n} > 0 \quad (8)$$

with \vec{n} the normal vector to the boundary $\partial G(\vec{\pi})$ and with $\partial_{1,\vec{\chi}}I$ the intensity spatial derivative in the differentiation direction $\vec{\chi}$ and $\partial_{2,\vec{\gamma}}I$ the intensity angular derivative in the rotation direction $\vec{\gamma}$. The intensity spatial derivative $\partial_{1,\vec{u}}I$ is a results of $\vec{\chi}$ decomposition (in a sum of the transport direction $\vec{\omega}$ and the surface the tangent vector \vec{u} , see appendix H) on the surface local frame. The sensitivity surface source $S_{b,\vec{\pi}}$ is described explicitly in the next paragraph and stated for three limits of boundaries radiative properties: black surfaces, purely diffuse surfaces and purely specular surfaces.

Intermediate summary The model for I was (see Eq. 2 and Eq. 4)

$$\begin{cases} \vec{\nabla} I \cdot \vec{\omega} = \mathcal{C}[I] + S & \vec{x} \in G \\ I = \mathcal{C}_b[I] + S_b & \vec{x} \in \partial G; \vec{\omega} \cdot \vec{n} > 0 \end{cases} \quad (9)$$

The model for s is (see Eq.7 and Eq.8)

$$\begin{cases} \vec{\nabla} s \cdot \vec{\omega} = \mathcal{C}[s] + S_{\vec{\pi}}[I] & \vec{x} \in G \\ s = \mathcal{C}_b[s] + S_{b,\vec{\pi}}[I, \partial_{1,\vec{u}}I, \partial_{1,\vec{\chi}}I, \partial_{2,\vec{\gamma}}I] & \vec{x} \in \partial G; \vec{\omega} \cdot \vec{n} > 0 \end{cases} \quad (10)$$

The main difference is the following:

- In the standard radiative transfer model, the sources S and S_b are given quantities (functions of the volume and surface properties), but in the model for s , the sources $S_{\vec{\pi}}$ and $S_{b,\vec{\pi}}$ depend on I , $\partial_{1,\vec{u}}I$, $\partial_{1,\vec{\chi}}I$ and $\partial_{2,\vec{\gamma}}I$. In pure mathematical terms, they are sources in the model for s only if this model is decoupled from the radiative transfer model, the model of the spatial derivative and the model of the angular derivative. But the complete physics implies that the models are coupled: $S_{b,\vec{\pi}}$ expresses part of this coupling via I , $\partial_{1,\vec{u}}I$, $\partial_{1,\vec{\chi}}I$ and $\partial_{2,\vec{\gamma}}I$ at the boundary. $S_{\vec{\pi}}$ expresses the rest of this coupling via I in the medium.

The surface source at the boundary condition for the geometric sensitivity $s = s(\vec{x}, \vec{\omega}, \vec{\pi})$ is (see appendix G):

$$\begin{aligned} S_{b,\vec{\pi}} = & -\alpha (\mathcal{C}[I] + S) \\ & -\beta \partial_{1,\vec{u}} S_b - \partial_{2,\vec{\gamma}} S_b + \partial_{\vec{\pi}} S_b \\ & -\beta \partial_{1,\vec{u}} \mathcal{C}_b[I] + \partial_{\vec{\pi}} \mathcal{C}_b[I] \\ & -\partial_{2,\vec{\gamma}} \rho(\vec{x}, -\vec{\omega}) \int_{\mathcal{H}'} p_{\Omega'}(-\vec{\omega}'|\vec{x}, -\vec{\omega}) d\vec{\omega}' I \\ & -\rho(\vec{x}, -\vec{\omega}) \partial_{2,\vec{\gamma}} \left(\int_{\mathcal{H}'} p_{\Omega'}(-\vec{\omega}'|\vec{x}, -\vec{\omega}) d\vec{\omega}' I' \right) \\ & -\beta \mathcal{C}_b[\partial_{1,\vec{u}}I] + \mathcal{C}_b[\partial_{1,\vec{\chi}}I] + \mathcal{C}_b[\partial_{2,\vec{\gamma}}I] \end{aligned} \quad (11)$$

Geometric sensitivity boundary condition for a black surface For a black surface at temperature T_b the intensity boundary condition (Eq. 4) becomes:

$$I = S_b = I^{eq}(T_b) \quad \vec{x} \in \partial G(\vec{\pi}); \vec{\omega} \cdot \vec{n} > 0 \quad (12)$$

And the boundary condition for the geometric sensitivity $s = s(\vec{x}, \vec{\omega}, \vec{\pi})$ is:

$$s = S_{b,\vec{\pi}}[I] \quad \vec{x} \in \partial G(\vec{\pi}); \vec{\omega} \cdot \vec{n} > 0 \quad (13)$$

with

$$\begin{aligned} S_{b,\vec{\pi}} = & -\alpha (\mathcal{C}[I] + S) \\ & -\beta \partial_{1,\vec{u}} S_b - \partial_{2,\vec{\gamma}} S_b + \partial_{\vec{\pi}} S_b \end{aligned} \quad (14)$$

with $\partial_{2,\vec{\gamma}}S_b = \partial_{2,\vec{\gamma}}I^{eq}(T_b) = 0$ and $\partial_{\vec{\pi}}S_b = 0$. If the surface temperature T_b is homogeneous along the boundary therefore $\partial_{1,\vec{u}}S_b = 0$. Otherwise the geometric sensitivity will depends on the surface derivative of the thermal emission:

$$S_{b,\vec{\pi}} = -\alpha(\mathcal{C}[I] + S) - \beta\partial_{1,\vec{u}}I^{eq}(T_b) \quad (15)$$

Geometric sensitivity boundary condition for diffuse surfaces For a diffuse surface the reflection probability density function is $p_{\Omega'}(-\vec{\omega}'|\vec{x}, -\vec{\omega}) = \frac{\vec{\omega}\cdot\vec{n}}{\pi}$. Two angular terms of the sensitivity boundary condition simplifies (see appendix I):

$$\partial_{2,\vec{\gamma}}\left(\int_{\mathcal{H}'} p_{\Omega'}(-\vec{\omega}'|\vec{x}, -\vec{\omega})d\vec{\omega}'I'\right) = 0 \quad (16)$$

and

$$\mathcal{C}_b[\partial_{2,\vec{\gamma}}I] = \int_{\Omega'} (\vec{\omega}' \wedge \vec{n}) \cdot \vec{\gamma}I(\vec{x}, \vec{\omega}', \vec{\pi})d\vec{\omega}' \quad (17)$$

The boundary condition for the geometric sensitivity $s = s(\vec{x}, \vec{\omega}, \vec{\pi})$ becomes:

$$s = \mathcal{C}_b[s] + S_{b,\vec{\pi}}[I, \partial_{1,\vec{u}}I, \partial_{1,\vec{x}}I] \quad \vec{x} \in \partial G(\vec{\pi}); \vec{\omega}\cdot\vec{n} > 0 \quad (18)$$

with

$$\begin{aligned} S_{b,\vec{\pi}} = & -\alpha(\mathcal{C}[I] + S) \\ & -\beta\partial_{1,\vec{u}}S_b - \partial_{2,\vec{\gamma}}S_b + \partial_{\vec{\pi}}S_b \\ & -\beta\partial_{1,\vec{u}}\mathcal{C}_b[I] + \partial_{\vec{\pi}}\mathcal{C}_b[I] \\ & -\partial_{2,\vec{\gamma}}\rho(\vec{x}, -\vec{\omega})\int_{\mathcal{H}'} p_{\Omega'}(-\vec{\omega}'|\vec{x}, -\vec{\omega})d\vec{\omega}'I \\ & -\beta\mathcal{C}_b[\partial_{1,\vec{u}}I] + \mathcal{C}_b[\partial_{1,\vec{x}}I] \\ & + \int_{\Omega'} (\vec{\omega}' \wedge \vec{n}) \cdot \vec{\gamma}I(\vec{x}, \vec{\omega}', \vec{\pi})d\vec{\omega}' \end{aligned} \quad (19)$$

Geometric sensitivity boundary condition for specular surfaces For a specular surface the reflection probability density function is $p_{\Omega'}(-\vec{\omega}'|\vec{x}, -\vec{\omega}) = \delta(\vec{\omega}' - \vec{\omega}_{spec})$ with $\vec{\omega}_{spec} = \vec{\omega} - 2(\vec{\omega} \cdot \vec{n})\vec{n}$. Acknowledging that the rotation direction $\vec{\gamma}$ can be reframed as the sum of a tangent and normal vector in the surface local frame: $\vec{\gamma} = \mu\vec{\gamma}_t + \eta\vec{\gamma}_n$ (see appendix I), two angular terms of the sensitivity boundary condition simplifies:

$$\begin{aligned} \partial_{2,\vec{\gamma}}\left(\int_{\mathcal{H}'} p_{\Omega'}(-\vec{\omega}'|\vec{x}, -\vec{\omega})d\vec{\omega}'I'\right) &= -\partial_{2,\vec{\gamma}_{spec}}I(\vec{x}, \vec{\omega}_{spec}, \vec{\pi}) \\ &= -\mu\partial_{2,\vec{\gamma}_t}I(\vec{x}, \vec{\omega}_{spec}, \vec{\pi}) + \eta\partial_{2,\vec{\gamma}_n}I(\vec{x}, \vec{\omega}_{spec}, \vec{\pi}) \end{aligned} \quad (20)$$

and

$$\begin{aligned} \mathcal{C}_b[\partial_{2,\vec{\gamma}}I] &= \partial_{2,\vec{\gamma}}I(\vec{x}, \vec{\gamma}_{spec}, \vec{\pi}) \\ &= \mu\partial_{2,\vec{\gamma}_t}I(\vec{x}, \vec{\omega}_{spec}, \vec{\pi}) + \eta\partial_{2,\vec{\gamma}_n}I(\vec{x}, \vec{\omega}_{spec}, \vec{\pi}) \end{aligned} \quad (21)$$

The boundary condition for the geometric sensitivity $s = s(\vec{x}, \vec{\omega}, \vec{\pi})$ becomes:

$$s = \mathcal{C}_b[s] + S_{b,\vec{\pi}}[I, \partial_{1,\vec{u}}I, \partial_{1,\vec{x}}I, \partial_{2,\vec{\gamma}_t}I] \quad \vec{x} \in \partial G(\vec{\pi}); \vec{\omega}\cdot\vec{n} > 0 \quad (22)$$

with

$$\begin{aligned} S_{b,\vec{\pi}} = & -\alpha(\mathcal{C}[I] + S) \\ & -\beta\partial_{1,\vec{u}}S_b - \partial_{2,\vec{\gamma}}S_b + \partial_{\vec{\pi}}S_b \\ & -\beta\partial_{1,\vec{u}}\mathcal{C}_b[I] + \partial_{\vec{\pi}}\mathcal{C}_b[I] \\ & -\partial_{2,\vec{\gamma}}\rho(\vec{x}, -\vec{\omega})\int_{\mathcal{H}'} p_{\Omega'}(-\vec{\omega}'|\vec{x}, -\vec{\omega})d\vec{\omega}'I \\ & -\beta\mathcal{C}_b[\partial_{1,\vec{u}}I] + \mathcal{C}_b[\partial_{1,\vec{x}}I] \\ & + 2\mu\partial_{2,\vec{\gamma}_t}I(\vec{x}, \vec{\omega}_{spec}, \vec{\pi}) \end{aligned} \quad (23)$$

3 Boundary discontinuities at the junction of two plane surfaces

We have set up a transport model for s . The corresponding source terms define the emission, in the elementary solid angle $d\vec{\omega}$ around $\vec{\omega}$,

- of any elementary volume $dv \equiv d\vec{x}$ around $\vec{x} \in G$:

$$\text{Volume emission: } S_{\vec{\pi}}[I] dv d\vec{\omega} \quad (24)$$

- of any elementary surface $d\sigma \equiv d\vec{x}$, of normal \vec{n} , around $\vec{x} \in \partial G$

$$\text{Surface emission: } S_{b,\vec{\pi}}[I, \partial_{1,\vec{a}}I, \partial_{1,\vec{x}}I, \partial_{2,\vec{\gamma}}I](\vec{\omega} \cdot \vec{n}) d\sigma d\vec{\omega} \quad (25)$$

When the boundary is discrete as an ensemble of plane surfaces, typically an ensemble of triangles, then the intensity in a given direction becomes discontinuous at the edge \mathcal{L}_{12} between adjacent plane surfaces ($\mathcal{S}_1, \mathcal{S}_2$). This discontinuity arise either because the intensity sources are different on the two plane surfaces (different surface temperatures for thermal emission), or because of different reflection properties or different surface orientations. In the geometric sensitivity model this apparent discontinuity is captured by the spatial derivative in the surface source $S_{b,\vec{\pi}}$. The spatial derivative will therefore account for the intensity spatial discontinuity on the discrete boundary. It is shown in PART 2 that the boundary discontinuities lead to localized sources along the triangles edges and in the geometric sensitivity model these linear sources will only appear as a result of the coupling with the spatial derivative model at the boundaries.

4 Path statistics and Monte Carlo

Notice: This is a preliminary version of the final paper, consequently only the theoretical framework is included in this paper. Monte-Carlo algorithms and results will be provided soon, along with analytical solutions.

Our main point in this text is that the model of the geometric sensitivity is so similar to the model of intensity (the radiative transfer model) that the whole radiative transfer literature about path statistics and Monte Carlo simulation can be directly reinvested to numerically estimate geometric sensitivities. In this last section, we illustrate the practical meaning of this statement. The technical steps that we will highlight with some specificity are the following:

- Via its volume and surface sources the model of geometric sensitivity is coupled to the radiative transfer model (at the boundaries via $S_{b,\vec{\pi}}$ and in the medium via $S_{\vec{\pi}}$), to the spatial derivative transport model (at the boundary via $S_{b,\vec{\pi}}$) and to the angular derivative model (at the boundary via $S_{b,\vec{\pi}}$). This couplings can be handled using the very same Monte Carlo techniques as those recently developed for the coupling of radiative transfer with other heat-transfer modes[2, 3, 4, 5], or the coupling of radiative transfer with electromagnetism and photosynthesis[6, 7, 8, 9]. In both cases, the main idea is double randomisation: in standard Monte Carlo algorithms for pure radiative transfer, when a volume source or a surface source is required it is known (typically the temperature is known for infrared radiative transfer); if it is not known but a Monte Carlo algorithm is available to numerically estimate the source as an average of a large number of sampled Monte Carlo weights, then in the coupled problem the source can be replaced by only one sample. The resulting coupled algorithm is rigorously unbiased thanks to the law of expectation (“the expectation of an expectation is an expectation”). In practice, this means that the Monte Carlo algorithms estimating geometric sensitivities can be designed as if the sources were known, and when a source is required that depends on $I(\vec{x}', \vec{\omega}', \vec{\pi})$ then one single radiative path is sampled as if estimating the intensity $I(\vec{x}', \vec{\omega}', \vec{\pi})$ with any available Monte Carlo algorithm. When a source is required that depends on $\partial_{1,\vec{x}}I(\vec{x}', \vec{\omega}', \vec{\pi})$ then on single spatial derivative path is sampled as if estimating the spatial derivative $\partial_{1,\vec{x}}I(\vec{x}', \vec{\omega}', \vec{\pi})$ with any available Monte Carlo algorithm (see PART 1). When a source is required that depends on $\partial_{2,\vec{\gamma}}I(\vec{x}', \vec{\omega}', \vec{\pi})$ the one single angular derivative path is sampled as if estimating the angular derivative $\partial_{2,\vec{\gamma}}I(\vec{x}', \vec{\omega}', \vec{\pi})$ with any available Monte Carlo algorithm (see PART 2). When the boundaries are discrete as in a set of plane triangles solving the spatial derivative requires to sample linear sources as described in PART 1.

We provide hereafter some examples of algorithms that illustrate this point. They estimate s at a location \vec{x} in a direction $\vec{\omega}$. Each example is implemented and tested against exact solutions:

- Solution 1: the solution provided by Chandrasekhar for a uniform flux in a stratified heterogeneous scattering atmosphere[15] (see Appendix J). This one-dimension solution is cut by a three-dimension closed boundary (a sphere or a cube) and the boundary conditions are adjusted to insure that Chandrasekhar’s solution is still satisfied. In Chandrasekhar’s solution, there is no volume absorption; when we need to add volume absorption, we compensate it by introducing an adjusted volume emission insuring that Chandrasekhar’s solution is again still satisfied.

- Solution 2: a transparent slab between a black isothermal surface at T_{hot} and an emitting/reflecting diffuse surface of temperature T_{cold} everywhere except for a square subsurface where the temperature is T_{hot} ;

These algorithms sample Monte Carlo weights noted w_Z for each quantity Z , meaning that N samples $w_{Z,1}, w_{Z,2} \dots w_{Z,N}$ are required to estimate Z as $\tilde{Z} = \frac{1}{N} \sum_{i=1}^N w_{Z,i}$,

- w_I for the intensity I when referring to a standard Monte Carlo algorithm estimating the solution of the radiative transfer equation;
- w_s for the geometric sensitivity;

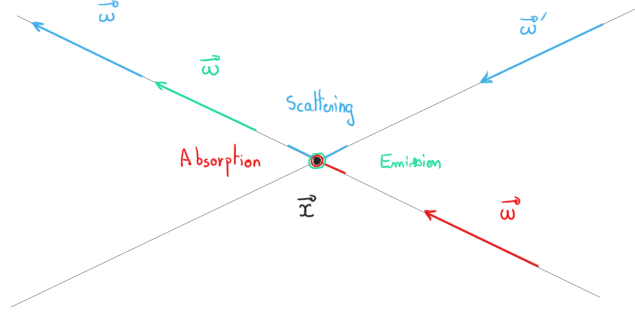


Figure 2: Sources (emission) and collisions (absorption and scattering) within the volume. The formulation of Eq. 3 favors a reciprocal/adjoint interpretation thanks to the micro-reversibility relation $p_{\Omega'}(-\vec{\omega}'|\vec{x}, -\vec{\omega}) = p_{\Omega'}(\vec{\omega}|\vec{x}, \vec{\omega}')$. The physical picture then becomes that of a photon initially in direction $-\vec{\omega}$ scattered in direction $-\vec{\omega}'$.

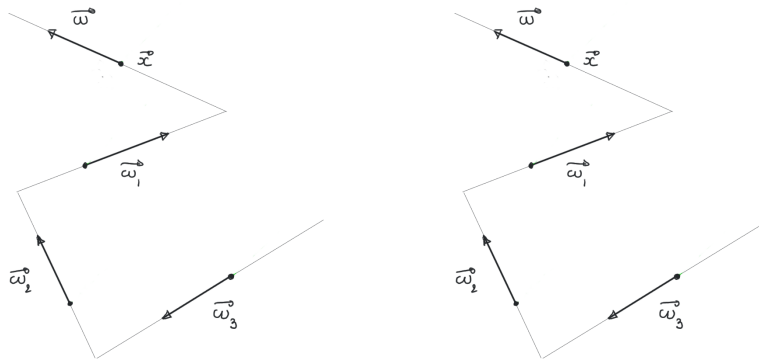


Figure 3: Left: a multiple-scattering photon trajectory leading to location \vec{x} and transport direction $\vec{\omega}$. Right: its correspondence for the geometric sensitivity. Nothing changes.

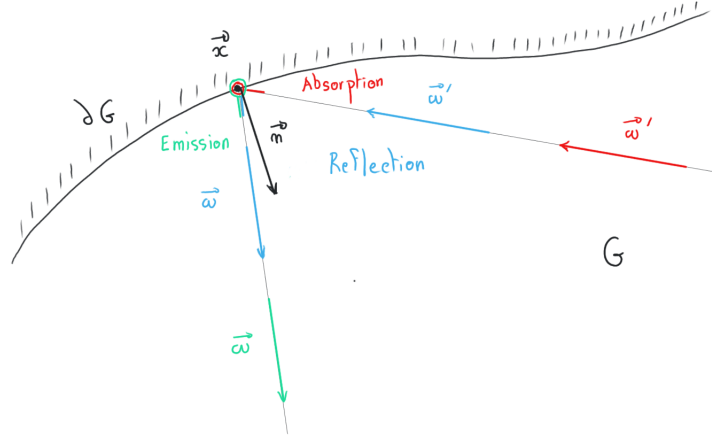


Figure 4: Sources (emission) and collisions (absorption and reflection) at the boundary. The formulation of Eq. 4 favors a reciprocal/adjoint interpretation thanks to the micro-reversibility relation $(\vec{\omega} \cdot \vec{n})\rho(\vec{x}, -\vec{\omega})p_{\Omega',b}(-\vec{\omega}'|\vec{x}, -\vec{\omega}) = -(\vec{\omega}' \cdot \vec{n})\rho(\vec{x}, \vec{\omega}')p_{\Omega,b}(\vec{\omega}|\vec{x}, \vec{\omega}')$. The physical picture then becomes that of a photon initially in direction $-\vec{\omega}$ reflected in direction $-\vec{\omega}'$.

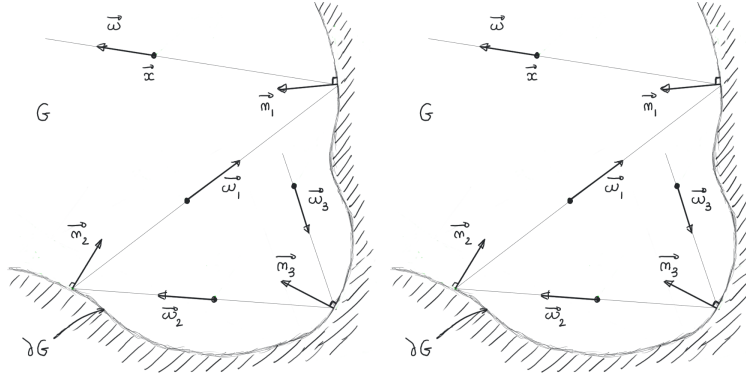


Figure 5: **Left:** a multiple-reflection photon trajectory leading to location \vec{x} and transport direction $\vec{\omega}$ for diffuse surfaces. **Right:** its correspondence for geometric sensitivity. Nothing changes.

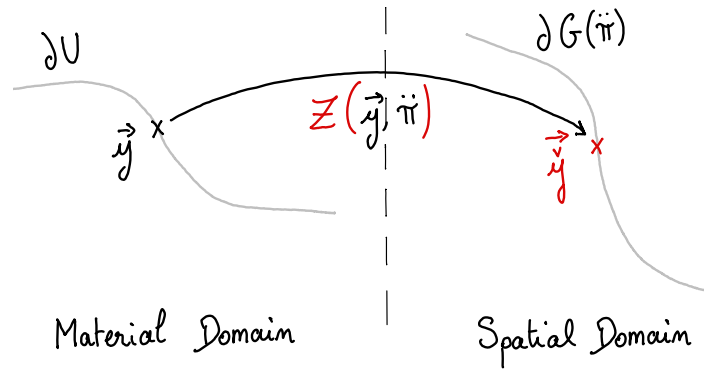


Figure 6: Relation between the material domain and the spatial domain. The application \mathcal{Z} state the spatial boundary $\partial G(\bar{\pi})$ from the material boundary ∂U for any $\bar{\pi}$ values ($\mathcal{Z} : \partial U \times \mathbb{R} \rightarrow \partial G(\bar{\pi})$ or $\vec{y} = \mathcal{Z}(\vec{y}, \bar{\pi})$).

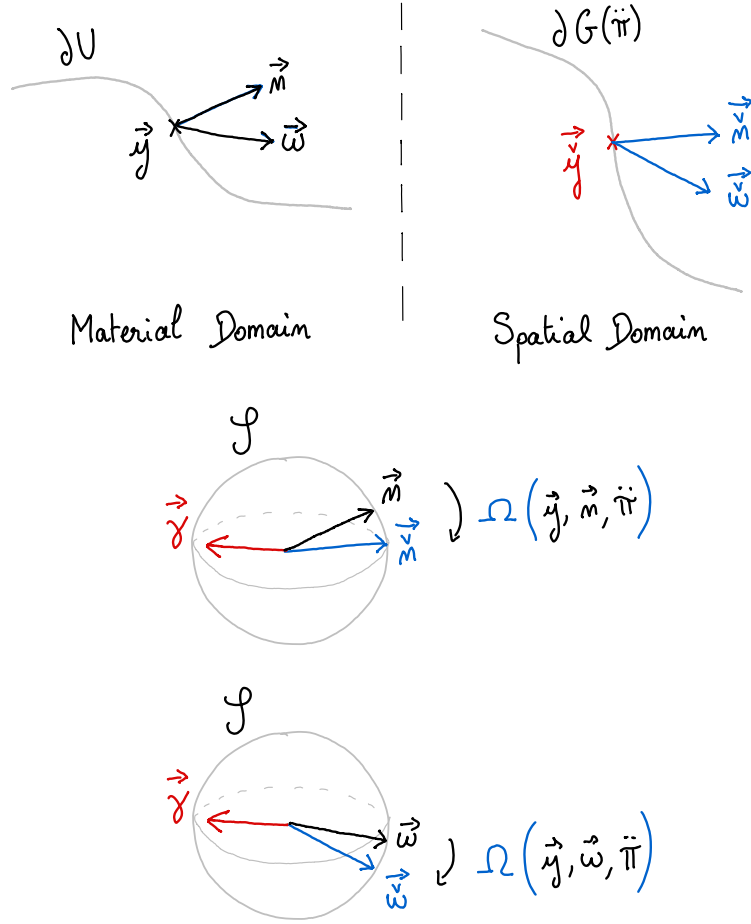


Figure 7: Relation between the material domain local frame (oriented by \vec{n}) and the spatial domain local frame (oriented by $\vec{\tilde{n}}$). The application Ω links any unit vector of the material local frame to their image in the spatial domain local frame ($\Omega : \partial U \times \mathcal{S} \times \mathbb{R} \rightarrow \mathcal{S}$ or $\vec{\omega} = \Omega(\vec{y}, \vec{\omega}, \bar{\pi})$).

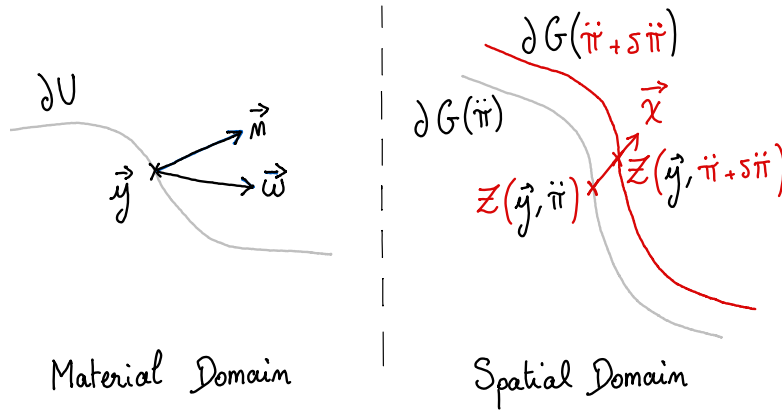


Figure 8: The deformation vector $\vec{\chi}$ describes the boundary deformation induced by a perturbation of the geometrical parameter $\bar{\pi}$ at any position of the boundary \vec{y} . For any position on the boundary and $\bar{\pi}$ values the deformation vector $\vec{\chi} = \partial_{\bar{\pi}} \mathcal{L}(\vec{y}, \bar{\pi})$.

G Derivation of the geometric sensitivity boundary condition

Starting from the equivalence between the material intensity and spatial intensity outgoing respectively the material and spatial boundaries we differentiate the equality $I = L$:

$$\partial_{\vec{\pi}} I(\vec{y}, \vec{\omega}, \vec{\pi}) = \partial_{\vec{\pi}} L(\vec{y}, \vec{\omega}, \vec{\pi}) \quad (26)$$

G.1 Differentiation of the spatial intensity boundary condition

$$\partial_{\vec{\pi}} I(\vec{y}, \vec{\omega}, \vec{\pi}) = \partial_{1, \vec{\chi}} I(\vec{y}, \vec{\omega}, \vec{\pi}) + \partial_{2, \vec{\gamma}} I(\vec{y}, \vec{\omega}, \vec{\pi}) + s(\vec{y}, \vec{\omega}, \vec{\pi}) \quad (27)$$

Acknowledging that the boundary properties are attached to the boundary, and anticipating the next steps of the sensitivity boundary condition derivation, we retained the following approach to deal with the spatial derivative of the boundary outgoing intensity $\partial_{1, \vec{\chi}} I$ (the same choices are made in PART 1):

- $\vec{\chi}$ is decomposed as the sum of two vectors, one collinear to the direction of sight $\vec{\omega}$, the other parallel to a direction \vec{u} to the boundary (see figure 9 and Appendix H), i.e.

$$\vec{\chi} = \alpha \vec{\omega} + \beta \vec{u} \quad (28)$$

with

$$\alpha = \frac{\vec{\chi} \cdot \vec{n}}{\vec{\omega} \cdot \vec{n}}; \quad \beta = \|\vec{\chi} - \alpha \vec{\omega}\|; \quad \vec{u} = \frac{\vec{\chi} - \alpha \vec{\omega}}{\beta} \quad \text{or} \quad \beta \vec{u} = \frac{(\vec{\omega} \wedge \vec{\chi}) \wedge \vec{n}}{\vec{\omega} \cdot \vec{n}} \quad (29)$$

The spatial derivative in direction $\vec{\chi}$ can then be addressed by successively considering the spatial derivative in direction $\vec{\omega}$ and the spatial derivative in direction \vec{u} :

$$\partial_{1, \vec{\chi}} I = \alpha \partial_{1, \vec{\omega}} I + \beta \partial_{1, \vec{u}} I \quad (30)$$

The spatial derivative in the direction of the line of sight is simply the transport term of the radiative transfer equation 2. It can therefore be replaced by field collisions and sources:

$$\partial_{1, \vec{\omega}} I = \mathcal{C}[I] + S \quad (31)$$

The spatial derivative in a direction tangent to the boundary can finally be obtained by a straightforward differentiation of the incoming radiation equation 4 (see also PART 1):

$$\partial_{1, \vec{u}} I = \mathcal{C}_b[\partial_{1, \vec{u}} I] + \partial_{1, \vec{u}} \mathcal{C}_b[I] + \partial_{1, \vec{u}} S_b \quad (32)$$

The angular derivative in the rotation direction $\vec{\gamma}$ can be obtained by the same straightforward differentiation of the incoming radiation equation 4 (see also PART 2):

$$\begin{aligned} \partial_{2, \vec{\gamma}} I &= \partial_{2, \vec{\gamma}} S_b \\ &+ \partial_{2, \vec{\gamma}} \rho(\vec{y}, -\vec{\omega}) \int_{\mathcal{H}'} p_{\Omega'}(-\vec{\omega}' | \vec{y}, -\vec{\omega}) I(\vec{y}, \vec{\omega}', \vec{\pi}) \\ &+ \rho(\vec{y}, -\vec{\omega}) \partial_{2, \vec{\gamma}} \left(\int_{\mathcal{H}'} p_{\Omega'}(-\vec{\omega}' | \vec{y}, -\vec{\omega}) I(\vec{y}, \vec{\omega}', \vec{\pi}) \right) \end{aligned} \quad (33)$$

G.2 Differentiation of the material intensity boundary condition

In the material domain, the intensity boundary condition is:

$$L = \mathcal{C}_b[L] + S_b \quad \vec{y} \in \partial U; \vec{\omega} \cdot \vec{n} > 0 \quad (34)$$

Differentiating the material intensity in Eq. 26 therefore gives:

$$\partial_{\vec{\pi}} L = \partial_{\vec{\pi}} \mathcal{C}_b[L] + \mathcal{C}_b[\partial_{\vec{\pi}} L] + \partial_{\vec{\pi}} S_b \quad \vec{y} \in \partial U; \vec{\omega} \cdot \vec{n} > 0 \quad (35)$$

with

$$\begin{aligned} \partial_{\vec{\pi}} \mathcal{C}_b[L] &= \partial_{\vec{\pi}} \rho(\vec{y}, -\vec{\omega}) \int_{\mathcal{H}'} p_{\Omega'}(-\vec{\omega}' | \vec{y}, -\vec{\omega}) d\vec{\omega}' L(\vec{y}, \vec{\omega}', \vec{\pi}) \\ &+ \rho(\vec{y}, -\vec{\omega}') \int_{\mathcal{H}'} \partial_{\vec{\pi}} p_{\Omega'}(-\vec{\omega}' | \vec{y}, -\vec{\omega}) d\vec{\omega}' L(\vec{y}, \vec{\omega}', \vec{\pi}) \end{aligned} \quad (36)$$

and with

$$\mathcal{C}_b[\partial_{\vec{\pi}}L] = \rho(\vec{y}, -\vec{\omega}) \int_{\mathcal{H}'} p_{\Omega'}(-\vec{\omega}'|\vec{y}, -\vec{\omega}) d\vec{\omega}' \partial_{\vec{\pi}}L(\vec{y}, \vec{\omega}', \vec{\pi}) \quad (37)$$

where $L(\vec{y}, \vec{\omega}', \vec{\pi})$ is the intensity incoming the material surface ∂U and is equal to the intensity incoming the spatial domain surface $\partial G(\vec{\pi})$:

$$L(\vec{y}, \vec{\omega}', \vec{\pi}) = I(\vec{y}, \vec{\omega}', \vec{\pi}) \quad (38)$$

so that

$$\begin{aligned} \partial_{\vec{\pi}}L(\vec{y}, \vec{\omega}', \vec{\pi}) &= \partial_{\vec{\pi}}I(\vec{y}, \vec{\omega}', \vec{\pi}) \\ &= \partial_{1, \vec{\chi}}I(\vec{y}, \vec{\omega}', \vec{\pi}) + \partial_{2, \vec{\gamma}}I(\vec{y}, \vec{\omega}', \vec{\pi}) + s(\vec{y}, \vec{\omega}', \vec{\pi}) \end{aligned} \quad (39)$$

and finally

$$\partial_{\vec{\pi}}L = \partial_{\vec{\pi}}\mathcal{C}_b[I] + \mathcal{C}_b[\partial_{1, \vec{\chi}}I] + \mathcal{C}_b[\partial_{2, \vec{\gamma}}I] + \mathcal{C}_b[s] + \partial_{\vec{\pi}}S_b \quad (40)$$

G.3 Geometric sensitivity boundary condition

Starting from differentiating $I = L$ the boundary condition for the geometric sensitivity $s = s(\vec{y}, \vec{\omega}, \vec{\pi})$ is:

$$s = \mathcal{C}_b[s] + S_{b, \vec{\pi}}[I, \partial_{1, \vec{u}}I, \partial_{1, \vec{\chi}}I, \partial_{2, \vec{\gamma}}I] \quad \vec{y} \in \partial G(\vec{\pi}); \vec{\omega} \cdot \vec{n} > 0 \quad (41)$$

with

$$\begin{aligned} S_{b, \vec{\pi}} &= -\alpha(\mathcal{C}[I] + S) \\ &\quad - \beta \partial_{1, \vec{u}}S_b - \partial_{2, \vec{\gamma}}S_b + \partial_{\vec{\pi}}S_b \\ &\quad - \beta \partial_{1, \vec{u}}\mathcal{C}_b[I] + \partial_{\vec{\pi}}\mathcal{C}_b[I] \\ &\quad - \partial_{2, \vec{\gamma}}\rho(\vec{y}, -\vec{\omega}) \int_{\mathcal{H}'} p_{\Omega'}(-\vec{\omega}'|\vec{y}, -\vec{\omega}) d\vec{\omega}' I \\ &\quad - \rho(\vec{y}, -\vec{\omega}) \partial_{2, \vec{\gamma}} \left(\int_{\mathcal{H}'} p_{\Omega'}(-\vec{\omega}'|\vec{y}, -\vec{\omega}) d\vec{\omega}' I' \right) \\ &\quad - \beta \mathcal{C}_b[\partial_{1, \vec{u}}I] + \mathcal{C}_b[\partial_{1, \vec{\chi}}I] + \mathcal{C}_b[\partial_{2, \vec{\gamma}}I] \end{aligned} \quad (42)$$

H Projection on the surface

$\vec{\chi}$ is decomposed using the non-orthogonal basis $(\vec{\omega}, \vec{m}, \vec{t})$:

$$\vec{\chi} = \alpha \vec{\omega} + \zeta \vec{m} + \xi \vec{t} \quad (43)$$

Taking the scalar product of $\vec{\chi}$ with \vec{n} , $\vec{\omega} \wedge \vec{t}$ and $\vec{\omega} \wedge \vec{m}$ leads to

$$\begin{aligned} \alpha &= \frac{\vec{\chi} \cdot \vec{n}}{\vec{\omega} \cdot \vec{n}} \\ \zeta &= \frac{\vec{\chi} \cdot (\vec{\omega} \wedge \vec{t})}{\vec{m} \cdot (\vec{\omega} \wedge \vec{t})} \\ \xi &= \frac{\vec{\chi} \cdot (\vec{\omega} \wedge \vec{m})}{\vec{t} \cdot (\vec{\omega} \wedge \vec{m})} \end{aligned} \quad (44)$$

Replacing \vec{m} with $\vec{t} \wedge \vec{n}$ and using standard algebra (line 2: circulation property of triple products; line 3: development of double vectorial products; line 4: $\vec{t} \cdot \vec{n} = 0$ and $\vec{t} \cdot \vec{t} = 1$),

$$\begin{aligned} \vec{m} \cdot (\vec{\omega} \wedge \vec{t}) &= (\vec{t} \wedge \vec{n}) \cdot (\vec{\omega} \wedge \vec{t}) \\ &= ((\vec{\omega} \wedge \vec{t}) \wedge \vec{t}) \cdot \vec{n} \\ &= (-\vec{t} \cdot \vec{t}) \vec{\omega} + (\vec{\omega} \cdot \vec{t}) \vec{t} \cdot \vec{n} \\ &= -\vec{\omega} \cdot \vec{n} \end{aligned} \quad (45)$$

Similarly $\vec{t} \cdot (\vec{\omega} \wedge \vec{m}) = \vec{\omega} \cdot \vec{n}$ and we get

$$\begin{aligned}\alpha &= \frac{\vec{\chi} \cdot \vec{n}}{\vec{\omega} \cdot \vec{n}} \\ \zeta &= -\frac{\vec{\chi} \cdot (\vec{\omega} \wedge \vec{t})}{\vec{\omega} \cdot \vec{n}} \\ \xi &= \frac{\vec{\chi} \cdot (\vec{\omega} \wedge \vec{m})}{\vec{\omega} \cdot \vec{n}}\end{aligned}\tag{46}$$

By definition, $\beta \vec{u} = \zeta \vec{m} + \xi \vec{t}$ and observing (line 1: development of double vectorial products; line 2: replacement of $\vec{\chi}$ with its development; line 3: $\alpha = \frac{\vec{\chi} \cdot \vec{n}}{\vec{\omega} \cdot \vec{n}}$)

$$\begin{aligned}(\vec{\chi} \wedge \vec{\omega}) \wedge \vec{n} &= -(\vec{\omega} \cdot \vec{n})\vec{\chi} + (\vec{\chi} \cdot \vec{n})\vec{\omega} \\ &= -(\vec{\omega} \cdot \vec{n}) (\alpha\vec{\omega} + \zeta\vec{m} + \xi\vec{t}) + (\vec{\chi} \cdot \vec{n})\vec{\omega} \\ &= -(\vec{\omega} \cdot \vec{n}) (\zeta\vec{m} + \xi\vec{t})\end{aligned}\tag{47}$$

we get

$$\beta \vec{u} = \frac{(\vec{\omega} \wedge \vec{\chi}) \wedge \vec{n}}{\vec{\omega} \cdot \vec{n}}\tag{48}$$

I Projections for the angular derivatives

I.1 Projections of the rotation direction

On the surface local frame (oriented by the normal vector \vec{n}), the rotation direction vector $\vec{\gamma}$ can be decomposed using a normal and a tangent components:

$$\vec{\gamma} = \mu\vec{\gamma}_t + \eta\vec{\gamma}_n\tag{49}$$

with

$$\vec{\gamma}_n = \vec{n} \quad ; \quad \vec{\gamma}_t = \frac{\vec{\gamma} - \eta\vec{\gamma}_n}{\|\vec{\gamma} - \eta\vec{\gamma}_n\|} \quad ; \quad \eta = \vec{\gamma} \cdot \vec{n} \quad ; \quad \mu = \|\vec{\gamma} - \eta\vec{\gamma}_n\|\tag{50}$$

J Chandrasekhar's exact solution for heterogeneous multiple-scattering atmospheres

In a heterogeneous, purely scattering and infinite medium, with plane parallel stratified intensity field, the radiative transfer equation has an analytical solution $I(\tau, \mu)$ ([15]):

$$I(\tau, \mu) = \frac{\eta(0)}{4\pi} + \frac{3}{4\pi} j[(g-1)\tau + \mu]\tag{51}$$

with $\eta(0)$ and j being constants, g is the asymmetric coefficient, τ is the optical thickness normal to the plane of stratification and μ the direction cosine. \vec{e}_1 being the plane normal unit vector and a vector of the Cartesian coordinate system $(\vec{e}_1, \vec{e}_2, \vec{e}_3)$ we state the normal optical thickness as:

$$\tau = \int_0^{\vec{x} \cdot \vec{e}_1} k_s(l) dl\tag{52}$$

with \vec{x} the position in the infinite medium. The cosine $\mu = \vec{\omega} \cdot \vec{e}_1$ with $\vec{\omega}$ the transport direction. We state the analytical intensity \mathcal{L} as $\mathcal{L}(\vec{x}, \vec{\omega}) = I(\tau, \mu)$.

References

- [1] Maxime Roger, Stephane Blanco, Mouna El Hafi, and Richard Fournier. Monte carlo estimates of domain-deformation sensitivities. *Phys. Rev. Lett.*, 95:180601, Oct 2005.
- [2] Richard Fournier, Stéphane Blanco, Vincent Eymet, Mouna El Hafi, and Christophe Spiesser. Radiative, conductive and convective heat-transfers in a single monte carlo algorithm. In *Journal of Physics: Conference Series*, volume 676, page 012007. IOP Publishing, 2016.

-
- [3] Léa Penazzi, Stéphane Blanco, Cyril Caliot, C. Coustet, Mouna El-Hafi, Richard A Fournier, Mathieu Galtier, Loris Ibarrart, and Maxime Roger. Toward the use of Symbolic Monte Carlo for Conduction-Radiation Coupling in Complex Geometries. In RAD-19 - 9th International Symposium on Radiative Transfer, page 8 p., Athens, Greece, June 2019. Begellhouse.
- [4] Morgan Sans, Olivier Farges, Vincent Schick, and Gilles Parent. Solving transient coupled conductive and radiative transfers in porous media with a monte carlo method: Characterization of thermal conductivity of foams using a numerical flash method. International Journal of Thermal Sciences, 179:107656, 2022.
- [5] JM Tregan, S Blanco, C Caliot, J Dauchet, M El Hafi, V Eymet, R Fournier, O Farges, J Gautrais, and M Roger. Transient conducto-radiative heat transfer in a single monte carlo algorithm: Handling the nonlinearity. In 9th International Symposium on Radiative Transfer, RAD-19, 2019.
- [6] Jérémi Dauchet, Stéphane Blanco, Jean-François Cornet, Mouna El Hafi, Vincent Eymet, and Richard Fournier. The practice of recent radiative transfer monte carlo advances and its contribution to the field of microorganisms cultivation in photobioreactors. Journal of Quantitative Spectroscopy and Radiative Transfer, 128:52–59, 2013. Eurotherm Seminar on Computational Thermal Radiation in Participating Media IV.
- [7] Jérémi Dauchet, Stéphane Blanco, Jean-François Cornet, and Richard Fournier. Calculation of the radiative properties of photosynthetic microorganisms. Journal of Quantitative Spectroscopy and Radiative Transfer, 161:60–84, 2015.
- [8] Julien Charon, Stéphane Blanco, Jean-François Cornet, Jérémi Dauchet, Mouna El Hafi, Richard Fournier, Mira Kaissar Abboud, and Sebastian Weitz. Monte carlo implementation of schiff s approximation for estimating radiative properties of homogeneous, simple-shaped and optically soft particles: Application to photosynthetic micro-organisms. Journal of Quantitative Spectroscopy and Radiative Transfer, 172:3–23, 2016. Eurotherm Conference No. 105: Computational Thermal Radiation in Participating Media V.
- [9] Victor Gattepaille, Jérémi Dauchet, Fabrice Gros, Matthieu Roudet, Caroline Supplis, and Jean-François CORNET. Integral formulations of multi-scale models for the optimization of solar photo-catalytic processes. In International Congress/3rd days of GdR Solar Fuels : Artificial photosynthesis and Solar Fuels, Paris, France, 2018.
- [10] J. Delatorre, G. Baud, J.J. Bézian, S. Blanco, C. Caliot, J.F. Cornet, C. Coustet, J. Dauchet, M. El Hafi, V. Eymet, R. Fournier, J. Gautrais, O. Gourmel, D. Joseph, N. Meilhac, A. Pajot, M. Paulin, P. Perez, B. Piaud, M. Roger, J. Rolland, F. Veynandt, and S. Weitz. Monte carlo advances and concentrated solar applications. Solar Energy, 103:653–681, 2014.
- [11] Cyril Caliot, Hadrien Benoit, Emmanuel Guillot, Jean-Louis Sans, Alain Ferriere, Gilles Flamant, Christophe Coustet, and Benjamin Piaud. Validation of a Monte Carlo Integral Formulation Applied to Solar Facility Simulations and Use of Sensitivities. Journal of Solar Energy Engineering, 137(2), 04 2015. 021019.
- [12] Olivier Farges, Jean-Jacques Bézian, Hélène Bru, Mouna El Hafi, Richard Fournier, and Christophe Spiesser. Life-time integration using monte carlo methods when optimizing the design of concentrated solar power plants. Solar Energy, 113:57–62, 2015.
- [13] M. Sans, M. El Hafi, V. Eymet, V. Forest, R. Fournier, and N. Villefranque. Null-collision meshless monte-carlo - a new reverse monte-carlo algorithm designed for laser-source emission in absorbing/scattering inhomogeneous media. Journal of Quantitative Spectroscopy and Radiative Transfer, page 107725, 2021.
- [14] Najda Villefranque, Richard Fournier, Fleur Couvreur, Stéphane Blanco, Céline Cornet, Vincent Eymet, Vincent Forest, and Jean-Marc Tregan. A path-tracing monte carlo library for 3-d radiative transfer in highly resolved cloudy atmospheres. Journal of Advances in Modeling Earth Systems, 11(8):2449–2473, 2019.
- [15] Subrahmanyam Chandrasekhar. Radiative transfer. Courier Corporation, 2013.

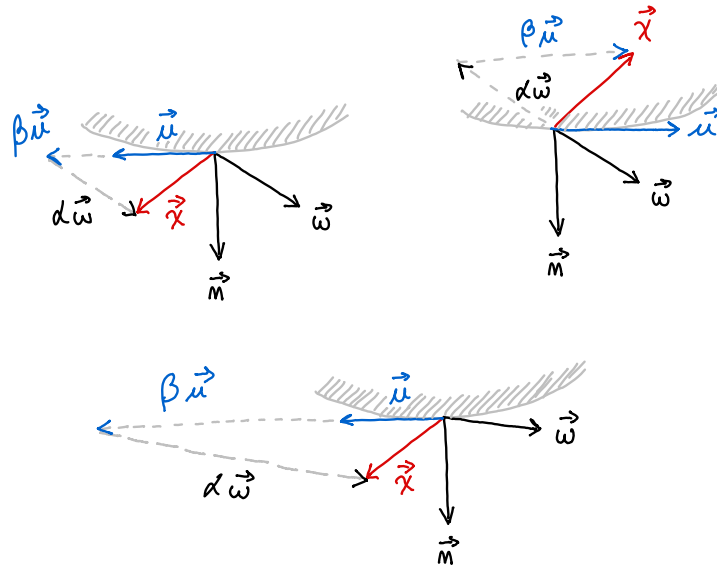


Figure 9: At the boundary, the differentiation direction $\vec{\chi}$ is decomposed by projection along the transport direction $\vec{\omega}$ and along a unit vector \vec{u} tangent to the boundary: $\vec{\chi} = \alpha\vec{\omega} + \beta\vec{u}$ with α that can be positive or negative and β always positive. Four configurations are illustrated. The bottom right configuration illustrates that when the transport direction is nearly tangent to the surface, then the coefficient β can take very large values. This will be an important point when discussing convergence issues for Monte Carlo simulations. β appears indeed as a factor in front of the collision operator, which is translated by the Monte Carlo weight being multiplied by β at each reflection, possibly leading to very large weight values.